

Universidade do Minho
Escola de Engenharia

Marta Susana Machado Fernandes Development of Bacterial Cellulose Composites as an Alternative to Leather

Marta Susana Machado Fernandes

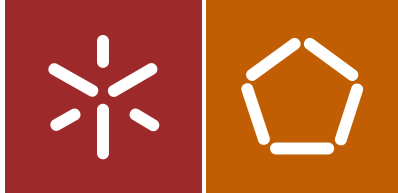
Development of Bacterial Cellulose
Composites as an Alternative to Leather



UNIÃO EUROPEIA
Fundo Europeu
de Desenvolvimento Regional

UMinho | 2021

setembro de 2021



Universidade do Minho
Escola de Engenharia

Marta Susana Machado Fernandes

Development of Bacterial Cellulose
Composites as an Alternative to Leather

Tese de Doutoramento
Doutoramento em Engenharia Têxtil

Trabalho efetuado sob a orientação de
Professor Doutor António Pedro Garcia de Valadares
Souto
Doutor Fernando Octávio de Queirós Dourado

DIREITOS DE AUTOR E CONDIÇÕES DE UTILIZAÇÃO DO TRABALHO POR TERCEIROS

Este é um trabalho académico que pode ser utilizado por terceiros desde que respeitadas as regras e boas práticas internacionalmente aceites, no que concerne aos direitos de autor e direitos conexos.

Assim, o presente trabalho pode ser utilizado nos termos previstos na licença abaixo indicada.

Caso o utilizador necessite de permissão para poder fazer um uso do trabalho em condições não previstas no licenciamento indicado, deverá contactar o autor, através do RepositóriUM da Universidade do Minho.

Licença concedida aos utilizadores deste trabalho



Atribuição-NãoComercial-SemDerivações
CC BY-NC-ND

<https://creativecommons.org/licenses/by-nc-nd/4.0/>

ACKNOWLEDGEMENTS

At the conclusion of the PhD, I would like to acknowledge to the people who supported me.

I would like to start by expressing my gratitude to my supervisor and forever mentor Professor António Pedro Souto. He gave me the opportunity to join his research group in 2010 and his teaching expertise and enthusiasm for science allowed me to grow as a researcher throughout all these years. He was a great professor, a great person, and a friend. It was an honor to have him in my life. I am and always will be deeply thankful to him.

I would like to deliver a word of appreciation and gratitude to my supervisor Doctor Fernando Dourado for all the support and guidance throughout this research work. Thank you very much for your advice and valuable suggestions.

I would like to acknowledge Professor Miguel Gama for giving me the opportunity to participate in the Project “BUILD – Bacterial Cellulose Leather” and always support the progress of the work with his scientific knowledge.

Finally, I would like to express my appreciation and thanks to all my colleagues for the moments we shared in the labs, Ângela, Vítor, Andrea, Isabel, Joaquim Jorge, Marta, Gonul, Ana Isabel, Xinyu, Lu’u, Derya, Sofia, Rui, Patrícia, Inês, Mónica.

Thank you all. It was a great pleasure to work and learn from you.

This project was supported by FEDER funding on the Programa Operacional Regional do Norte (NORTE2020) within the scope of the project NORTE-01-0247-FEDER-003435 (“BUILD–Bacterial Cellulose Leather”).



STATEMENT OF INTEGRITY

I hereby declare having conducted this academic work with integrity. I confirm that I have not used plagiarism or any form of undue use of information or falsification of results along the process leading to its elaboration.

I further declare that I have fully acknowledged the Code of Ethical Conduct of the University of Minho.

University of Minho, September 13, 2021

Full name: Marta Susana Machado Fernandes

Signature: 

Resumo

Desenvolvimento de compósitos de celulose bacteriana como alternativa ao couro

O couro é um material natural amplamente usado nas indústrias do têxtil e do calçado. No entanto, o seu processo produtivo juntamente com o processo de crescimento dos animais apresenta um elevado impacto ambiental e humano. Com os consumidores cada vez mais atentos às questões ambientais e de bem-estar animal, existe uma procura crescente por alternativas sustentáveis e sem crueldade animal.

Este trabalho visou o desenvolvimento de compósitos de celulose bacteriana (CB), como material estruturante, e óleos vegetais ativados e outros polímeros hidrofóbicos, como agentes flexibilizantes e hidrofobizantes, como um produto alternativo ao couro. Para isto, foi testada uma nova abordagem para a modificação da CB, combinando simplicidade, potencial para aplicação à grande escala e baixo custo, com base no uso de um processo simples de esgotamento para a incorporação dos polímeros na matriz da CB. Todas as combinações resultaram em compósitos hidrofóbicos (ângulo de contato máximo de 138°). Primeiramente foram usados dois polímeros comerciais hidrofóbicos da indústria têxtil, um amaciador à base de polidimetilsiloxano (PDMS) e um hidrofobizante à base de perfluorocarbono (PFC). Os compósitos obtidos eram respiráveis (permeabilidade ao vapor de água máxima de $373 \text{ g}\cdot\text{m}^{-2}\cdot 24 \text{ h}^{-1}$) e com performance satisfatória relativamente às propriedades mecânicas (força de rotura máxima de 48.4 MPa). Para aumentar o teor de base biológica no compósito, foi usado óleo de soja epoxidado acrililado (AESO) numa mistura com um polímero à base de PDMS e polietilenoglicol (PEG) 400. Os compósitos de CB possuíam performances distintas, manipuláveis variando a percentagem de polímero. Posteriormente, foram desenvolvidos compósitos com a resina de AESO previamente emulsionada e em misturas com PDMS, PFC e PEG, resultando em compósitos termicamente estáveis (até 200°C) e, globalmente, com propriedades mecânicas adequadas para a aplicação pretendida (força de rotura máxima de 35.9 MPa). Por fim, validou-se o desenvolvimento de compósitos usando um sistema redox ecológico para a polimerização do AESO, bem como o acabamento com um biocida e o tingimento dos compósitos.

A associação de óleos vegetais ativados com membranas de CB constituiu uma abordagem inovadora e promissora para o desenvolvimento de um produto amigo do ambiente, quase exclusivamente composto de materiais biológicos e recicláveis, com potencial para aplicação nas indústrias do têxtil e do calçado, contribuindo para a redução da dependência do couro animal.

Palavras-chave: celulose bacteriana; óleos vegetais ativados; biocompósitos; alternativa ao couro; sustentabilidade.

Abstract

Development of bacterial cellulose composites as an alternative to leather

Leather is a natural material widely used in the textile and footwear industries. However, its production process together with the animal growth process has a high environmental and human impact. With consumers increasingly aware of environmental and animal welfare issues, there is a growing demand for sustainable and cruelty-free alternatives to leather.

This work aimed the development of composites comprising bacterial cellulose (BC), as structural material, and activated vegetable oils and other hydrophobic polymers, as flexibilizing and hydrophobizing agents, as an alternative product to leather. For this, it was tested a novel approach for the modification of BC, combining simplicity, potential for large-scale application and low cost, based on the use of a simple process of exhaustion for the incorporation of the polymers into the BC matrix. All the combinations resulted in hydrophobic composites (maximum contact angle of 138°). Firstly, two commercial hydrophobic polymers from the textile industry were used, a softener based on polydimethylsiloxane (PDMS) and a hydrophobizer based on perfluorocarbon (PFC). The obtained composites were breathable (maximum water vapor permeability of $373 \text{ g}\cdot\text{m}^{-2}\cdot 24 \text{ h}^{-1}$) and with satisfactory performance regarding mechanical properties (maximum tensile strength of 48.4 MPa). To increase the bio-based content in the composite, the acrylated epoxidized soybean oil (AESO) was tested in a mixture with the PDMS-based polymer and polyethylene glycol (PEG) 400. The BC composites owned distinct performances, manipulated by varying the percentage of polymer. Then, composites were developed with the AESO resin previously emulsified and in mixtures with PDMS, PFC and PEG, resulting in composites thermally stable (up to $200 \text{ }^\circ\text{C}$) and, overall, with suitable mechanical properties for the proposed application (maximum tensile strength of 35.9 MPa). Finally, it was validated the development of composites using an ecological redox system for the polymerization of AESO, as well as the finishing with a biocide and the dyeing of the composites.

The association of activated vegetable oils with BC membranes constituted an innovative and promising approach for the development of an environmentally friendly product, almost exclusively composed of biological and recyclable materials, with potential for application in the textile and footwear industries, contributing to the reduction of the animal hide dependency.

Keywords: bacterial cellulose; activated vegetable oils; biocomposites; leather alternative; sustainability.

Table of content

DIREITOS DE AUTOR E CONDIÇÕES DE UTILIZAÇÃO DO TRABALHO POR TERCEIROS.....	ii
ACKNOWLEDGEMENTS.....	iii
STATEMENT OF INTEGRITY.....	iv
Resumo	v
Abstract.....	vi
Acronyms and abbreviations.....	xi
Figure index	xiii
Table index.....	xv
Chapter 1	1
Introduction.....	1
1.1. Preamble.....	1
1.2. Structure of the thesis	4
Chapter 2	6
Literature overview	6
2.1. The leather industry and its environmental impact	6
2.2. Synthetic alternatives to leather	9
2.3. Eco-friendly alternatives to leather	11
2.3.1. Alternatives to leather obtained from sustainable natural resources.....	11
2.3.2. Alternatives to leather obtained by biofabrication	14
2.4. Bacterial cellulose	17
2.4.1. Bacterial cellulose production and properties.....	17
2.4.2. General applications of bacterial cellulose	20
2.4.3. BC in the textile and shoe industry	22
<i>2.4.3.1. BC for the fashion industry.....</i>	<i>22</i>
<i>2.4.3.2. BC coated on fibers, yarns, fabrics.....</i>	<i>25</i>
<i>2.4.3.3. Development of BC macrofibers.....</i>	<i>27</i>
<i>2.4.3.4. Improvement of BC flexibility, hydrophobicity, and mechanical properties</i>	<i>28</i>
<i>2.4.3.5. BC purification, bleaching, and dyeing.....</i>	<i>30</i>
2.5. Vegetable oils	32
Chapter 3	35
Development of BC/PDMS/PFC composites	35
3.1. Abstract.....	35
3.2. Introduction	36
3.3. Materials and methods	37
3.3.1. Materials	37

3.3.2. Composites production	38
3.3.3. Physical-chemical properties evaluation	38
3.3.3.1. <i>Scanning electron microscopy (SEM)</i>	38
3.3.3.2. <i>Atomic force microscopy (AFM)</i>	39
3.3.3.3. <i>Fourier transform infrared (FT-IR) analysis</i>	39
3.3.3.4. <i>Surface energy</i>	39
3.3.3.5. <i>Water vapor permeability (WVP) and static water absorption (SWA)</i>	40
3.3.3.6. <i>Mechanical properties</i>	40
3.3.4. Statistical analysis	41
3.4. Results and discussion	41
3.4.1. Scanning electron microscopy (SEM)	41
3.4.2. Atomic force microscopy (AFM)	43
3.4.3. Fourier transform infrared (FT-IR)	44
3.4.4. Water contact angle (CA) and surface free energy (SFE)	45
3.4.5. Water vapor permeability (WVP) and static water absorption (SWA)	48
3.4.6. Mechanical properties	50
3.5. Conclusion	52
Chapter 4	53
Development of BC/PDMS/PEG/AESO composites	53
4.1. Abstract	53
4.2. Introduction	54
4.3. Materials and methods	54
4.3.1. Materials	54
4.3.2. Composites production	54
4.3.3. Physical-chemical properties evaluation	56
4.3.3.1. <i>Fourier transform infrared (FT-IR) spectroscopy</i>	56
4.3.3.2. <i>Scanning electron microscopy (SEM)</i>	56
4.3.3.3. <i>Wettability</i>	56
4.3.3.4. <i>Water vapor permeability (WVP)</i>	56
4.3.3.5. <i>Mechanical properties</i>	57
4.4. Results and discussion	57
4.4.1. ATR FT-IR analyses of BC and BC composites	57
4.4.2. Scanning electron microscopy (SEM)	59
4.4.3. Wettability	61
4.4.4. Water vapor permeability (WVP)	62
4.4.5. Mechanical properties	63
4.5. Conclusion	64
Chapter 5	65

Development of BC/emulsified AESO composites	65
5.1. Abstract.....	65
5.2. Introduction	66
5.3. Materials and methods	68
5.3.1. Materials	68
5.3.2. Preparation of the acrylated epoxidized soybean oil (AESO) mixture	68
5.3.3. Determination of the required hydrophilic–lipophilic balance (HLB) and AESO emulsion stability evaluation	69
5.3.4. Exhaustion of BC membranes with emulsified AESO	70
5.3.5. Production of composites with different polymers	70
5.3.6. Characterization of the BC-based composites	72
5.3.6.1. <i>Scanning electron cryomicroscopy (Cryo-SEM)</i>	72
5.3.6.2. <i>Scanning electron microscopy (SEM)</i>	72
5.3.6.3. <i>Fourier transform infrared (FT-IR) spectroscopy.....</i>	72
5.3.6.4. <i>Contact angle (CA) and surface free energy (SFE).....</i>	73
5.3.6.5. <i>Differential scanning calorimetry (DSC)</i>	73
5.3.6.6. <i>Thermogravimetric analysis (TGA).....</i>	73
5.3.6.7. <i>Mechanical properties.....</i>	73
5.4. Results and discussion	74
5.4.1. Emulsions stability and diffusion into BC	74
5.4.2. Morphological Analysis	76
5.4.3. Fourier transform infrared (FT-IR).....	78
5.4.4. Surface wettability and surface free energy	80
5.4.5. Thermal properties	82
5.4.6. Mechanical properties.....	85
5.5. Conclusion	86
Chapter 6	88
Development of BC-based composites polymerized with H₂O₂/AA, finishing and dyeing... 88	
6.1. Abstract.....	88
6.2. Introduction	89
6.3. Materials and methods	90
6.3.1. Materials	90
6.3.2. Development of composites with AESO emulsion polymerized before and after the exhaustion process.....	90
6.3.2.1. <i>Emulsion polymerization and development of the composites</i>	90
6.3.2.2. <i>Characterization of the composites</i>	92
6.3.3. Finishing and dyeing	92
6.3.3.1. <i>Antimicrobial finishing.....</i>	92
6.3.3.2. <i>Dyeing of the composites.....</i>	93

6.4.	Results and discussion	94
6.4.1.	Properties of the composites	94
6.4.2.	Antimicrobial activity	97
6.4.3.	Dyeing	98
6.5.	Conclusion	99
Chapter 7		100
Conclusions and suggestions for future work		100
7.1.	Main conclusion	100
7.2.	Suggestions for future work	102
Chapter 8		103
References		103

Acronyms and abbreviations

A

AESO	Acrylated epoxidized soybean oil
AFM	Atomic force microscopy
ATR	Attenuated total reflection

B

BAC	Benzalkonium chloride
BC	Bacterial cellulose

C

CA	Contact angle
CAB	Cellulose acetate butyrate
CFUs	Colony forming units
CHP	Cumene hydroperoxide
CNT	Carbon nanotubes
COD	Chemical oxygen deficiency
CONP	Cobalt naphthenate
Cryo-SEM	Scanning electron cryomicroscopy

D

DSC	Differential scanning calorimetry
DTG	Derivative thermogravimetry

E

ENM	Electrospun nanofibrous membrane
EU	European Union

F

FT-IR	Fourier transform infrared
-------	----------------------------

H

H	Hydrophobizer
HLB	Hydrophilic–lipophilic balance
HS	Hestrin-Scharmm

M

MLAU	Lauryl methacrylate
------	---------------------

O

OCA	Oil contact angle
OLEDs	Organic light-emitting diode
O/W	Oil-in-water

P

PDMS	Polydimethylsiloxane
------	----------------------

PEG	Polyethyleneglycol
PFC	Perfluorocarbon
PFOA	Perfluorooctanoic acid
PFOS	Perfluorooctane sulfonate
PLLA	Poly(L-lactic acid)
PU	Polyurethane
PVA	Polyvinyl alcohol
PVC	Poly(vinyl chloride)
R	
Ra	Roughness average
RMS	Root mean square
S	
S	Softener
SDS	Sodium dodecyl sulfate
SEM	Scanning electron microscopy
SFE	surface free energy
SMD-LED	Surface mounted device-light-emitting diode
SWA	Static water absorption
T	
TDS	Total dissolved solids
TEMPO	(2,2,6,6-tetramethylpiperidin-1-yl)oxyl
TGA	Thermogravimetric analysis
U	
USD	United States Dollar
V	
VOs	Vegetable oils
W	
WCA	Water contact angle
WVP	Water vapor permeability
Y	
YSC	Yarn supercapacitor

Figure index

Figure 1. Schematic representation of the strategies here taken towards the preparation of BC composites.	3
Figure 2. Schematic illustration of the biosynthesis of cellulose molecules and their assembly into nanofibers.	18
Figure 3. SEM micrographs of BC (a,f) and BC composites (10S (b,g); 10H (c,h); 10S + H (d,i); and 50S + H (e,j)), and photos showing the malleability (sample BC-50S + H) (l).	42
Figure 4. AFM micrographs and results of average roughness (Ra) and root mean square roughness (RMS) of BC and BC composites.	43
Figure 5. FT-IR spectra of BC, PDMS (S) and PFC (H) based formulations, and BC composites.....	45
Figure 6. Contact angles over time of the BC composites produced with S (a), H (b), with S and H applied sequentially, and BC (c).	47
Figure 7. Total surface energy, dispersive and polar components, determined with the Wu method, using the initial contact angles of water, PEG 200 and glycerol.....	48
Figure 8. Water vapor permeability and mass per unit area.....	49
Figure 9. Static water absorption.	50
Figure 10. ATR-FT-IR spectra of BC and BC composites.....	58
Figure 11. SEM images of BC and BC composites.....	60
Figure 12. Contact angle of BC and BC composites.....	61
Figure 13. Water vapor permeability of BC and BC composites.....	62
Figure 14. Stress-strain averaged curves of BC and BC composites obtained up to the rupture point.....	63
Figure 15. Optical micrographs (100× magnification) of freshly prepared AESO emulsions with different HLB and after 10 min of emulsification: (a) HLB 5.20, (c) HLB 7.00, (d) HLB 9.00, and (e) HLB 11.33; and visual appearance of AESO emulsions at different times of emulsification after 10 days storage: (b) HLB 5.20 and (f) HLB 11.33.	75
Figure 16. CryoSEM images: (a) BC membrane, (b) after exhaustion with AESO emulsion for 9 days at 40 °C (Sample 1), (c) after exhaustion with AESO emulsion for 9 days at 40 °C + 3 h at 90 °C (Sample 2); and (d) SEM image of the Sample 1 after drying at 40 °C.....	76
Figure 17. SEM images of BC and BC composites: surface and cross-section images, (a,e) BC; (b,f) BC/AESO; (c,g) BC/AESO/PEG/S; (d,h) BC/AESO/PEG/H; and cross-section images (i) BC/AESO/PEG, (j) BC/AESO/S, (k) BC/AESO/H, and (l) BC/AESO/PEG/S/H. Magnification: 15,000× (scale: 5 μm) (a) and 10,000× (scale: 10 μm) (b–l).	77
Figure 18. FT-IR spectra of BC and the composites.	80
Figure 19. Water contact angle over time.	81
Figure 20. Static water contact angle and surface free energy.....	82
Figure 21. (a) DSC thermograms and (b) TGA curves of weight percentage of dried BC and BC composites...	84
Figure 22. Stress strain curves of dried BC and BC composites.	86
Figure 23. TGA curves (solid lines) and respective derivative (dashed lines) of BC and BC composites.	96
Figure 24. Evolution of the storage modulus (E') versus temperature at 1 Hz for BC (inserted graph) and BC composites as obtained by dynamic mechanical analysis.....	97
Figure 25. Antibacterial activity of the BC composites surface-functionalized with benzalkonium chloride-based product against Escherichia coli and Staphylococcus aureus.	98

Figure 26. Photos of the dyed BC composites. Letters (a–i) correspond to the experimental conditions described in Section 6.3.3.2. Simultaneous dyeing and production of the BC-based composites (a–f) and dyeing of dry composites (g–i).....99

Table index

Table 1. Properties of leather.....	7
Table 2. Advantages and disadvantages of synthetic leathers.	10
Table 3. Advantages and disadvantages of natural, synthetic, and vegetable leather.	11
Table 4. Examples of commercial alternatives to leather obtained from sustainable natural resources.....	14
Table 5. Examples of alternatives to leather obtained by biofabrication.	16
Table 6. Properties of bacterial cellulose	19
Table 7. Examples of BC potential applications.	21
Table 8. Summary table on the exploitation of BC for the fashion industry.	24
Table 9. Coating of fibers, yarns, and fabrics with BC nanofibers.	26
Table 10. BC macrofibers.	28
Table 11. Improvement of BC properties for textile applications.	29
Table 12. BC purification, bleaching, and dyeing.....	31
Table 13. Characteristics of the finishing polymers used. ^a	37
Table 14. Mass per unit area and percentage of polymers in brackets.....	42
Table 15. Average contact angle values (°) measured for drops of water, PEG 200 and glycerol.....	46
Table 16. Thickness, Young's modulus, tensile strength, and elongation at break.....	51
Table 17. Formulations used in the production of BC composites.	55
Table 18. Thickness, mass per unit area and polymers content of BC composites.....	57
Table 19. Combinations of surfactants used to study the effect of HLB on the AESO emulsion stability.	70
Table 20. Proportions of the polymers in the aqueous mixture used in the production of BC composites.....	71
Table 21. Thickness, mass per unit area and polymer content of the composites.	78
Table 22. Thermal degradation data obtained from DSC, TGA and DTG curves of dried BC and BC composites.	84
Table 23. Tensile strength and elongation at break of dried BC and BC composites.....	86
Table 24. Proportions of each component in the mixtures used in the production of BC composites.	91
Table 25. Conditions used in the antimicrobial finishing of BC composites.	92
Table 26. Properties of the BC and BC composites.....	95

To Professor Pedro Souto

*“Prometo-te que estarei
em tudo aquilo que te ensinei e
que aprenderás por ti.”*

Chapter 1

Introduction

1.1. Preamble

In recent years, one of the problems the world has been facing concerns climate change, caused primarily by greenhouse gas emissions. In 2015, the United Nations announced 17 Sustainable Development Goals, challenging organizations to work in ways that improve human life and planet quality. Two of these goals rely on the availability and sustainable management of water and sanitation for all and ensure sustainable consumption and production patterns. These goals can be achieved namely by reducing pollution and minimizing the release of hazardous chemicals and materials, and through efficient management of the planet's natural resources (United Nations, 2015).

The leather industry sector presents a production chain of high economic and social value. Worldwide, per year, more than 20 billion square feet of leather and 4.5 billion pairs of upper leather shoes are produced. The market value of hides, skins, leather, and leather footwear is more than 82 billion USD (FAO, 2015). However, leather processing has a high environmental and human impact, with large amounts of chemicals and water being used. In the whole process, for each ton of raw skin, about 500 kg of chemicals are added (Black *et al.*, 2013), and 30,000 to 50,000 L of water are consumed (Sathish *et al.*, 2016). Worldwide, the leather industry generates per year 548 billion L of wastewater (Sathish *et al.*, 2016) and 600,000 tons of solid waste classified as dangerous (Bizzi *et al.*, 2020). In addition, the livestock sector, from which animals' skins are obtained to produce leather, consumes a large amount of natural resources, contributing to 14.5% of the global greenhouse gas emissions. The majority of these emissions comes from the feed production stage, followed by deforestation due to the expansion of pasturelands and croplands for livestock production (Rojas-Downing *et al.*, 2017).

For decades, the development of leather analogues has been pursued by the scientific community and leather industry. This effort led to the appearance of various materials, some synthetic, other naturals.

Despite the increasing interest and market pull, the market penetration of these alternative products has been relatively modest.

This research intends to develop an ecological alternative to leather by the production of composites from bacterial cellulose (BC) and different polymers, in particular activated vegetable oils, contributing to the reduction of the animal hide dependency, and thus, to a more environmentally sustainable approach towards making available, to a wide and important market, a natural-based raw material for leather applications.

BC is a biopolymer produced by bacteria fermentation in the form of a gelatinous film that consists of a porous 3D structure of pure cellulose nanofibers with excellent mechanical properties and high specific surface area (Wu *et al.*, 2016). Nevertheless, the hydrophilic nature of BC and the loss of flexibility and porosity upon drying due to the collapse of the 3D network has limited its application in the textile and footwear industry. Surface functionalization strategies have been usually used to modify the surface properties of cellulosic materials, to improve its compatibility with hydrophobic matrices, often being detrimental to the mechanical and physico-chemical properties of BC (Hu *et al.*, 2011; K.-Y. Lee *et al.*, 2011; Frone *et al.*, 2018). The alternative and new strategy here proposed uses BC as structuring material, capable of housing emulsified hydrophobic polymers as flexibilizing and hydrophobizing agents, as a simple approach to overcome these constraints (Figure 1). In this approach, impregnation of the BC was achieved by an exhaustion process, a method widely used in textile dyeing.

The work here done was framed within the Portuguese project BUILD – Bacterial Cellulose Leather, supported by the program COMPETE 2020. This project involved the Centre of Biological Engineering (CEB/UM) and the Centre for Textile Science and Technology (2C2T/UM) from University of Minho, Satisfibre, S.A., a spinoff from CEB/UM, KYAIA - Fortunato O. Frederico & C^a Lda, a major Portuguese shoe manufacturer company and the Technological Center for Footwear in Portugal (CTCP).

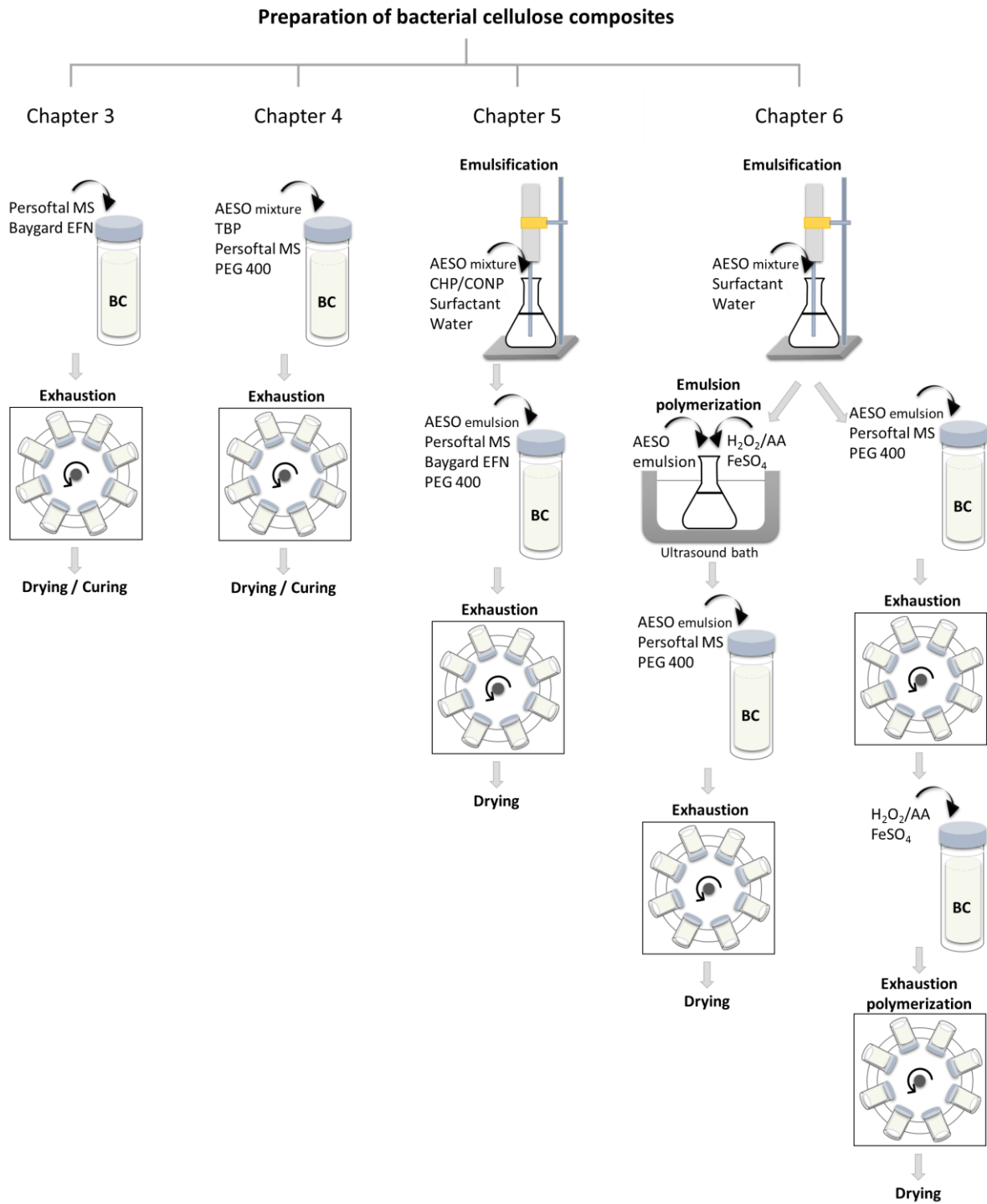


Figure 1. Schematic representation of the strategies here taken towards the preparation of BC composites.

1.2. Structure of the thesis

This thesis is organized in the following chapters (Figure 1):

Chapter 1. Introduction

This chapter presents the purpose of the research and the thesis outline.

Chapter 2. Literature overview

This chapter includes a comprehensive overview of the leather industry and its impact on the environment, the existing synthetic alternatives to leather, and the efforts made more recently in the development of ecological alternatives. Additionally, the bacterial cellulose properties and applications are reported, and its potential for the textile and footwear industries, including the scientific studies, are reviewed. Finally, efforts towards the development of composites based on modified soybean oil are also summarized.

Chapter 3. Development of BC/PDMS/PFC composites

In this chapter, a novel approach is tested for the bulk and surface modification of bacterial cellulose. Malleable, breathable, and water impermeable BC-based nanocomposites were developed by impregnating BC membranes with two commercial hydrophobic polymers used in textile finishing, Persoftal MS (polydimethylsiloxane (PDMS)) and Baygard EFN (perfluorocarbon (PFC)), by an exhaustion process. The properties of the obtained bio-based composites were characterized.

The work here done resulted in the following publication:

Fernandes, M., Gama, M., Dourado, F. and Souto, A. P. (2019) "Development of novel bacterial cellulose composites for the textile and shoe industry," *Microbial Biotechnology*, 12(4), pp. 650–661.

Chapter 4. Development of BC/PDMS/PEG/AESO composites

In chapter 4, in order to yield a high bio-based content composite with hydrophobic character, the acrylated epoxidized soybean oil (AESO) resin was incorporated into the bulk of BC membranes, in a mixture containing also the PDMS-based polymer and polyethyleneglycol (PEG) 400, as a plasticizer, allowing to obtain a product with greater elasticity, as well as, contributing to improve the interfacial adhesion between the BC and the other polymers. The properties of the obtained bio-based composites were characterized.

The work here done resulted in the following publication:

Silva, F. A. G. S., Fernandes, M., Souto, A. P., Ferreira, C., Dourado, F. and Gama, M. (2019) “Optimization of bacterial nanocellulose fermentation using recycled paper sludge and development of novel composites,” *Applied Microbiology and Biotechnology*, 103(22), pp. 9143–9154.

Chapter 5. Development of BC/emulsified AESO composites

In this chapter, bio-based composites comprising bacterial cellulose and acrylated epoxidized soybean oil previously emulsified were developed. In the first part, the optimum conditions for the emulsification of AESO were studied. The required hydrophilic–lipophilic balance (HLB) and the AESO emulsion stability were evaluated. Then, a stable AESO emulsion was used to develop BC-based composites. PEG, PDMS- and PFC-based polymers were also added to the emulsion, with the mixtures being diffused into the BC 3D nanofibrillar matrix by an exhaustion process. The properties of the obtained bio-based composites were characterized.

The work here done resulted in the following publication:

Fernandes, M., Souto, A. P., Gama, M. and Dourado, F. (2019) “Bacterial cellulose and emulsified AESO biocomposites as an ecological alternative to leather,” *Nanomaterials*, 9(12), pp. 1710–1727.

Chapter 6. Development of BC-based composites polymerized with H₂O₂/AA, finishing and dyeing

In this chapter, the polymerization of the AESO emulsion using an ecological redox system, peroxide hydrogen and L-ascorbic acid, before exhaustion process, were tested. Also, the finishing with a biocide and the dyeing of the BC-based composites were tested. The properties of the obtained bio-based composites were characterized.

The work here done resulted in the following publication:

Fernandes, M., Souto, A. P., Dourado, F. and Gama, M. (2021) “Application of bacterial cellulose in the textile and shoe industry: Development of biocomposites,” *Polysaccharides*, 2(3), pp. 566–581.

Chapter 7. Conclusions and suggestions for future work

This chapter presents the major conclusions of the thesis and future perspectives for this research work.

Chapter 2

Literature overview

2.1. The leather industry and its environmental impact

The world production of leather is approximately 20 billion square feet per year and are produced about 4.5 billion pairs of leather shoes (FAO, 2015). With a 50% share in the EU, footwear, in general, remains the dominant sector for finished leather. Also in the EU, the garment industry occupies approximately 20%, furniture and car upholstery represent 17%, and the leather goods sector 13% (Black *et al.*, 2013).

As a high-value noble material, leather has a unique structure that offers advantageous properties such as mechanical strength, flexibility, and breathability. The leather-making operation involves a sequence of complex chemical and mechanical processes, necessary to transform the animals' skins, a byproduct of meat industry, into a functional material. The different processing steps can be divided into the main sets of operations: beamhouse, tanning, post-tanning, and finishing. In the first phase, different processes are carried out to restore moisture, remove tissue and fat, and give flexibility. The tanning process consists of stabilizing the collagen fibers. In the post-tanning operations, touch properties, softness, and uniformity are improved by filling the weaker areas, and in the final step, leather is finished to enhance its appearance (Black *et al.*, 2013; Laurenti *et al.*, 2016). Tanning is the most important operation which provides permanent stability to the material. It can be done with vegetable or mineral tanning agents, but chromium agent is the most used because it offers superior softness, high thermal and water stability and it is less time-consuming (Dixit *et al.*, 2015).

Structurally, leather is characterized by a three-dimensional network of bundles of collagen fibers (about 80 μm in diameter), composed of fibers (1–4 μm), which in turn are composed of microfibrils (0.08–0.10 μm). Each microfibril consists of several protofibrils (about 1.5 μm), formed by bundles of polypeptide chains (Hiokki, 2014). Collagen fibrils have inherent strength and their arrangement is crucial in physical properties, such as strength, smoothness, and aesthetic properties. The hierarchical structure

is complex with different layers, the grain on the outer surface, and the corium beneath. The corium presents more collagen, highly oriented and compacted, which offers most of the strength to leather (Basil-Jones *et al.*, 2010). The capillaries among collagen fibers together with the hydrophilic groups on the collagen chains make leather permeable to water vapor (Ugbaja *et al.*, 2016). Table 1 presents some properties of leather. Regarding the alternative products mentioned in the next sections, no data on their properties was found.

Table 1. Properties of leather

Property		References
Fiber diameter	about 80 μm	(Hiokki, 2014)
Static water absorption	147.5–240 $\text{mL}\cdot 100\text{g}^{-1}\cdot 24\text{ h}^{-1}$ 249.57 / 307.19 $\text{mL}\cdot 100\text{ g}^{-1}$ (chrome, vegetable)	(Kılıç <i>et al.</i> , 2017) (Zengin <i>et al.</i> , 2016)
Dynamic water absorption	103.31–136.31% (24 h) 52.06 / 99.61% (chrome, vegetable)	(Nasr, 2017) (Zengin <i>et al.</i> , 2016)
Water vapor permeability	2.6 $\text{mg}\cdot\text{cm}^{-2}\cdot\text{h}^{-1}$ 1.41–5.43 $\text{mg}\cdot\text{cm}^{-2}\cdot\text{h}^{-1}$ 18.71–114.34 / 330.54–337.82 $\text{mg}\cdot\text{cm}^{-2}\cdot\text{h}^{-1}$ (finished, unfinished) 23.7–42 $\text{g}\cdot\text{m}^{-2}\cdot\text{h}^{-1}$ (coated, uncoated)	(Tamilselvi <i>et al.</i> , 2019) (Nasr, 2017) (Ugbaja <i>et al.</i> , 2016) (Gulbinieni, Jankauskaite and Arcilauskaite, 2003)
Water vapor sorption	33–79 $\text{g}\cdot\text{m}^{-2}$	(Gulbinieni, Jankauskaite and Arcilauskaite, 2003)
Tensile strength	33.0–34.3 $\text{N}\cdot\text{mm}^{-2}$ 13.07–22.53 $\text{N}\cdot\text{mm}^{-1}$ 276.02–329.29 $\text{kg}\cdot\text{cm}^{-2}$ 18–26 $\text{N}\cdot\text{mm}^{-2}$ 6.6–10.9 $\text{N}\cdot\text{mm}^{-2}$	(Tamilselvi <i>et al.</i> , 2019) (Kılıç <i>et al.</i> , 2017) (Nasr, 2017) (Sureshkumar <i>et al.</i> , 2012) (Sudha <i>et al.</i> , 2009)
Elongation	38.8–41.2% 56.07–84.63% 48.19–68.36% 38–42% 58%	(Tamilselvi <i>et al.</i> , 2019) (Kılıç <i>et al.</i> , 2017) (Nasr, 2017) (Sureshkumar <i>et al.</i> , 2012) (Sudha <i>et al.</i> , 2009)
Tear strength	50.3–52.7 $\text{N}\cdot\text{mm}^{-1}$ 80.55–114.4 $\text{N}\cdot\text{mm}^{-1}$ 69.23–86.94 $\text{kg}\cdot\text{cm}^{-1}$ 56–60 $\text{N}\cdot\text{mm}^{-1}$	(Tamilselvi <i>et al.</i> , 2019) (Kılıç <i>et al.</i> , 2017) (Nasr, 2017) (Sureshkumar <i>et al.</i> , 2012)
Stitch tear strength (double hole)	167.09–208.58 $\text{N}\cdot\text{mm}^{-1}$ 37.9–52.9 $\text{N}\cdot\text{mm}^{-1}$	(Kılıç <i>et al.</i> , 2017) (Sudha <i>et al.</i> , 2009)

Despite its global use through mankind history and its economic value, the leather industry is considered one of the most polluting industries (Yorgancioglu, Başaran and Sancakli, 2020). Consequently, leather production is accompanied by several challenges associated to the high environmental impact and increasing consumer demand for eco-friendly products, as well as increasing regulatory constrains towards the reduction of the environmental impact. Nowadays, consumers are becoming more aware of

the ecological problems and activist campaigns for environmental, animal welfare and human health risk issues are being targeted in the tanning industry (Klerk, Kearns and Redwood, 2019).

Worldwide, more than 90% of the tanneries use chromium compounds (Fontaine *et al.*, 2019). While the tanning process uses trivalent chromium (Cr(III)), which can cause allergies only in extensive amounts, it can be oxidized into the hexavalent form (Cr(VI)), a very strong oxidant with mutagenic, teratogenic, and carcinogenic effects on living organisms (Wiśniewska *et al.*, 2019). The poor absorption of chromium during the tanning process (50 to 70%) results in a waste of material and creates ecological imbalances. The post-tanning process also results in significant changes in the concentration of total dissolved solids (TDS), chemical oxygen deficiency (COD), and pollution with heavy metals (Dixit *et al.*, 2015).

This industry consumes large quantities of water and chemicals and generates a large amount of wastes (Yorgancioglu, Başaran and Sancakli, 2020). In the whole process, for each ton of raw skin, about 500 kg of chemicals are added (Black *et al.*, 2013), and 30000 to 50000 L of water are consumed (Sathish *et al.*, 2016). Most of these chemicals are discharged without treatment into rivers, leaving a large amount of pollution (Kanagaraj *et al.*, 2015). Per ton of processed skin, 150 kg of leather are produced and the remaining 850 kg contribute to solid waste, of which 450 kg are collagen waste and 400 kg other animal waste with 30 m³ of effluent (Kanagaraj *et al.*, 2015). Worldwide, the industry generates 548 billion L of wastewater per year (Sathish *et al.*, 2016). The wastewater (untreated) is characterized by a high chemical and biochemical oxygen deficiency, and a high salt and chemical content (Black *et al.*, 2013). Solid waste consists of organic matter, such as protein and fat, and chemicals (Black *et al.*, 2013). Most of this waste results from shaving and trimming steps where 40–50% of the tanned leather are lost, generating, worldwide and per year, about 600,000 tons of solid waste classified as dangerous (Bizzi *et al.*, 2020). A large amount of sludge generated in this industry makes the solid waste treatment system highly inactive due to the non-biodegradability of the tanned leather. Also, leather has a slow biodegradability and the treatment with different chemicals during the tanning process makes it resistant to chemical, thermal, and microbiological degradation. This, in turn, affects agricultural activities and degrades the groundwater system. These residues are also a threat to the ecology and the aquatic system in the vicinity of the tanneries, particularly from accidental releases of chemicals and process residues. Air emissions can also be toxic and contain substances such as sulfides, ammonia, organic solvents, particles in the emission of gases from the energy supply, and other incineration processes, representing a threat to the atmosphere (Black *et al.*, 2013; Dixit *et al.*, 2015). Natural leather has an energy consumption associated with the manufacturing process of around 24,600–27,000 kcal·kg⁻¹ of leather, which corresponds to a carbon footprint in CO₂ of 4.1–4.5 kg CO₂·kg⁻¹ of leather (Wool, 2013).

2.2. Synthetic alternatives to leather

The development of alternatives to leather has long been pursued, leading to the appearance of various synthetic materials. These commercial products comprise essentially three main product categories: compact coated fabrics, poromerics, and microfibrinous (Table 2).

Compact coated fabrics synthetic leathers are obtained by depositing (coating) or transferring a polymer onto a structuring substrate consisting of a textile. These emerged in the 1950s with the development of synthetic leather obtained from poly (vinyl chloride) (PVC), with the launch of products such as Naugahyde (U.S. Rubber Company). Although having a pleasant appearance, are easy to clean, are scratch resistant, and are inexpensive, these first generation of PVC products was rigid, heavy, with a cold touch, and impermeable to water vapor, allowing human sweat to accumulate at the interface between the coating and the fabric, causing delamination of the composite. In general, these materials can be used, rather than natural leather, in applications such as upholstery, based on its price and quality (Hole and Whittaker, 1971; Wool, 2013; Schenk, 2014).

Poromeric synthetic leathers emerged in the 1960s as an alternative to those coated with PVC or polyurethane (PU). By this time, the term “coagulation” emerged in the textile and coating market. (Hemmrich, Fikkert and Berg, 1993). This typology of synthetic leathers is achieved mainly by impregnating a textile base with PU solutions or dispersions containing organic solvents, followed by a heat treatment step, where temperature cycles are used. The successive cooling, through several baths that comprise mixtures of dimethylformamide and water with decreasing concentration of dimethylformamide, induces the contraction of the polymer, compacting the entire matrix of the composite. The composite is then coated superficially with a new hygroscopic polymeric layer. When submerged in water, this outer layer coagulates, creating porous structures. The structure of the porous surface layer and the method of processing it largely determines its sensory values, which include tactile sensation and appearance, as well as characteristics such as moisture transfer, surface resistance, flexural strength, and water resistance. The disadvantage of these processes is that they produce large amounts of waste that contain organic solvents (Schenk, 2014; Züribig, Kruse and Buchkremer, 2015). The development of these microporous materials made it possible to overcome the lack of breathability, to the detriment of mechanical properties. However, although the microporous coating resembles the grain layer of the leather, the textile structure base does not show a smooth transition from thicker to thinner fibers. The intermediate layer between the textile structure and the microporous coating acts as

a support for greater tensile strength and tear resistance, but also leads to lower elongation at break (Hole and Whittaker, 1971).

The latest class of leather analogues includes bicomponent fibers. This newer class of synthetic leather, where Clarino™ and Lorica® are also included, appeared in the 70s and 80s, and, like the previous ones, are produced by the coagulation method, the main difference between these products is in the substrate they use (Schenk, 2014). These analogues consist of fully synthetic nonwovens obtained by co-extruding microfibers from two immiscible polymers. After extrusion of the microfibers, they are cross-linked and the polymeric matrix is removed by extraction with organic solvents, leaving aggregates of microfibers (Kuraray, 2018).

Table 2. Advantages and disadvantages of synthetic leathers.

Synthetic leather	Advantages	Disadvantages
Compact coated fabrics, 1950's Fabric coated with PVC or PU	<ul style="list-style-type: none"> • Good appearance • Easy to clean • Cheap 	<ul style="list-style-type: none"> • Rigid and heavy • Cold touch • Impermeable to water vapor • Delaminate easily
Poromerics, 1960's Fabric coated with coagulated PU	<ul style="list-style-type: none"> • Pleasant touch and appearance • Porous structure • Breathable • Resistant to bending and delamination 	<ul style="list-style-type: none"> • Highly polluting process
Microfibrous, 1970's Microfibers	<ul style="list-style-type: none"> • Soft • Flexible • Impermeable • Breathable 	<ul style="list-style-type: none"> • 100% synthetic

Regarding the environmental impact, PVC synthetic leather presents energy consumption, carbon footprint, and water consumption in the range of 6,600–28,200 kcal·kg⁻¹, 3.4–4 kg CO₂·kg⁻¹, and 19–57.5 L·kg⁻¹, respectively. The thermal degradation of these polymers may contribute to the release of toxic compounds to the environment such as dioxins (polychlorinated organic compounds with known adverse effects on human and animal health). In the case of PU, except for water, energy consumption is higher than that of natural leather, 27.660–30.600 kcal·kg⁻¹ and 24,600–27,000 kcal·kg⁻¹, PU and leather, respectively, leaving a carbon footprint of 5–5.6 kg CO₂·kg⁻¹ and 170–510 L water·kg⁻¹, with no possibility of recycling this water. In this comparison, polyamides are currently the best alternatives to the manufacture of synthetics, not due to their energy (32,400–36,000 kcal·kg⁻¹), environmental (6.7–10 kg CO₂·kg⁻¹), and water (138–414 L·kg⁻¹) consumptions, but because they use less polluting processes (Wool, 2013).

2.3. Eco-friendly alternatives to leather

With the consumers becoming more aware and concerned about environmental protection, the search for leather substitutes derived from renewable resources has increased. Table 3 presents the main advantages and disadvantages of leather, synthetic ‘leather’, and the most recent alternatives to leather, vegetable ‘leather’.

Table 3. Advantages and disadvantages of natural, synthetic, and vegetable leather.

	Natural leather	Synthetic ‘leather’	Vegetable ‘leather’
Advantages	<ul style="list-style-type: none"> • Based on renewable resources • Upcycles waste • Attractive properties, such as mechanical strength, breathability, flexibility, softness, and durability 	<ul style="list-style-type: none"> • Animal-free • Resembles real leather • Versatility in shape and size 	<ul style="list-style-type: none"> • Animal-free • Based on renewable resources • Upcycles waste • Biodegradable • Versatility in shape and size
Disadvantages	<ul style="list-style-type: none"> • Based on animal hides and skins • Limited in shape and size • Imperfections • High water and chemicals consumptions and generates large amounts of wastes (wastewater, solid waste, and atmospheric emissions) • Uses chromium compounds • High environmental and human impact • Slow biodegradability • High costs associated with animal farming and with the tanning process 	<ul style="list-style-type: none"> • Based on petroleum • Not renewable • Not biodegradable 	<ul style="list-style-type: none"> • Coated with synthetic polymers to achieve a leather-like appearance* • Lack of homogeneity and strength* • Limited production capacity*

* depending on the type of vegetable ‘leather’

2.3.1. Alternatives to leather obtained from sustainable natural resources

Contrarily to natural leather and synthetic analogues, these leather alternatives that have emerged more recently (2000-2020) derive from abundant sustainable materials and are animal-free. In general, they are produced by non-toxic processes and are biodegradable, while having acceptable durability for use in articles that are normally made from natural leather. These materials also have greater versatility in terms of shape and size, which is limited in the case of leather obtained from animal hides and skins. Examples of these materials include vegetable sources (cork, wood, pineapple plant and areca palm leaves, cactus),

fungi (mushrooms), using by-products (grape marc, coffee grounds, discarded fruit), or developed through biofabrication (collagen, mycelium, and bacterial cellulose) (Table 4).

Cork is a material that has made a great contribution to the development of alternatives to leather. It is a natural and sustainable material with a closed-cell structure that gives it unique properties such as versatility, lightness, elasticity, flexibility, resistance to compression, impermeability to gases and liquids, good electrical, thermal and acoustic insulation, high friction coefficient, high resistance to abrasion, anti-static, hypoallergenic, non-toxicity and biodegradability, ideal for numerous applications, such as for the production of leather analogues (cork skin) (Silva *et al.*, 2005; Gil, 2015; Gonçalves *et al.*, 2015). For the production of 'cork skin', natural cork or agglomerated blocks are first laminated in very thin layers, then they are impregnated by melting with a polymeric material and, finally, they are compressed under heat and pressure (Duarte and Bordado, 2015). To obtain better mechanical properties, another support/reinforcement layer (textile, plastic material) is added. This product may contain another layer of finishes (varnishes, resins, paints) (Sá, 2011).

Nuo (formerly Ligneah) is another vegan and sustainable material made of real wood. It consists of a thin wood veneer bonded with an environmentally friendly backing material (cotton) through a low environmental impact adhesive, to provide strength and ensure its processing. The wood surface is micro-laser etched in a fine texture of different geometric patterns. This material is flexible, it can be bent in all directions and is very soft (Schorn & Groh, 2020).

Piñatex, a product developed by Ananas Anam, is obtained from fibers from the leaves of the pineapple plant and marketed as an alternative to leather (Ananas-anam, 2017). According to the patent of this leather analogue, the product consists of a non-woven structure. For its production, initially, the fibers of the pineapple leaves are extracted after cutting the fruit of the plant, cleaned and cut, and then mixed with up to 20% of a fusible polymer (polyester) that will work as a binder. After the production of the nonwoven, it is mechanically needle bonded, followed by a heat treatment to melt the added polymer. Afterwards, another polymer can be laminated to one or both sides of the nonwoven. Finally, commercial finishes used in leather finishing are applied (Hijosa *et al.*, 2013).

Designer Tjeerd Veenhoven created Palmetti, a handmade product produced by impregnating leaves of the Areca palm (*Chrysalidocarpus lutescens*) with natural oil. In addition to the ecological benefits of offering a 100% biodegradable and vegan alternative to animal leather, this product also helps financially a poor community of artisans in India, where the designer started a social activity (Palmleather, 2017).

MuSkin is a material created by the Italian company GradoZero Espace and produced from mushrooms of the species *Phellinus ellipsoideus*. It is presented as a vegan alternative to animal leather and 100% biodegradable. After extraction, the material is treated using only natural products, such as waxes, which give it special characteristics. This vegetable leather has a soft touch, like suede, and consistency and texture like cork. It has good thermal properties, moisture transfer, water repellency, and is non-toxic. However, it has several limitations, namely in terms of the inhomogeneity of the surface (visible defects), mechanical properties, and limited size and productive capacity (50 m²·month⁻¹) (Life Materials, 2017; Riccio, 2017).

Recently, a new ecological material called Desserto has emerged. This vegan leather was developed by two Mexican innovators, Adrián López and Marte Cázarez, and they use nopal cactus as raw material. The production process consists of harvesting the mature leaves every 6-8 months from organically grown cactus plants; after cutting they are cleaned, mashed, and then sun dried for three days until achieving the desired humidity. The organic raw material is then processed to make it part of their patented formula and can be also dyed naturally. All the process has an average duration of 3–4 weeks. Their production capacity is 500,000 linear meters a month and they have, so far, created car seats, shoes, handbags, and even apparel. This vegan leather is eco-friendly, animal cruelty-free, and lasts up to 10 years (Fibre2Fashion, 2020; Stewart, 2020).

The Designer Don Kwaning created a leather-like material made from linoleum, a material produced from plant-based oils and resins combined with minerals or fine powders and commonly used as flooring. They can obtain a double-sided material more flexible and stronger by introducing a textile layer in the center and pressing it with two out-layers of a mixture of linseed oil and jute. This material, called Lino, can be used as a vegetal alternative to leather in furniture design and upholstery (Live kindly, 2018; Rixtel, 2019).

With the world running out of raw materials, the use of wastes to create innovative materials can contribute to making a change. Vegea is a product of biological and vegan origin developed in 2016 in Italy and which has aroused interest. The material consists of a fabric coated with lignocellulose and oils present in the by-products of vinification, grape marc. With the development of these new eco-sustainable technical fabrics from vegetable raw materials, the company intends to create an alternative to the use of non-renewable fossil sources, implementing new models of circular agriculture and economy (Vegea, 2017). Alice Genberg created a leather-like material from coffee grounds waste. The process consists of collecting the coffee waste from cafés, and after rinsing and drying the material is ground to obtain a fine powder, then it is mixed with 100% natural binders and additives and pressed into a sheet (Genberg,

2019). Designer Uyen Tran has developed a leather alternative called Tômtex that is made from seafood shells and coffee grounds. After collecting seafood waste, chitin is extracted and mixed with coffee waste, and the mixture is placed in a mold and left to dry for two days (Hahn, 2020). The Italian company Frumat developed a vegan leather-like material called Apple Ten Lork that is made from apple cores and skins, a biological industrial waste product (Materials District, 2019). Fruit leather Rotterdam has also developed an eco-friendly process that converts leftover mangoes into a durable leather-like material that involves mashing, cooking, and drying (Fruit leather, 2020).

Table 4. Examples of commercial alternatives to leather obtained from sustainable natural resources.

Leather alternatives	Raw material	Producer / Creator
Cork skin	Cork	Pelcor
Nuo (formerly Ligneah)	Wood	Nuo Design (MyMantra)
Piñatex	Pineapple plant leaves	Ananas Anam
Palmetti	Areca palm leaves	Tjeerd Veenhoven
MuSkin	Mushrooms (<i>Phellinus ellipsoideus</i>)	GradoZero Espace
Desserto	Nopal cactus	Adrián López Velarde and Marte Cázarez
Lino leather	Linoleum (plant-based oils/resins), jute	Don Yaw Kwaning
Vegea	Grape marc	VEGEA srl
Coffee leather	Coffee grounds waste	Alice Genberg
Tômtex	Seafood shells and coffee grounds waste	Uyen Tran
Apple Ten Lork	Apples waste	Frumat
Fruit leather	Discarded fruit	Fruit leather Rotterdam

2.3.2. Alternatives to leather obtained by biofabrication

With the increasing search for more sustainable leather alternatives, some progress has been done focused on biofabrication processes. The metabolic processes of living organisms such yeast, fungi, and

bacteria produce yeast-derived collagen, fungal biomass, and bacterial cellulosic materials, respectively, which are being explored for the development of leather substitutes (Table 5).

Modern Meadow is a Brooklyn startup founded in 2011 that is developing a process for making leather without using animal skins. The process involves culturing collagen protein from animal cells, which is then structured in a material that replicates natural leather. For the transformation of raw synthetic leather into leather, collagen sheets are subjected to a simplified tanning process, which requires 80% less of the chemicals used in traditional tanning. Unlike traditional leather, with this technology, the shape and size can be adjusted, eliminating the waste resulting from the imperfections that exist in traditional leather and, in the future, it may be possible to improve the product's properties such as strength or flexibility. In 2017 they launched their first branded biofabricated leather material called Zoa™ (Leber, 2016; Hao, 2017; Modern Meadow, 2020).

The startup MycoWorks (San Francisco) was founded in 2013, and in 2015 they started producing a sustainable and versatile leather-like material made with mushrooms (mycelium). They called it Reishi™ and is described as soft, malleable, and waterproof material that in the future may replace leather and foams in shoes. This type of leather is made from pure mycelium, the key ingredient, in the form of microscopic threads formed at the base of the mushrooms. The company mainly uses *Ganoderma lucidum*, also known as the Reishi mushroom. In the production of this material, fungi are collected from nature, and pieces of mycelium are placed in bottles with discarded organic material (agricultural waste). After a few days, the fibers of the mycelium expand, forming a 3D structure of microscopic threads. The mycelium can be cultivated and manipulated in a multitude of textures and shapes, by changing the growth environment, developing differently according to the available nutrients, temperature, light, humidity, and gas in the environment. It is also possible to add other materials, such as oils, to obtain a product with different characteristics, more resistant or flexible, heavy or light. Despite the advantage that a piece the size of a bovine skin can be produced in a few weeks, the process takes place in a closed circuit (without waste) and with a variety of shapes and textures achievable. However, the material has not yet been tested for a series of important characteristics, such as biological decomposition or durability/use behavior (Peters, 2016; Robinson, 2016; Tu, 2016). The company Bolt Threads also started to produce a vegan alternative leather made from mushroom roots called Mylo™. The process consists of growing the mycelium cells on beds of renewable organic matter with controlled temperature and humidity, in order to make the mycelium grow upward and assemble into an organized interconnected 3D network. The mycelium mat is then harvested and processed, tanned and dyed, and

imprinted with the desired pattern. The resulted material has a leather-like look and is durable and abrasion-resistant (Bolt Threads, 2020).

Other alternatives to leather produced by biofabrication for application in the textile and footwear industries are that consisting of bacterial cellulose. Some of these examples are presented in Table 5 and are described later in section 2.4.3.

Table 5. Examples of alternatives to leather obtained by biofabrication.

Biofabricated leather	Materials used	Creator
Zoa™	Collagen	Modern Meadow
Reishi™	Mycelium (Reishi mushrooms)	MycoWorks
Mylo™	Mycelium	Bolt Threads
BioCouture project	Bacterial cellulose (kombucha-green tea)	Suzanne Lee
ScobyTec BNC	Bacterial cellulose (kombucha-black tea)	SCT Materials Corporation
Soya C(o)u(l)ture project	Bacterial cellulose (soya waste)	XXLab
Malai	Bacterial cellulose (coconut water)	Malai Design & Materials

2.4. Bacterial cellulose

Cellulose is an almost inexhaustible and sustainable natural polymeric raw material and, being an alternative to products derived from the petrochemical industry, it is considered as one of the most promising renewable resources for the growing investment in ecological and biocompatible products with a performance at the same or better level than conventional non-renewable materials (Klemm *et al.*, 2005; Wan *et al.*, 2009; Hu *et al.*, 2014; Tang *et al.*, 2015). It can be obtained from plants, some species of bacteria, algae, fungi, and tunicates (Klemm *et al.*, 2005; Mishra, Sabu and Tiwari, 2018).

Bacterial cellulose (BC) is a biopolymer produced by fermentation by bacteria such as the genus *Komagataeibacter*. Under static culture conditions, BC is produced as a gelatinous film that consists of a 3D structure of pure cellulose nanofibers. Despite having a chemical composition identical to that of vegetable cellulose, BC differs in terms of structure and mechanical properties, presenting several distinct advantages (Lee, Blaker and Bismarck, 2009; Wan *et al.*, 2009; Retegi *et al.*, 2012; Wu *et al.*, 2016).

2.4.1. Bacterial cellulose production and properties

BC is synthesized in a multi-step process involving individual enzymes, catalytic complexes, and regulatory proteins (Lee *et al.*, 2014). Figure 2 illustrates the bacterial cellulose biosynthesis process (Portela *et al.*, 2019; Zhong, 2020). In the first stage, the glucose in the medium is transported into the bacteria and the polymerization of the glucose molecules occurs between the outer membrane and the cell's cytoplasm, forming 1,4- β – glucosidic chains. Then, these chains are secreted through cellulose synthase complex (each cell has 50 to 80 pores along its axis) and 10-15 chains form a 1.5 nm wide protofibril. The organization and crystallization of the protofibrils through hydrogen bonds give rise to microfibrils with 2 to 4 nm in diameter and, finally, the microfibrils are grouped on an bundle with 20 to 100 nm in diameter, thus forming a cellulose film with a three-dimensional structure that composes BC (Iguchi, Yamanaka and Budhiono, 2000; Castro *et al.*, 2011; K.-Y. Lee *et al.*, 2014; Rajwade, Paknikar and Kumbhar, 2015).

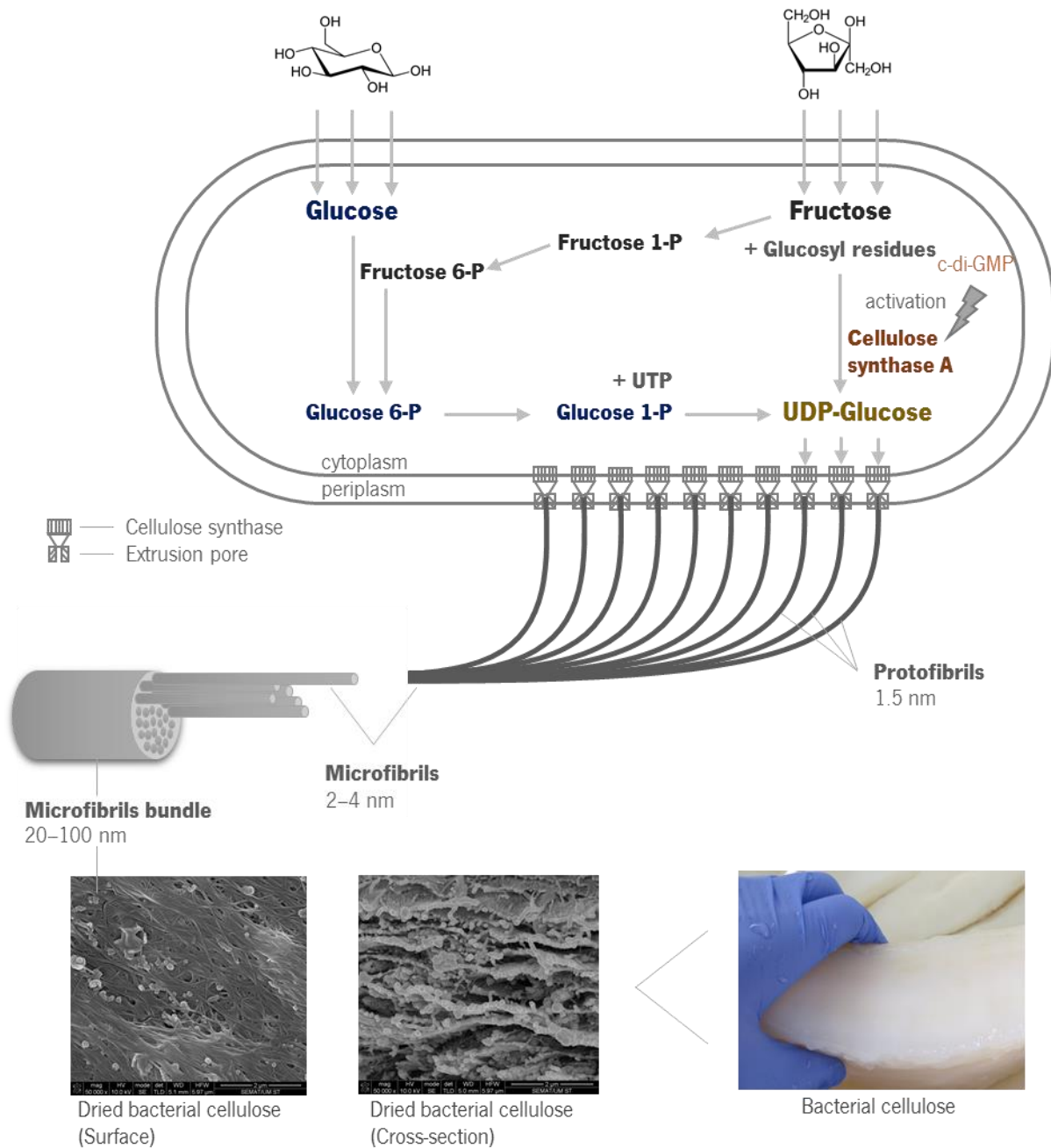


Figure 2. Schematic illustration of the biosynthesis of cellulose molecules and their assembly into nanofibers.

Under static culture, BC production takes place in the form of uniformly spaced layers parallel to the air/liquid interface. At the beginning of biosynthesis, the inoculum bacteria increase their population through the consumption of oxygen dissolved in the medium and, since they are aerobic, they accumulate at the air/liquid interface of the culture medium. During this time, they synthesize a certain amount of cellulose into the liquid phase, descending as the biosynthesis progresses. The new cells diffuse through the cellulose matrix synthesized to the air/liquid interface to start producing a new layer, and so on, until

the nutrients in the medium are exhausted (Budhiono *et al.*, 1999; Klemm *et al.*, 2011; Ruan *et al.*, 2016). Table 6 summarizes the properties of bacterial cellulose. (Lee, Blaker and Bismarck, 2009)

Table 6. Properties of bacterial cellulose

Properties		References
Degree of polymerization	up to 8000	(Wu <i>et al.</i> , 2016)
Crystallinity	60–90%.	(Klemm <i>et al.</i> , 2005)
Nanofibers' diameter	20–100 nm	(Wu <i>et al.</i> , 2016)
Nanofibers' length	1–9 μm	(Foresti, Vázquez and Boury, 2017)
Density	1.50 $\text{g}\cdot\text{cm}^{-3}$ 1.25 $\text{g}\cdot\text{cm}^{-3}$	(Hervy <i>et al.</i> , 2018) (Lee, Blaker and Bismarck, 2009)
Surface area	2.7–37 $\text{m}^2\cdot\text{g}^{-1}$	(Kim, Nishiyama and Kuga, 2002)
Water absorption	610.5% 320%	(Potivara and Phisalaphong, 2019) (Rathinamoorthy <i>et al.</i> , 2019)
Water vapor permeability	765.95–1045.55 $\text{g}\cdot\text{m}^{-2}\cdot 24 \text{ h}^{-1}$ $2.38\times 10^{-11} \text{ g}\cdot\text{m}^{-1}\cdot\text{s}^{-1}\cdot\text{Pa}^{-1}$ 151 $\text{g}\cdot\text{m}^{-2}\cdot 24 \text{ h}^{-1}$ $1.26\times 10^{-10} \text{ g}\cdot\text{m}^{-1} \text{ h}^{-1}\cdot\text{Pa}^{-1}$ $1-11\times 10^{-13} \text{ g}\cdot\text{m}^{-1}\cdot\text{s}^{-1}\cdot\text{Pa}^{-1}$	(Kamal, Misnon and Fadil, 2020) (Cazón, Velázquez and Vázquez, 2019) (Rathinamoorthy <i>et al.</i> , 2019) (Jebel and Almasi, 2016) (Tomé <i>et al.</i> , 2010)
Young's modulus	1044 MPa 5–17 GPa 93.8 MPa 138 GPa 114 GPa 15–35 GPa	(Cazón, Velázquez and Vázquez, 2019) (Potivara and Phisalaphong, 2019) (Jebel and Almasi, 2016) (Hu <i>et al.</i> , 2011) (Lee, Blaker and Bismarck, 2009) (Klemm <i>et al.</i> , 2005)
Tensile strength	20.8 MPa 70–300 MPa 26.3 MPa 2 GPa 200–300 MPa	(Cazón, Velázquez and Vázquez, 2019) (Potivara and Phisalaphong, 2019) (Jebel and Almasi, 2016) (Hu <i>et al.</i> , 2011) (Klemm <i>et al.</i> , 2005)
Elongation	2.3% 0.5%–5.0% 6.1% 1.5–2.0%	(Cazón, Velázquez and Vázquez, 2019) (Potivara and Phisalaphong, 2019) (Jebel and Almasi, 2016) (Klemm <i>et al.</i> , 2005)

The properties of cellulose produced by bacteria can be controlled by changing the conditions of the fermentation, such as the type of strain, the composition of the culture medium, and environmental factors, namely pH, temperature, dissolved oxygen content, and type of culture (static or with agitation) (K.-Y. Lee *et al.*, 2014; Douglass *et al.*, 2018). Its uniqueness is due, in the first place, to the fact that it is free of lignin, hemicellulose, and pectin, which are present in the cellulose of plants, and therefore there is no need for extra processing to remove them (Lee, Blaker and Bismarck, 2009; Wu *et al.*, 2016). At the microstructure level, BC presents a porous interconnected structure. The particular mechanical properties result from its randomly organized three-dimensional network of interconnected nanofibers,

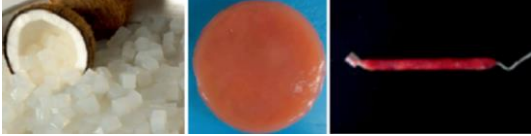

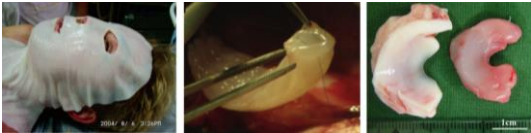
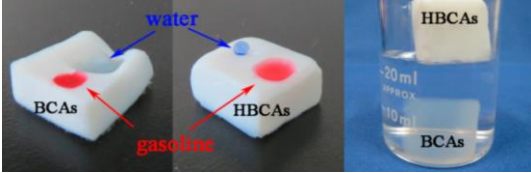


with a diameter of 20-100 nm and a few micrometers in length, resulting in a high specific surface area (Tang *et al.*, 2015; Wu *et al.*, 2016), properties which are very advantageous for the production of composite materials (Lee, Blaker and Bismarck, 2009). These nanofibers can be oriented uniaxially by the application of tension during drying (K.-Y. Lee *et al.*, 2014). Regarding physical properties, BC exhibits high crystallinity, which, coupled with its' 3D nanofibrillar architecture, results in a high Young's modulus. It also has a high degree of polymerization, high water holding capacity, and high moldability *in situ* (during fermentation) and *ex situ* (after fermentation) (Lee, Blaker and Bismarck, 2009; Wu *et al.*, 2016).

2.4.2. General applications of bacterial cellulose

The unique properties of BC compared to vegetable cellulose have supported the development of several applications in different areas, such as food, paper, biomedical, aerogel, electronic devices, and textile and footwear industries (Table 7).

Despite this wide range of possible applications of BC, only a few products reached commercialization, particularly in the food, biomedical and cosmetic areas (Jang *et al.*, 2017). BC's main commercialization exists in the form of *nata de coco*, a gelatinous product resulting from the fermentation of coconut water that is preserved in syrup and often served with fruit, drinks, creams, or ice cream. Pure cellulose can also be safely processed in various foods, acting as a thickener, stabilizer, gelling agent, or low-calorie substitute (Dourado *et al.*, 2016; Jang *et al.*, 2017; Gama and Dourado, 2018). In relation to electronic products, high-fidelity loudspeakers, and headphones with acoustic diaphragms from BC are marketed by Sony Corporation (Iguchi, Yamanaka and Budhiono, 2000). However, the biomedical area is the one that has received more attention, with several medical products already commercialized, with the treatment of burns and skin wounds being the main application of BC membranes (Ludwicka *et al.*, 2016). In terms of cosmetics, BC facial masks are widely known in Asian markets (Jang *et al.*, 2017).

Table 7. Examples of BC potential applications.

Sector	Applications	
Food	<ul style="list-style-type: none"> • Food: <i>nata de coco</i>, artificial meat (Dourado <i>et al.</i>, 2016) • Additive: thickener, stabilizer, gelling agent, emulsifier, bonding agent (Jozala <i>et al.</i>, 2016) • Food packaging: sausage casings (Padrão <i>et al.</i>, 2016) 	 <p>(Dourado <i>et al.</i>, 2016)</p>
Paper	<ul style="list-style-type: none"> • Packaging (Pradipasena, Chollakup and Tantratian, 2018) • Paper restoration (Santos <i>et al.</i>, 2016) • Ultra-filtration membranes (Mautner <i>et al.</i>, 2015) 	 <p>(Santos <i>et al.</i>, 2016)</p>
Biomedical	<ul style="list-style-type: none"> • Wound care (Czaja <i>et al.</i>, 2007) • Tissue engineering: blood vessels (Schermer <i>et al.</i>, 2014), meniscus implant (Bodin <i>et al.</i>, 2007), urethral reconstruction (Huang <i>et al.</i>, 2015) • Drug delivery (Abeer, Mohd and Martin, 2014) 	 <p>(Czaja <i>et al.</i>, 2007) (Schermer <i>et al.</i>, 2014) (Bodin <i>et al.</i>, 2007)</p>
Aerogels	<ul style="list-style-type: none"> • Filtration/separation • Thermal and acoustic insulation (Sai <i>et al.</i>, 2014, 2015) 	 <p>(Sai <i>et al.</i>, 2015)</p>
Electronic devices	<ul style="list-style-type: none"> • OLEDs (Nogi and Yano, 2008; Pinto <i>et al.</i>, 2015) • Acoustic Membranes (Iguchi, Yamanaka and Budhiono, 2000) • Solar cells (Pleumphon <i>et al.</i>, 2017) 	 <p>(Nogi and Yano, 2008) (Pinto <i>et al.</i>, 2015)</p>
Textile and footwear	<ul style="list-style-type: none"> • Clothing (Lee, 2011; Chan, Shin and Jiang, 2018) • Footwear (Costa, Rocha and Sarubbo, 2017; Rotor, 2017) 	 <p>(Chan, Shin and Jiang, 2018) (Costa, Rocha and Sarubbo, 2017)</p>

2.4.3. BC in the textile and shoe industry

Regarding the application of BC in the clothing and footwear sectors, the first proof of concept of the use of BC as an alternative to leather was made in the 1990s, in the Philippines, where handmade BC was pressed and tanned to produce a material with similar properties to leather (Rotor, 2017). In this last decade, the well-known fashion designer Suzanne Lee, in England, expanded the possibility of using BC in the manufacture of clothing and footwear in an artistic and ecological project called BioCouture. BC was produced handmade, from fermentation with a consortium of microorganisms (kombucha) in a nutrient medium enriched with sugar; then cellulose sheets were washed, adjusted to a pre-defined shape, depending on the final piece to be obtained, dried, and dyed (Lee, 2011). The German start-up ScobyTec developed a vegan alternative to leather made of bacterial cellulose produced from kombucha, which they used to make various products, like gloves, children's shoes, and business handbags. The material called ScobyTec BNC possesses high mechanical strength and is non-flammable (Material District, 2019). In the project SOYA C(O)U(L)TURE, settled by the Indonesian collective XXlab, bacterial cellulose was produced from the liquid waste in tofu production. The cellulose sheets were further pressed, dried, colored, and coated (Sick-Leitner, 2015). The company Malai Design & Materials from India is also using by-products to produce bacterial cellulose but in this case coconut water. The obtained BC sheets are processed and can be modified by incorporating natural fibers, resins, and gum to create a leather-like material (Raut, 2019).

Several academic studies have been conducted with the intention of developing bacterial cellulose-based materials for the textile and fashion industry (Table 8, Table 9, Table 10, Table 11 and Table 12).

2.4.3.1. BC for the fashion industry

The receptivity of BC films produced from kombucha culture with different incubation times, carbon sources, and medium concentrations by professional designers was studied through a qualitative assessment, in terms of comfort and appearance, and it was concluded that BC is useful for fashion applications (Ng and Wang, 2015, 2016). The acceptance of BC in apparel or other related products by the consumers was also explored through an online survey based on visual images of a vest prototype (Lee, 2016; Lee, Li and Nam, 2016). In another work, the acceptance of BC, produced from the kombucha fermented medium, as a novel material for fashion was evaluated subjectively. The participants accepted BC for fashion accessories, but not as a clothing material, based on its thinness, translucency,

unpleasant odor, and skin-like and worn appearance. However, material texture and novelty were found to be favorable characteristics (Ghalachyan, 2018).

The moldability of BC and the possibility of growing it in any shape are advantageous for the development of fashion products. Materials in the form of 2D sheets, singular 3D, and multiple 3D to be used in fashion creation were produced by exploring BC growth (Ng and Wang, 2016). BC-based 3D art integrating SMD-LED through conductive threads was developed by molding BC using a preform (Ng, 2017). The peculiarity of BC to be produced in the desired shape was used to produce clothing with zero-waste. Each part of the garment was fermented to the required size and shape, then dyed and finished with animal oil or wax (Chan, Shin and Jiang, 2018). The moldability of BC was also studied by placing wet BC, produced along with a natural dye extract, in a preform, followed by drying (Tyurin *et al.*, 2019).

The attention given to BC to be used alternatively to leather and cotton-based products is due to its leather-like appearance and cellulose content. The influence of nitrogen and carbon sources on the production of BC was studied and the properties compared with natural leather. The BC nonwoven obtained presented a leather-like appearance and its tensile strength was two times higher, but half the elongation, when compared with bovine top-grain leather (Yim, Song and Kim, 2017). BC properties were also compared with cotton fabric in order to analyze its potentiality in the apparel and textile industry. The authors concluded that BC presents good folding endurance and the tensile strength is acceptable for clothing purposes, but properties related to moisture management should be improved (Rathinamoorthy *et al.*, 2019). The effect of drying temperature on BC properties was studied by analyzing BC obtained through kombucha tea fermentation and dried at different temperatures. It was concluded that BC material is sensitive to drying temperature, it becomes stiffer and loses strength when dried at higher temperatures. And, although the water vapor permeability is compared to coated fabric and leather, further improvement is needed for its application in the fashion industry (Domskiene, Sederaviciute and Simonaityte, 2019).

Table 8. Summary table on the exploitation of BC for the fashion industry.

Study type	Methodology	Results	Reference
Subjective analysis of BC material / Self-grown fashion	Development of BC using black tea, green tea, wine, beer, fresh milk, and coconut juice as carbon sources and selection of the best one based on visual and tactile factors. Optimization of the growing conditions and evaluation of its comfort and appearance properties. Exploration of the BC growth and moldability.	BC grown from 15 g·L ⁻¹ of green tea concentration broth on 6 day cultivation was proposed as the most optimal for self-grown fashion creation. Self-grown fashion prototypes.	(Ng and Wang, 2015, 2016)
Online survey	An online survey using visual images of a BC nonwoven material and a vest prototype.	Participants presented interest in BC material, but they did not perceive this material as good as other currently available sustainable materials.	(Lee, 2016; Lee, Li and Nam, 2016)
Subjective analysis of BC material	BC production using the kombucha, in the static condition, for 4 weeks. Dyeing with red onion skins by boiling in the dye bath for 40 min, then rinsed. Purification, dyeing, and coating with vegetable-based glycerine, by hand. After drying, designing a women's bag and evaluation using group discussions.	Participants accepted BC for fashion accessories, but not as a clothing material.	(Ghalachyan, 2018)
BC 3D art integrating SMD-LED	Production of BC using kombucha for 9–15 days and dyeing with natural blue and red dyes by immersion. Creation of origami pattern by laying wet BC on a template, then design circuitry is placed on top of it and is covered with a second layer of BC, followed by drying.	Kombucha-based 3D art.	(Ng, 2017)
Tailored shape BC	Grow BC in the tailored shape and size, by using panel-shaped cultivation and by using contact surface blocking cultivation.	Zero waste prototype.	(Chan, Shin and Jiang, 2018)
Moldability of BC	Production of BC in static condition for 2 weeks along with a natural dye extract (added one day before the removal). The dyed films were applied to a preform made of epoxy resin and dried by hot airflow.	BC presents moldability with potential in the clothing design.	(Tyurin <i>et al.</i> , 2019)
Comparison of BC with natural leather	Production of BC in the static condition, for 12 days using various nitrogen and carbon sources. Washing with distilled water at 100–105 °C for 5 min and drying at 25 °C for 24 h.	Green tea and sucrose are the optimum nitrogen and carbon sources. BC has a leather-like appearance and when compared with top-grain leather	(Yim, Song and Kim, 2017)

		of similar thickness, BC presented a tensile strength two times higher, but half the elongation.	
Comparison of BC with cotton fabric	Production of BC using <i>Acetobacter xylinum</i> strain in green tea, under static conditions, for 3 weeks. Purification with 2% NaOH, at 90 °C, for 30 min, followed by washing with distilled water until neutral pH.	BC presents lower tensile strength, elongation, and air and water vapor permeability value than the woven cotton fabric. Water absorbency and water holding capacity are superior to the cotton fabric.	(Rathinamoorthy <i>et al.</i> , 2019)
Effect of drying temperature on the BC properties	BC production using kombucha under static conditions, for 7 days. Washed with distilled water and squeezed to reduce its water content. Dried at different temperatures until constant weight.	BC is sensitive to drying temperature. Higher temperatures created rapid water loss and brittle properties. WVP = 2,775–3,050 g·m ⁻² 24 h ⁻¹ , which are compared with laminated fabric and leather. Hydrophilic with a water contact angle of 64°.	(Domskiene, Sederaviciute and Simonaityte, 2019)

2.4.3.2. BC coated on fibers, yarns, fabrics

An approach to the use of BC in the textile industry consists of coating fibers, yarns, or fabrics with BC nanofibers, increasing the surface area and the mechanical properties of the obtained composites (Table 9). The interfacial adhesion of natural fibers, such as hemp and sisal fibers, with biopolymers significantly increased by adding those fibers to the BC culture medium before fermentation (Pommet *et al.*, 2008). In order to develop wearable electronics, cotton yarns were first soaked in BC nanofiber suspension, under sonication, to increase the surface area before the deposition of pyrrole (Q. Xu *et al.*, 2016). Hybrid fabrics (wool/BC, silk/BC, cotton/BC, cellulose acetate/BC, nylon/BC, polyester/BC, Kevlar®/BC, viscose rayon/BC, Bemlise®/BC) were developed by producing BC with different fabrics added to the culture medium. In order to obtain double-sided coating, the fabrics were inverted during the experiments. Although BC was produced at the surface of all fabrics, it showed no affinity for the non-cellulosic material and easily peeled off during the NaOH washing step (Mizuno *et al.*, 2012). A similar procedure was used to develop cotton, polyester and rayon hybrid fabrics where the BC coating increased the thickness and bursting strength and decreased the penetration of water through the composite fabrics and the water vapor permeability (Kamal *et al.*, 2018). A method to produce BC/ENM (regenerated cellulose electrospun nanofibrous membrane) hybrid fabrics with targeted dimensions was developed through in situ self-assembly, by adding a polypropylene mesh template to the fermentation medium. The growth of BC nanofibers into the empty voids of the mesh improved the fabric performance by decreasing the

surface hydrophobicity and water uptake, while increasing the tensile strength of the composite (Naeem *et al.*, 2019).

Table 9. Coating of fibers, yarns, and fabrics with BC nanofibers.

Study type	Methodology	Results	Reference
Natural fibers coated with BC nanofibers	BC production under agitated conditions for one week with hemp and sisal fibers in the culture medium. A purified single fiber was embedded in a PLLA or CAB melt droplet.	5–6% BC adheres to the fibers. Mechanical properties of sisal remain, but hemp deteriorates. The interfacial adhesion of the natural fibers with biopolymers increased.	(Pommet <i>et al.</i> , 2008)
YSC based on hierarchically structured BC nanofiber coated cotton	Cotton yarn soaked in BC nanofiber suspension under sonication. BC coated cotton yarn was dipped into a pyrrole aqueous solution. Assembly of Yarn supercapacitor by soaking into PVA/H ₂ SO ₄ gel electrolyte.	YSC with excellent mechanical stability, high flexibility, and high capacitance retention.	(Q. Xu <i>et al.</i> , 2016)
Hybrid fabrics	BC production in static conditions with Multifiber Test fabric (wool, silk, cotton, cellulose acetate, nylon, polyester), Kevlar®, and viscose rayon and Bemlise® nonwovens fabrics in the culture medium.	BC was produced on the surfaces of all fabrics, but it was peeled off from the non-cellulosic fabrics during the NaOH washing.	(Mizuno <i>et al.</i> , 2012)
Hybrid fabrics	BC production in static conditions for 7 days with cotton, polyester, and rayon fabrics in the culture medium.	The thickness and bursting strength increased. Water impact penetration and water vapor permeability decreased. BC produced on polyester fabric is easily peeled-off.	(Kamal <i>et al.</i> , 2018)
BC/ENM (electrospun nanofibrous membrane) hybrid fabrics	BC/ENM seamless tubular hybrid fabric was produced through <i>in situ</i> self-assembly approach by fermentation under the static condition for 7 days. ENM was supported by a PP mesh held by a pair of aligned rubber rollers which are driven every 24 h.	Properties of the ENM were improved: Thickness and weight gain: 33.90% and 39.02%. Hydrophobicity and water uptake decreased. Tensile strength increased.	(Naeem <i>et al.</i> , 2019)

2.4.3.3. Development of BC macrofibers

The production of macrofibers from oriented BC nanofibers, with promising potential applications such as smart textiles and for structural reinforcement, can also be developed (Table 10).

Macrofibers obtained in a continuous process based on aligned BC nanofibers by wet spinning were developed in a process where the cellulose suspensions were first prepared by TEMPO oxidation. Then, the suspensions were spun into an acetone coagulation bath and dried. Subsequently, the filaments with a controlled humidity were stretched to align the BC nanofibers. These macrofiber filaments were subjected to cross-linking by multivalent ions, to prevent the decrease of the mechanical properties due to the weakening of the interfacial linkage between the nanofibers in a high moisture environment (Yao *et al.*, 2017). BC macrofibers with improved mechanical properties were also prepared by wet-drawn stripes of BC membranes by using a tensile testing machine, to improve the filament alignment. Then the wet-drawn samples were twisted into macrofibers with nine turns per inch and then dried at 90 °C under tension to reduce the voids and to induce a strong interfilament hydrogen bonding. These macrofibers can be shaped and dyed, possessing interesting potential for application in the textile industry (Wang *et al.*, 2017). In another work, the alignment of BC nanofibers was achieved via a simple one-step solvent-assisted drawing. Films of BC were first soaked in N-methyl-2-pyrrolidinone solvent, then they were wet-drawn, followed by hot-pressing drying at 60 °C. To obtain ultrathin films with high tensile strength and high toughness, layers of the BC film were removed using tape (mechanical exfoliation). These films were then soaked in water and twisted, resulting in strong fibers. The production of multifunctional fibers, namely dyed fibers, CNT/BC fibers, and CoFe₂O₄/BC magnetic fibers, was also shown by soaking aligned BC ultrathin films in the respective solutions followed by sonicating, and after that twisting and drying (Wu *et al.*, 2020). Hierarchical helical nanocomposite macrofibers were developed using a wet-spinning method by extruding mixtures of BC nanofibers dispersions and alginate through a capillary needle into a CaCl₂ coagulation bath, forming filaments with aligned BC nanofibers. Then, two single BC/alginate gel filaments were twisted together into hierarchical helical BC/alginate macrofibers with certain twist levels according to a multilevel wet-twisting process. The alignment of BC contributes to ultimate mechanical properties, whereas the alginate matrix contributes to the stress transfer between BC nanofibers, resulting in a simultaneous improvement of the tensile strength, elongation, and toughness (Gao *et al.*, 2020).

Table 10. BC macrofibers.

Study type	Methodology	Results	Reference
BC macrofibers	BC nanofiber suspensions prepared by TEMPO oxidation and wet spinning into an acetone coagulation bath. Alignment of BC nanofibers by stretching and cross-linking by multivalent ions.	Young's modulus of 22.9 and 15.9 GPa and tensile strength of 357.5 and 262.2 MPa, dried and wet conditions, respectively.	(Yao <i>et al.</i> , 2017)
BC macrofibers	Alignment of BC nanofibers by wet-drawn stripes of BC membrane and twisted into macrofibers.	Young's modulus of 65.7 GPa, tensile strength of 826 MPa, and specific tensile strength of 598 MPa g ⁻¹ ·cm ³ .	(Wang <i>et al.</i> , 2017)
High strength ultrathin films and multifunctional fibers	BC films soaked in a solvent were wet drawn, followed by hot-pressing. Layers of the film were removed using tape. BC ultrathin films were soaked in water and twisted. Production of multifunctional fibers, namely dyed fibers, CNT/BC fibers, and CoFe ₂ O ₄ /BC magnetic fibers, by soaking aligned BC ultrathin films in the respective solutions.	Film: tensile strength of 758 MPa and toughness 42.3 MJ·m ⁻³ . Macrofibers: tensile strength of 954.2 MPa and toughness of 93.2 MJ·m ⁻³ .	(Wu <i>et al.</i> , 2020)
Hierarchical helical nanocomposite macrofibers	Wet spinning of BC/alginate dispersions into a CaCl ₂ coagulation bath. Gel filaments twisted together into hierarchical helical BC/alginate macrofibers.	Tensile strength of 535.4 MPa, elongation of 16.2 %, and toughness of 44.8 MJ·m ⁻³ .	(Gao <i>et al.</i> , 2020)

2.4.3.4. Improvement of BC flexibility, hydrophobicity, and mechanical properties

Despite its excellent properties, the hydrophilic nature of BC and the loss of flexibility and porosity upon drying (due to the collapsing of the 3D network) have limited its application in the textile and footwear industry. Some attempts have been taken to improve BC properties to be applied in the textile industry (Table 11). In order to improve the mechanical properties of BC and to reduce the water regain, PLA and PU-based biopolymers were embedded into BC by dip-coating and electrospinning. Although some improvement was observed in the tensile strength when BC was coated with PU-based biopolymer by electrospinning, further work is needed to, namely, reduce the moisture regain (Y.-A. Lee *et al.*, 2014; Lee, 2016). The hydrophobicity and flexibility of BC from kombucha were improved by immersing dried BC sheets in a textile softener solution followed by immersion in a hydrophobic finishing agent solution. BC was then dried at 120 °C for 1 min. From about 60° (native BC) the obtained hydrophobic composite had a water contact angle of 114° (Araújo, Silva and Gouveia, 2015). Laccase-assisted reactions allowed the functionalization of BC with poly(fluorophenol) and lauryl gallate oligomers, improving its

hydrophobicity and durability (in terms of its dimensional stability and tensile strength). For the functionalization with poly(fluorophenol), laccase was first entrapped onto the surface of the BC fibers and then used to in situ polymerize the fluorophenol. For the lauryl gallate oligomers functionalization, wet BC was submerged in lauryl gallate oligomers that were previously synthesized by laccase. The resulting materials also presented hydrophobic surfaces and durability (Song *et al.*, 2019, 2020). The flexibility and mechanical properties of BC were also improved by immersion in glycerol and coating with stearic acid (Kamiński *et al.*, 2020).

Table 11. Improvement of BC properties for textile applications.

Study type	Methodology	Results	Reference
Case study, BC and biopolymer composites	Production of BC with SCOBY, for 4 weeks. Purification by washing and boiling in water, followed by air-drying. Development of BC/biopolymer composites: PLA by dip-coating and aqueous castor oil-based PU dispersions by dip-coating and electrospinning.	Nonporous surface using the dip-coating method. PU-coating (electrospinning) provides some additional strength to the purified BC film, but no differences regarding water regain.	(Y.-A. Lee <i>et al.</i> , 2014; Lee, 2016)
Hydrophobic BC material	Production of BC from tea extract and HS medium, for 7 days. Purification with 0.1 N NaOH for 30 min at 80 °C, neutralization and washing with distilled water. Immersion of dried BC pellicle in a softener solution and then in a hydrophobic finishing, followed by drying for 1 min at 120 °C.	Hydrophobic material with a contact angle of 114°.	(Araújo, Silva and Gouveia, 2015)
Hydrophobic and durable BC	Swelling of BC using a NaOH solution under ultrasound, followed by addition of laccase for 30 min. Immersion of BC in fluorophenol solutions at 50 °C for 24 h, at 135 rpm, followed by washing with 1% SDS.	WCA increased from 54.5° to 120° and OCA from 46.5° to 87°. Improvement in the durability properties, tensile strength, and dimensional stability, after wetting.	(Song <i>et al.</i> , 2019)
Hydrophobic and durable BC	Production of lauryl gallate oligomers through laccase-mediated oligomerization. Swelling of BC using a NaOH solution under ultrasound, followed by incubation in lauryl gallate oligomers solution at 50 °C for 12 h, at 135 rpm. Washing with distilled water and drying.	WCA increased from 48.1° to 118°. Improvement in the durability properties, tensile strength, and dimensional stability, after wetting.	(Song <i>et al.</i> , 2020)

Flexible BC	Production of BC from kombucha, in static conditions for 2 weeks. Freeze-dried BC samples were added to a glycerol aqueous solution and autoclaved at 121 °C for 15 min. Then rinsing with distilled water and freeze-dried. Stearic acid ethanol solution was spread using a brush and streamed with hot air (70–75 °C).	BC with increased strength, elasticity, and inflammable properties.	(Kamiński <i>et al.</i> , 2020)
-------------	--	---	---------------------------------

2.4.3.5. BC purification, bleaching, and dyeing

The possibility of giving certain colors to the materials is a fundamental feature in the textile and footwear sectors. Several studies have been conducted for the color modification of BC, including bleaching, dyeing with natural and artificial dyes, and *in situ* and *ex situ* dyeing processes (Table 12). After cultivation, BC presents a natural yellowish-brown color derived from the culture medium. Washing of BC with 3% NaOH solution results in the effective removal of bacteria and the remnants of the culture medium that does not affect the BC nanoscale 3D network structure. In order to ensure the subsequent uniform dyeing and bright colors, bleaching with 5% H₂O₂ solution for 60 min at 90 °C removed the brown-yellow color of BC (white index of 73.15), without deforming the cellulose structure (Han, Shim and Kim, 2019). Recently, the effect of sodium hydroxide concentration on morphology, physical and chemical structure, and water vapor permeability (WVP) of BC membranes was studied. It was shown that by removing impurities, such as organic compounds, nucleic acids, and proteins generated by during the fermentation process, BC membrane breathability can be improved (Kamal, Misnon and Fadil, 2020).

Dyeing of BC was carried out by producing BC in the presence of a direct acid or basic dye in the culture media. Optical microscopy observation showed that the direct and basic dyestuffs stained the BC, but the acid one did not. Analysis of wide angle X-ray diffraction (WAXD) data indicated that direct dyestuffs inhibited the crystallization of BC above 0.05 wt% dyestuff concentration in the culture medium, but basic dyestuff had almost no influence on the BC's crystallization (Miyamoto *et al.*, 2014). In another work, in order to produce colored BC nonwovens, different natural and artificial dyes were added to the culture medium. Colors were successfully incorporated into the BC when natural dyes and the blue artificial dye were used, while other artificial dyes inhibited BC growth (Wood, Hang and Salusso, 2015). Shoe prototypes were developed using bacterial cellulose mats and the colors of the BC sheets were obtained by dyeing BC with red onion skins and coffee grounds leftovers (Nam and Lee, 2016). The dyeability of BC produced under static culture using *in situ* and *ex situ* methods was also studied using direct acid

and reactive dyestuffs. Although only the lower half of the BC was colored during the cultivation (*in situ* method), after drying it showed uniform color on both sides and presented clearer colors when compared with the dried BC colored by the *ex situ* method (Shim and Kim, 2019). An environmentally friendly process was developed for the bio-coloration of BC via phenolic oxidation by laccase immobilized onto BC. Specifically, flavonoids were successfully polymerized by the immobilized laccase, which gave rise to yellow, orange and dark brown oligomers that colored the BC. Best results were obtained with the flavonoids catechol and catechin (Song *et al.*, 2018). BC films were also dyed by immersion of BC into plant-based natural dye (*Clitoria ternatea L.* and *Hibiscus rosa-sinensis*) solutions, while retaining the crystallinity, thermal and mechanical properties of BC (Costa *et al.*, 2019).

Table 12. BC purification, bleaching, and dyeing.

Study type	Methodology	Results	Reference
Purification and bleaching	Cultivation of BC using HS medium for 8 days. Washing with NaOH and bleaching with different concentrations of H ₂ O ₂ .	3% NaOH better removal of impurities. 5% H ₂ O ₂ increased the whiteness (white index 73). Crystallinity increased 27% after three-step process.	(Han, Shim and Kim, 2019)
Purification	BC production in a coconut water-based culture medium with 10% of <i>Acetobacter xylinum</i> inoculum, in static conditions for 7 days. Washing with water and purification by soaking (24 h) with different percentages of NaOH (0–2%). Washing with water until neutral pH and air drying at 120 °C.	With higher % NaOH better removal of impurities, increment on the yield, thickness, and WVP of the BC. NaOH ≥ 2% WVP decreased.	(Kamal, Misnon and Fadil, 2020)
Dyeing (in-situ)	Production of BC with 0–0.5 wt% of dyestuffs (direct, acid, and basic) dispersed into the culture media, by shaking for 24 h. Filtration and purification with NaOH solution, followed by neutralization, filtration, and freeze-drying. Samples obtained with 0.5 wt% dyestuffs were washed with ethanol.	Direct and basic dyestuffs stain BC but acid dyestuff did not. Direct dyestuffs inhibited the crystallization of BC, while basic dyestuff had almost no influence on it.	(Miyamoto <i>et al.</i> , 2014)
Dyeing (natural and synthetic dyes)	Production of BC with natural dyes (turmeric, saffron, and beet) and artificial dyes (red, orange, yellow, green, blue, and violet) in the culture media, for 3 weeks. Drying at ambient conditions.	Natural dyes and the blue artificial dye were incorporated into BC. The addition of the rest of the artificial dyes inhibited BC growth.	(Wood, Hang and Salusso, 2015)

Shoe prototypes	Dyeing of BC with red onion skins and coffee grounds leftovers	Dark red and dark brown BC.	(Nam and Lee, 2016)
Dyeing (in-situ and ex-situ methods)	<i>In situ</i> dyeing by production BC with direct, reactive, and acid dyes and different carbon sources in the culture media, in the static condition, for 8 days, followed by washing with 3% NaOH and neutralization. <i>Ex situ</i> dyeing of BC with different temperatures and pH, for 30 min. Drying at 35 °C for 24 h.	<i>In situ</i> method - highest production yield using glucose as a carbon source and reactive dye. Ex-situ method - best results for dyeing BC produced with fructose with reactive dye, at 135 °C, and pH 3. <i>In situ</i> method allows a smoother surface and higher color strength than the <i>ex situ</i> .	(Shim and Kim, 2019)
Dyeing (flavonoids)	Production of BC in static condition for 8 days, followed by washing with distilled water and bleaching with H ₂ O ₂ solution. Swelling with NaOH solution and drying. Immobilization of laccase into BC by immersion, at room temperature and 4 °C, for 12 h. Laccase-mediated polymerization with catechol, catechin, ferulic acid and hydroquinone monomers by immersion overnight, followed by washing and drying.	Color depth is more pronounced in samples with laccase immobilized at 4 °C and increases with the incubation time. Catechol and hydroquinone gave rise to a dark brown and catechin and ferulic acid to yellow-orange.	(Song <i>et al.</i> , 2018)
Dyeing (natural dyes)	Production of BC in static condition for 10 days, followed by washing with tap water and purification with NaOH, and neutralization. Dyeing by immersion in a heated solution of natural pigments (extracted from <i>Clitoria ternatea</i> L. and <i>Hibiscus rosa-sinensis</i>) and mordants, for 30 min, followed by immersion in a solution containing 1% fixer and 2% of softener, for 15 min.	Submersion in distilled water for 5 days led to a reduction in fixation of 28.3% for the <i>Clitoria ternatea</i> L. dye and a 12.1% reduction for the <i>Hibiscus rosa-sinensis</i> dye. After the hand washing simulation, the color intensity decreases. Loss in mechanical properties after dyeing.	(Costa <i>et al.</i> , 2019)

2.5. Vegetable oils

Vegetable oils (VOs) are renewable resources abundantly available with an increasing number of industrial applications that offer advantages such as low cost, non-toxicity, and biodegradability (López and Santiago, 2013; Saithai *et al.*, 2013). Basically, these raw materials are composed of triglyceride molecules, whose main components are fatty acids (three) linked to glycerol esters. Fatty acids in the most common triglycerides, range from 14 to 22 carbons in length and have 0 to 3 double bonds (Khot *et al.*, 2001; Lu and Wool, 2004; López and Santiago, 2013). To increase their reactivity, double bonds can be replaced by more reactive functional groups using chemical reactions, such as epoxidation,

acryloylation, hydroxylation, or maleinization (Grishchuk and Karger-Kocsis, 2011; Saithai *et al.*, 2013; Senoz *et al.*, 2013; Gandini and Lacerda, 2015). VOs and their derivatives are already used in different areas, such as health and cosmetics, biodiesel, paints, varnishes and coatings for wood, and anti-corrosion agents for metals (López and Santiago, 2013). Among VOs, soybean oil is one of the most attractive due to its low price and abundant availability. Generally, their double bonds are epoxidized and then acryloylated, by reaction with carboxylic groups of acrylic acids, allowing their polymerization by free radicals (Gandini and Lacerda, 2015; Liu, Madbouly and Kessler, 2015). Acrylated epoxidized soybean oil (AESO) has been studied extensively in the production of composites with a high content of renewable resources. In general, these composites include different particles or fibers, such as microcrystalline cellulose (W. Liu *et al.*, 2017), regenerated cellulose fibers (Ramamoorthy *et al.*, 2014), coconut residues (Kocaman *et al.*, 2017), discarded cotton/polyester and denim fabrics (Ramamoorthy *et al.*, 2018; Temmink, Baghaei and Skrifvars, 2018), ramie fibers (Lee *et al.*, 2013), hemp fibers (Khot *et al.*, 2001; Akesson, Skrifvars and Walkenström, 2009; Liu *et al.*, 2018), flax and glass fibers (Khot *et al.*, 2001), or pyrolyzed fibers from chicken feathers (Senoz *et al.*, 2013).

Regarding the area of leather and analogues, AESO has been tested in goatskin leather finish. Compared to untreated leather, coated leather showed a reduction in the friction coefficient on the inner face, thus showing the possibility of using AESO as an ecological solution for leather finishing (Nunez, Santiago and Lopez, 2008). A recent patent (Wool, 2013) demonstrates the possibility of making ecological leather analogues; the process consists of mixing natural fibers with different types of epoxidized and acryloylated triglycerides. According to the patent, different vinyl monomers and a catalyst can be added to this mixture. The composite is then deposited in appropriate molds and subjected to hot pressing techniques such as Resin Transfer Molding or Sheet Compound Molding. In another work, an environmentally friendly substitute for leather was developed by reinforcing a mixture of AESO resin with cotton fabrics (Cao *et al.*, 2013). Later, it was used for the development of ecological shoes composed of organic cotton fabrics and AESO/MLAU resin (lauryl methacrylate) (50/50). The prototype comprising this composite was applied to the upper part of the shoe and tested on volunteers. Its performance was evaluated using a questionnaire where the participants described it as wearable, versatile, and practical. Despite presenting this product as water-resistant and breathable, tests have not been carried out to measure these properties (Cao *et al.*, 2014).

It is expected that by combining BC membranes, which have the unique properties already presented, with a biodegradable polymer, such as the AESO, it is possible to produce a truly green nanocomposite. In the literature, the works that have been developed with BC and modified soybean oil have a different

approach from the one intended in this research project. Highly porous UV curable and thermosetting nanocomposite foams from BC/AESO were developed by producing water-in-oil emulsions stabilized by BC nano-fibrils previously hydrophobized by acetylation and silylation (Blaker *et al.*, 2009). In another work, other monomers were added to AESO and the emulsions were polymerized by free radicals (Sousa *et al.*, 2017). It was also shown that it is possible to produce macroporous 3D polymers through microwave heating of liquid gas/AESO foams. The addition of BC allowed to significantly improve the stability of the foams, by obstructing the flow of liquid, and the mechanical properties, since it acts simultaneously as a nanofiller (Koon-Yang Lee *et al.*, 2011). Optically transparent composites with excellent mechanical properties were developed by impregnating BC films with epoxidized soy oil. To improve the dispersion of the nanofibers and the adhesion between the cellulose and the hydrophobic polymeric matrix, pressed BC films were acetylated (Retegi *et al.*, 2012).

Chapter 3

Development of BC/PDMS/PFC composites¹

3.1. Abstract

This research aimed at obtaining a malleable, breathable and water impermeable bacterial cellulose-based nanocomposites, by impregnating bacterial cellulose (BC) membranes with two commercial hydrophobic polymers used in textile finishing, Persoftal MS (polydimethylsiloxane (PDMS)) and Baygard EFN (perfluorocarbon (PFC)), by an exhaustion process. These hydrophobic products penetrated the BC membranes and adsorbed tightly onto the surface of the nanofibers, across the entire depth of the material, as demonstrated by scanning electron microscopy (SEM) and Fourier transform infrared (FT-IR) spectroscopy studies. The water static contact angles, drop absorption over time and vapor permeability values showed that the composites were impermeable to liquid water but permeable to water vapor. The mechanical properties of the BC-nanocomposites were improved after incorporation of the hydrophobic products, in some of the formulations tested, overall presenting a satisfactory performance. Thus, through a simple and cost-effective process, hydrophobized, robust, malleable and breathable nanocomposites based on BC were obtained, featuring promising properties for application in the textile and shoe industries.

¹ This chapter is based on the following publication:

Fernandes, M., Gama, M., Dourado, F. and Souto, A. P. (2019) "Development of novel bacterial cellulose composites for the textile and shoe industry," *Microbial Biotechnology*, 12(4), pp. 650–661.

3.2. Introduction

Bacterial cellulose (BC) consists of a 3D nanofibrillar arrangement of pure cellulosic fibers with a diameter of 20-100 nm and several micrometers in length, resulting in a high specific surface area (Tang *et al.*, 2015; Wu *et al.*, 2016), property which are very advantageous for the production of composite materials (Lee, Blaker and Bismarck, 2009; Wan *et al.*, 2009; Wu *et al.*, 2016). BC also exhibits high crystallinity, high degree of polymerization, high water holding capacity and high moldability (Lee, Blaker and Bismarck, 2009). These unique properties have sustained the elevator pitch of several BC applications in the biomedical field, pulp & paper, composites and foods (Andrade *et al.*, 2010; Dourado *et al.*, 2016; Fortunato *et al.*, 2016; Gonçalves *et al.*, 2016; Padrão *et al.*, 2016).

Despite these excellent properties, the loss of flexibility upon drying is a disadvantage for several applications such as in the textile and shoe industry. Due to the collapse of the 3D nanofibrillar BC network, a significant reduction in gas permeability also occurs, heavily reducing the material's breathability. Further, the hydrophilic nature of BC hinders the combination with hydrophobic polymer matrixes, an obstacle to the development of composites where both BC and the added polymer contribute to the final desirable properties. Several studies have been conducted on the chemical modification/hydrophobization of cellulose and of BC in particular, attempting to overcome these issues (Tomita, Tsuji and Kondo, 2009; Nisoa and Wanichapichart, 2010; Tomé *et al.*, 2010; Wan *et al.*, 2017).

The major limitations of *ex situ* BC modification methods concern with the size and nature of the reinforcing materials, namely, only soluble polymers and nano-submicron sized materials can penetrate into the BC 3D network. The bulk distribution of these particles within the BC pellicle is also heterogeneous, a feature further aggravated by the hydrophobic nature of certain polymer matrices, which have poor interfacial adhesion to native BC (Shah *et al.*, 2013).

Throughout this research, a novel approach was tested for the bulk and surface modification of BC, combining simplicity, potential for application at large scale and low cost, based on the use of an exhaustion process. Through this process, two hydrophobic commercial polymers, Persoftal MS Con.01, a softener based on polydimethylsiloxane (PDMS), and Baygard EFN, a hydrophobizer based on perfluorocarbon (PFC), were incorporated into the nanofibrillar matrix of BC, aiming at obtaining a malleable, breathable and water impermeable nanocomposite with strong potential of application in textile and shoe industries.

3.3. Materials and methods

3.3.1. Materials

BC membranes were offered by Satisfibre S.A. (Portugal). The commercial polymer formulations, Persoftal MS Conc.01 (a softener based on Polydimethylsiloxane - PDMS) and Baygard EFN (hydrophobizer based on Perfluorocarbon - PFC), both from Tanatex Chemicals, were offered by ADI Center Portugal.

Perfluorinated acrylate polymers have extremely low surface energy due to their side chain containing outwardly oriented perfluoro hydrophobic groups and are widely used in textile and leather coatings. The application of perfluorinated organic compounds with a long perfluoroalkyl chain (C_nF_{2n+1} , $n \geq 8$) has been restricted by the European Union due to its high bioaccumulation and difficult biodegradation (Zahid *et al.*, 2017). Thus, the hydrophobic product used in this work consisted of a C6-based Fluorocarbon polymer nano-emulsion without Perfluorooctane Sulfonate (PFOS) and less than 5 ppb Perfluorooctanoic Acid (PFOA). The characteristics of the products used are summarized in Table 13.

Table 13. Characteristics of the finishing polymers used.^a

	Softener (S) – Persoftal MS Conc.01	Hydrophobizer (H) – Baygard EFN
Chemical basis	Modified polysiloxane aqueous dispersion	Fluorocarbon polymer aqueous nano-emulsion
Ionicity	Non-ionic	Non-ionic
Density	0.99 g·cm ⁻³ (23°C)	1.1 g·cm ⁻³ (20°C)
Viscosity	405 mPa·s (23°C)	100 mPa·s (20°C)
Content	10–20% Siloxanes and Silicones, 3-((2-aminoethyl)amino)propyl Me, diMe, hydroxy-terminated (CAS: 75718-16-0) 3–5% Alcohols, C12-18, ethoxylated (CAS: 68213-23-0) 3–5% Alcohols, C10-14, ethoxylated (CAS: 66455-15-0) 0.1–1% Octamethylcyclotetrasiloxane (CAS: 556-67-2)	28% Fluorocarbon polymer 0.1–1% Alcohols, C16-20, ethoxylated (CAS: 106232-82-0)

^aInformation extracted from the technical sheets provided by the manufacturer.

3.3.2. Composites production

BC membranes (with about 2.5–3.0 cm in thickness, with a size of 12.0 × 13.0 cm and weighting 450 g) were squeezed to a final wet mass of 100 g (2.6% BC (w/w)). The compressed membranes were each treated by exhaustion in 100 mL of:

- i) an aqueous mixture containing either the softener (**S**) or the hydrophobizer (**H**), each, at different concentrations (1, 10, 25, and 50% (v/v)), or;
- ii) processed in two steps by exhaustion with 10, 25 and 50% (v/v) of softener **S**, followed by drying; afterwards, the dried composites were each impregnated with 50% (v/v) hydrophobizer **H** (further designated by 10S + H, 25S + H, and 50S + H).

It is expected that with the sequential application **S+H** a material with suitable properties for application in the textile and shoe industry can be achieved. Considering PDMS characteristics, it allows properties such as malleability, robustness and softness, permitting water vapor transmission. However, since the hydroxyl and amino-functional polar groups linked to PDMS in the softener used impart some hydrophilicity, the subsequent application of the PFC nano-emulsion will hydrophobize the surface.

The exhaustion process was carried out in an Ibelus machine equipped with an infrared heating system, using stainless-steel cups with a capacity of approximately 220 cm³, with a rotation of 50 rpm and 40 cycles. The desired temperature (30 °C) was achieved using a gradient of 2 °C·min⁻¹. The treatment lasted for 5 days at 30 °C, after which the samples were oven dried (WTC binder oven) at 25 °C for 48 hours, followed by a curing step for 30 min at 120 °C. To avoid shrinkage of the samples during drying and curing, the composite BC membranes were attached to a zinc-plated wire support.

3.3.3. Physical-chemical properties evaluation

3.3.3.1. Scanning electron microscopy (SEM)

BC composites were coated with a thin layer of gold-palladium. Analyses of the surface morphology and cross section of these composites were done using an ultra-high-resolution field emission gun SEM instrument (NOVA 200 Nano SEM, FEI, Hillsboro, OR, USA).

3.3.3.2. Atomic force microscopy (AFM)

Atomic force microscope images of the BC composites were collected in tapping mode using a Nanoscope III microscope from Digital Instruments (Santa Barbara, CA, USA), with antimony-doped silicon probes in contact mode in air. Images were captured at a scanning rate of 1.0 Hz and resolution of 512 pixels × 512 pixels. The roughness parameters, roughness average (Ra) and root mean square (RMS), were calculated using the average of three scans in different places for each sample in 10 μm × 10 μm area.

3.3.3.3. Fourier transform infrared (FT-IR) analysis

A Nicolet Avatar 360 FT-IR spectrophotometer (Madison, WI, USA) was used to record the FT-IR spectra of the BC sheet and BC composites. The spectra were collected in the attenuated total reflection mode (ATR) at a spectral resolution of 16 cm⁻¹, with 60 scans, over the range 400–4000 cm⁻¹ at room temperature. A background scan with no sample and no pressure was acquired before the spectra of the samples were collected.

3.3.3.4. Surface energy

Contact angles measurements were carried out in a Dataphysics instrument (Filderstadt, Germany) using OCA20 software (Germany) with a video system for the capture of images in static mode using the sessile drop method. A drop of 5 μL of distilled water was placed on the composite's surface with a microliter syringe and observed with a special charge-coupled device camera. After a water drop was deposited in the composites surface, the water contact angle was observed over time for 220 s. At least five measurements at different places were taken for each sample. The camera recorded an image every 0.04 s. To calculate the surface energy (γ_s) of the BC and the polar (γ_s^p) and dispersive (γ_s^d) components, the Wu method (harmonic-mean) was used, with the Equation (1) (Wu, 1971):

$$\gamma_{sl} = \gamma_s + \gamma_l - 4 \left[\frac{\gamma_s^d \gamma_l^d}{\gamma_s^d + \gamma_l^d} + \frac{\gamma_s^p \gamma_l^p}{\gamma_s^p + \gamma_l^p} \right], \quad (1)$$

The following liquids (*l*) with known surface energy and surface energy components were used: distilled water (γ : 72.8; γ^d : 29.1; γ^p : 43.7); polyethylene glycol 200 (γ : 43.5; γ^d : 29.9; γ^p : 13.6); and glycerol (γ : 63.4; γ^d : 37.4; γ^p : 26.0), units in mJ·m⁻² (Oliveira *et al.*, 2013).

3.3.3.5. *Water vapor permeability (WVP) and static water absorption (SWA)*

WVP was evaluated according to the Standard BS 7209:1990 (British Standards Institution, 1990). According to this method, the test specimen is sealed over the top of a test dish which contains 46 mL of distilled water and the assembly is placed on a rotating turntable and allowed to rotate, under isothermal conditions, for a period of one hour to establish the equilibrium of water vapor pressure gradient across the sample. After this period the assembly is weighted and allowed to rotate for 24 h, and is weighted again.

The result is represented by the following Equation (2) and expressed in $\text{g}\cdot\text{m}^{-2}\cdot 24\text{ h}^{-1}$.

$$WVP = \frac{24W}{At}, \quad (2)$$

where W is the mass (g) of water vapor lost in t hours, A is the area of the sample exposed to vapor (m^2), and t is the time between the various weightings (h).

SWA was measured by immersing the samples in distilled water, at room temperature, for 15, 30, 60 and 120 min. After the immersion time, the specimens were removed from the container and their surface moisture was removed by tissue paper. The content of water absorbed was weighed and the SWA was calculated through Equation (3).

$$SWA = \frac{M_t - M_0}{M_0}, \quad (3)$$

where M_t is the weight of specimen at a given immersion time and M_0 is the weight of the dried sample.

3.3.3.6. *Mechanical properties*

The overall width of the sample (25 mm) was fixed and a length that allows an initial distance between the clamps of the strength tester equipment (Hounsfield HSK100) of 75 mm was set out between grips; the samples were then submitted to tensile and tear. Three samples of each material were tested at a constant speed of $\text{mm}\cdot\text{min}^{-1}$.

3.3.4. Statistical analysis

Statistical analysis was performed using ORIGIN PRO 8 software. All data are presented as the mean \pm standard error of the mean. Statistical analysis included Shapiro-Wilks, Skewness and one-way ANOVA with Tukey post hoc tests whenever the results displayed a parametric distribution, otherwise Dunn-Sidak post hoc test was used.

3.4. Results and discussion

Simply defined, the exhaustion process used in textile technology involves placing the fabric or yarn in a chamber containing water and treatment products. The chamber is then sealed and the treatment solution heated, which results in the products transitioning from the water to the fabric or yarn. This procedure was adopted in this work to process BC membranes, incorporating different hydrophobic materials into the cellulosic porous network. Although several authors addressed the development of composites using BC fibers, very few papers use the intact membranes obtained by static fermentation. Thus, we believe this approach is innovative and, by preserving the mechanical properties and the three-dimensional BC membrane, fully exploits its potential as a nanocomposite scaffold.

3.4.1. Scanning electron microscopy (SEM)

The surface and cross-section morphologies of the BC and the composites produced with PDMS (**S** - softener) and PFC (**H** - hydrophobizer) polymers (Figure 3) were observed by SEM analysis. Dried BC (Figure 3a and f) exhibited a characteristic entangled nanofibrillar matrix disposed in layers with nanofibers of about 70 nm in thickness. Figure 3g (10S) and Figure 3h (10H) shows the increase in the nanofibers thickness, following polymer impregnation. Treating BC with increasing amounts of either **S** or **H** increased the mass per unit area of the BC composite (Table 14), especially with the former, possibly due to a higher penetration of the polymer into the BC matrix and/or higher affinity for the BC's hydroxyl groups. As observed in Figure 3b, the BC-10S composite presented thicker nanofibers, with higher surface coverage and a more compact, fused morphology, whereas BC-10H (Figure 3c) showed a more porous surface structure. Regarding the sequential impregnation of **S** and **H** (Figure 3d, e, i, j and Table 14), adding **H** to BC-S after drying did not impact significantly on the final composite's specific mass, suggesting limited absorption, as compared to samples treated with **S** alone. Actually, a slight decrease

in the composite's mass was observed as compared with treatments with **S** alone, possibly associated with desorption of **S** during the second stage of the sequential process.

As demonstrated further bellow (regarding the water vapor permeability values, Figure 8), despite the extensive coverage of the BC nanofibers and compact appearance of the dried composites (Figure 3), the porosity was not compromised, thus assuring the breathability of the composite. Figure 3k shows photos of the composite 50S + H, demonstrating that it can be easily folded without causing visible damage.

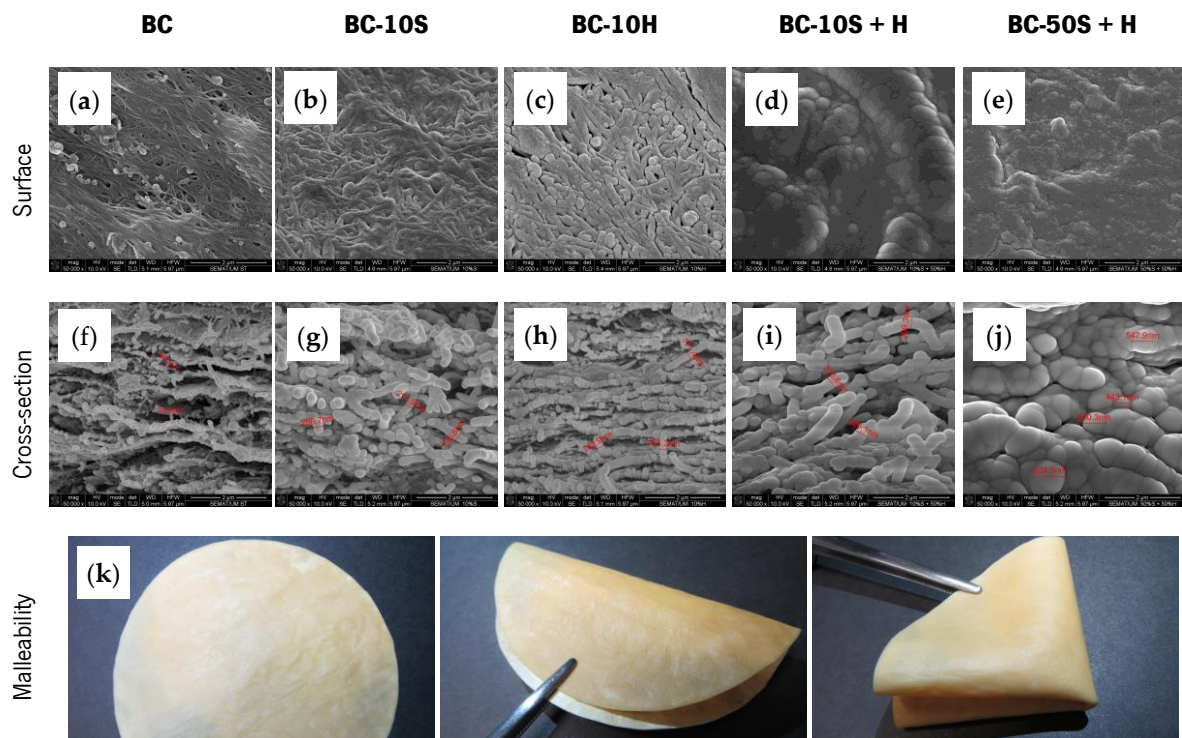


Figure 3. SEM micrographs of BC (**a,f**) and BC composites (10S (**b,g**); 10H (**c,h**); 10S + H (**d,i**); and 50S + H (**e,j**)), and photos showing the malleability (sample BC-50S + H) (**l**).

Table 14. Mass per unit area and percentage of polymers in brackets.

Mass per unit area ($\text{g}\cdot\text{m}^{-2}$) (% polymer)				
BC 54.9	BC-1S 78.9 (30%)	BC-10S 129.4 (58%)	BC-25S 173.2 (68%)	BC-50S 241.8 (77%)
	BC-1H 60.1 (9%)	BC-10H 84.6 (35%)	BC-25H 134.0 (59%)	BC-50H 197.0 (72%)
		BC-10S + H 85.0 (35%)	BC-25S + H 133.7 (59%)	BC-50S + H 222.6 (75%)

3.4.2. Atomic force microscopy (AFM)

The surface topography of the BC and its composites was also characterized using AFM. Figure 4 illustrates examples of three-dimensional AFM images of a scanned area of $10 \times 10 \mu\text{m}$, showing the values of the average roughness (Ra) and the root mean square (RMS) roughness.

The image recorded for the pure BC indicates that the dried membrane has an average surface roughness of 143 nm with a maximum height of 2.5 μm . Following polymer impregnation with 10S, the average roughness was reduced to 105 nm. It may be concluded that the micron-scale pores of the BC membrane became filled with the polymers, following treatment. In the case of 10H, no effect (within experimental variability) on the surface roughness was observed. These results are in accordance with the SEM observations, as above discussed. In contrast and associated with the highest increase in the mass per unit area, the addition of higher concentration of S increases the most (to 386 nm) the composite's surface roughness. Thereafter, these values decrease with the addition of more polymer **H** (BC-50S + H). Despite the 2-fold increase in the mass per unit area (Table 14), increasing the amount of **H** by 5 times (from 10H to 50H) only slightly increases the surface roughness.

It should be emphasized that the surface topography of the BC and BC composites were non-uniform, as can be noticed by the standard deviation values presented. The results from ANOVA tests show that Ra means difference are not significant at the 0.05 level, and RMS means are statistically different only between 50S with BC, 10S, 10H and 10S+H samples.

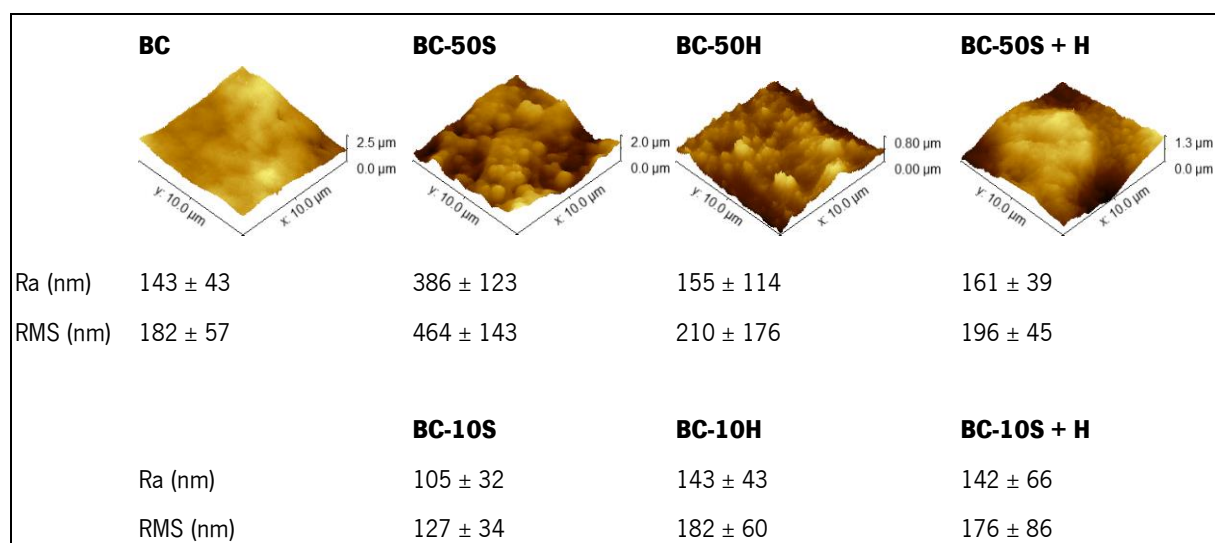


Figure 4. AFM micrographs and results of average roughness (Ra) and root mean square roughness (RMS) of BC and BC composites.

3.4.3. Fourier transform infrared (FT-IR)

FT-IR spectroscopy was used to characterize the composites. As seen in Figure 5, the spectrum of raw BC presents a band at around 3348 cm^{-1} that corresponds to O–H stretching. The absorption bands at 2985 cm^{-1} and 1419 cm^{-1} are assigned to the CH_2 and the peak at 1034 cm^{-1} to the vibrations of the glycosidic C–O–C bridges. The band at around 1635 cm^{-1} is assigned to adsorbed water (Garside and Wyeth, 2003; Yang *et al.*, 2017).

The main peaks for the samples treated with **S** based product are located at 3340 cm^{-1} (O–H and N–H stretching), 2962 cm^{-1} and 2916 cm^{-1} (asymmetric and symmetric CH_3 stretching in Si– CH_3), 1627 cm^{-1} and 1558 cm^{-1} (N–H deformation in amine groups), 1450 cm^{-1} and 1250 cm^{-1} (CH_3 asymmetric and symmetric bending in Si– CH_3), 1404 cm^{-1} (CH_2 bending), 1080 cm^{-1} and 1018 cm^{-1} (asymmetric and symmetric Si–O–Si stretching), 864 cm^{-1} and 787 cm^{-1} ($-\text{CH}_3$ rocking and Si–C stretching in Si– CH_3) (Hashem *et al.*, 2009; Cai *et al.*, 2010; Johnson *et al.*, 2013; Zhang *et al.*, 2018).

For BC samples treated with **H**, the main peaks observed are located at 3371 cm^{-1} (O–H stretching), 2916 cm^{-1} and 2854 cm^{-1} (C–H asymmetric and symmetric stretching), and at 1458 cm^{-1} (CH_2 in-plane bending). The characteristic peaks from the reactive acrylic group which is usually present in short-chain perfluorinated oligomers are detected at 1736 cm^{-1} (C=O stretching) and 1643 cm^{-1} (C=C stretching). Fluorinated functional groups are identifiable at 1350 cm^{-1} (terminal CF_3 group vibration), at 1234 cm^{-1} and 1188 cm^{-1} (asymmetric and symmetric stretching vibrations of CF_2 , respectively), and at 702 cm^{-1} (amorphous CF_2 deformation) (Mukherjee *et al.*, 2013; Joseph and Joshi, 2018).

The spectra obtained reveal the presence of the polymers in the interior (bulk) and exterior (surface) of the composites, when softener and hydrophobizer are used alone with BC. However, when combined formulations of **S + H** were used, **H** was not detected inside the composites.

The increase in the BC nanofibrils thickness (as observed by SEM) correlated well with the increase in the infrared absorption peaks' intensity, as the concentration of the applied products increased. Similar observations were recorded for all other mixtures (data not shown).

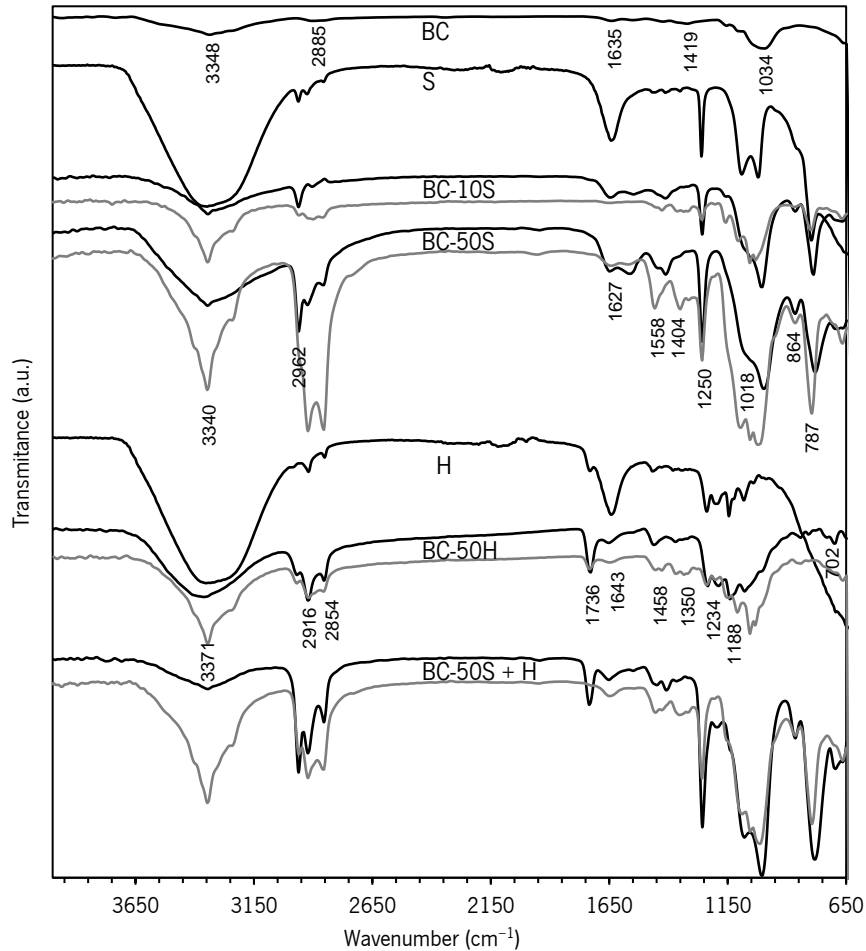


Figure 5. FT-IR spectra of BC, PDMS (S) and PFC (H) based formulations, and BC composites.

3.4.4. Water contact angle (CA) and surface free energy (SFE)

Hydrophobic surfaces may be obtained through the creation of hierarchical roughness or through the control of the surface chemistry, decreasing the surface energy (Mondal *et al.*, 2018). The introduction of hydrophobic polymers in BC membranes changed its surface wettability, as shown by static contact angle (Table 15) and water drop absorption over time (Figure 6), as assessed by contact angle (CA) measurements. As expected, the lowest water CA was measured on BC alone (63.8°). After incorporation of the polymers, overall, higher contact angles were obtained, indicative of more hydrophobic surfaces. It is important to mention that, alongside with surface chemistry, surface topography plays a role on wettability. The actual and apparent contact angle values can deviate from each other depending on the surface roughness. Surface hydrophobicity can be enhanced due to surface roughness (Zhao *et al.*, 2015). Thus, although slight differences were observed among the samples, these may be related to the surface topography and not just to the surface chemistry. As a

matter of fact, the BC fibres are well coated with **S** in the series of samples impregnated with 1% up to 50%, as observed by SEM; thus the differences observed cannot be assigned to surface chemistry only.

Table 15. Average contact angle values (°) measured for drops of water, PEG 200 and glycerol.

Sample	Water	PEG 200	Glycerol
BC	63.8 ± 4.7	38.3 ± 2.3	105.0 ± 4.1
BC-1S	126.2 ± 1.9	108.1 ± 2.2	126.4 ± 1.1
BC-10S	129.2 ± 0.5	115.2 ± 3.0	129.4 ± 1.3
BC-25S	128.4 ± 2.1	108.0 ± 2.8	125.3 ± 1.3
BC-50S	115.0 ± 4.4	98.4 ± 0.7	112.3 ± 1.5
BC-1H	89.4 ± 5.2	66.5 ± 1.7	125.7 ± 1.7
BC-10H	131.2 ± 2.7	101.2 ± 3.8	123.6 ± 2.7
BC-25H	128.3 ± 0.8	101.1 ± 1.0	127.3 ± 3.8
BC-50H	125.8 ± 2.5	101.5 ± 1.7	122.4 ± 3.3
BC-10S + H	135.4 ± 1.0	113.4 ± 1.8	124.7 ± 3.4
BC-25S + H	134.8 ± 1.0	117.4 ± 1.6	128.3 ± 1.1
BC-50S + H	127.6 ± 2.5	112.3 ± 0.9	123.7 ± 1.6

Despite the overall proximity in the values of the static contact angles between **S** and **H** composites, the later showed lower permeability to water, as observed from the significantly slower water absorption rates over time (Figure 6a and b). As a matter of fact, the use of **H** seems to provide water resistant properties more effectively. The reason for this clear trend is not obvious, taking in account the static contact angle or the surface energy (as discussed ahead), and may be related to the ultrastructure, namely porosity, of the composites.

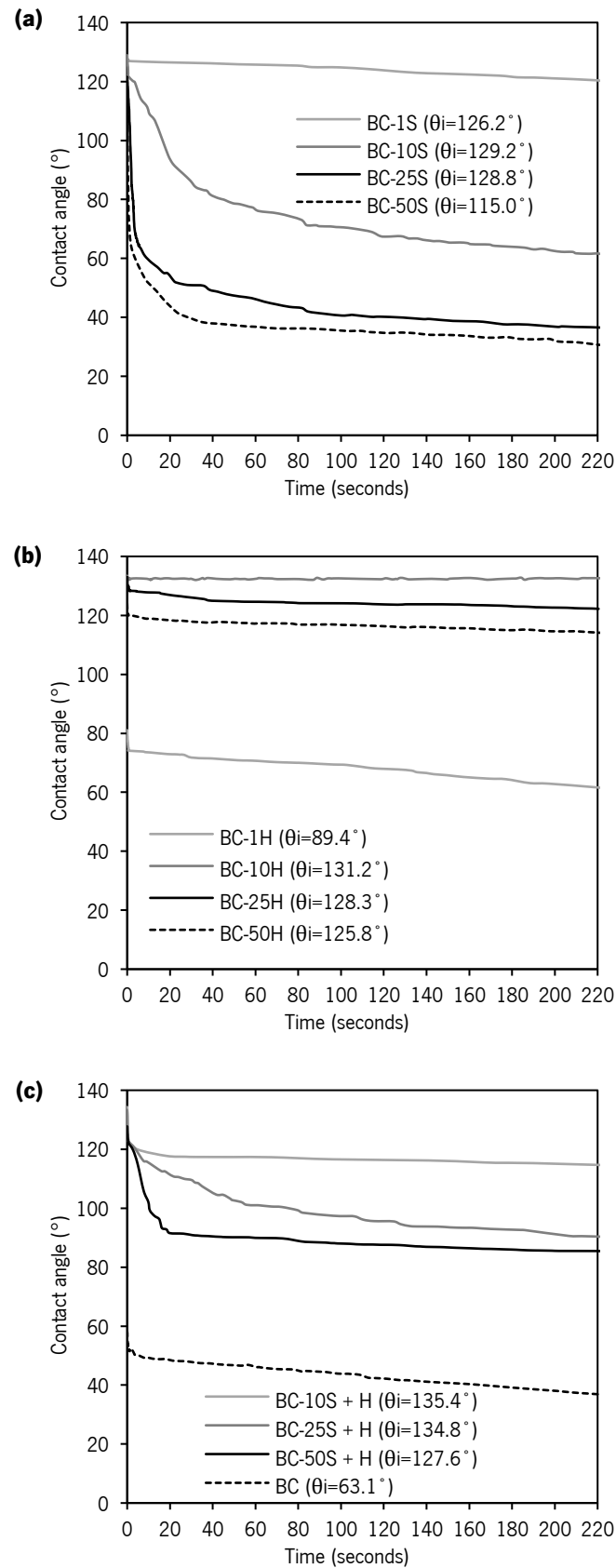


Figure 6. Contact angles over time of the BC composites produced with S **(a)**, H **(b)**, with S and H applied sequentially, and BC **(c)**.

The surface energy is an important variable to understand the wetting phenomena and can be determined from the measurement of the contact angles formed by liquids with different surface energies. Wu's approach (Wu, 1971) was used in this study for monitoring the surface energy and its components on the BC composites.

The polar and dispersive components of the surface free energy of unmodified BC and the BC composites are displayed in Figure 7. The results show that, overall, comparatively to BC, BC composites obtained by treatment with **S** or **H** and by sequential impregnation (**S+H**) had a noticeable decrease in the surface free energy, due to the reduction of the polar component.

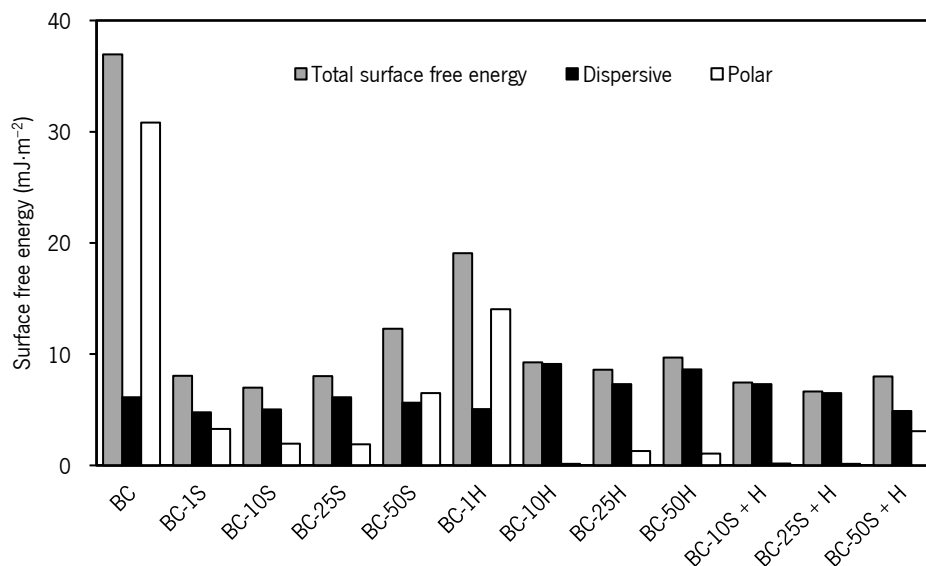


Figure 7. Total surface energy, dispersive and polar components, determined with the Wu method, using the initial contact angles of water, PEG 200 and glycerol.

3.4.5. Water vapor permeability (WVP) and static water absorption (SWA)

Breathability of textiles and leather products is commonly assessed through the measurement of water vapor permeability. This is very important for proper moisture management and to ensure the thermophysiological comfort of the human body. An adequate skin temperature balance must be achieved through perspiration and breathability (Tang, Kan and Fan, 2014; Mukhopadhyay, Preet and Midha, 2018).

As observed in Figure 8, the WVP values of the BC composites decreased when compared to the original dry BC. However, all BC composites were still breathable. Indeed, according to the technical report

ISO/TR20879 (ISO, 2007), that establishes the WVP performance requirements for upper footwear components, most of the composites are suitable to be used in footwear (casual footwear - $WVP \geq 192 \text{ g}\cdot\text{m}^{-2}\cdot 24 \text{ h}^{-1}$).

Also, with an increase in the amount of incorporated **S** or **H**, (as observed by the increase in the mass per unit area (Figure 8) and thickness (Table 18)) a decrease in the WVP was observed, as could be expected. In general, the sequential treatment using both polymers did not change significantly the WVP values, as compared to BC samples treated only with the softener.

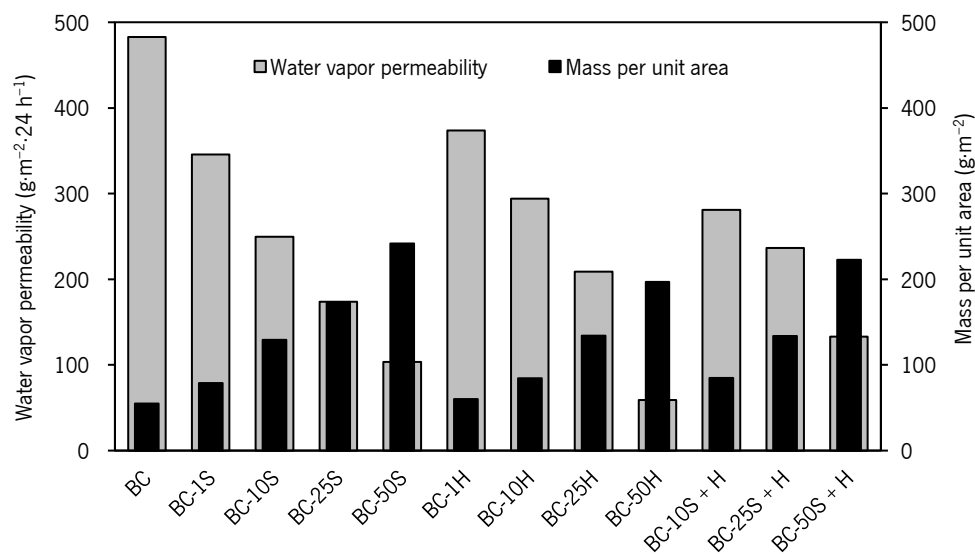


Figure 8. Water vapor permeability and mass per unit area.

The comfort of clothing and footwear is closely associated with both water vapor permeability and static water absorption. In the case of footwear, sweat is first absorbed by the lining and insole material and then the moisture is transferred to the exterior. The materials used inside the shoe should therefore have a good level of water absorption so that the sweat does not accumulate, causing discomfort. The recommended water absorption is a maximum of 60% after 120 min for uppers and a minimum of 100% for linings and insoles (Bitlisli *et al.*, 2005).

The static water absorption was in this work measured at 15, 30, 60 and 120 min. The results are shown in Figure 9. The composites with higher amounts of added polymers (50S, 50H and 50S + H) absorbed less than 60% of water after immersion for 120 min, thus being appropriate for uppers, whereas most of the other composites show an absorption higher than 100% and are more suitable to be used in linings and insoles.

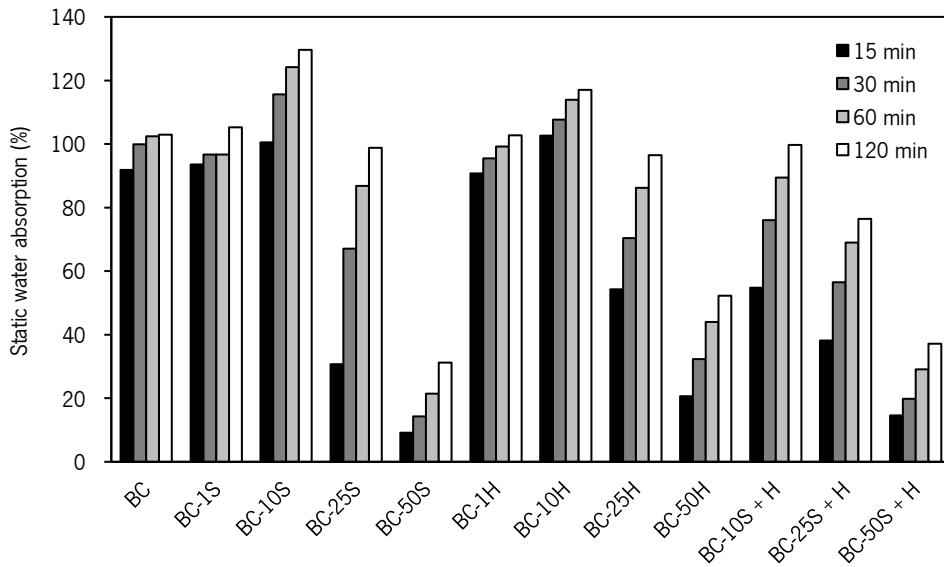


Figure 9. Static water absorption.

3.4.6. Mechanical properties

The characterization of the mechanical properties resulting from the tensile test are shown in Table 16. The tensile strength and elongation break of dried BC was found to be of 35.60 MPa and 3.44%, respectively. Incorporation of increasing amounts of **S** or **H** increased the thickness and the mass per unit area of the composites, while decreasing the WVP. Unexpectedly, the mechanical properties of the composite did not follow this progression. Regarding the incorporation of softener, maximum tensile strength values were of 42.64 MPa (1S), whereas the maximum elongation at break observed was 7.67% (50S). As for the hydrophobizer, the maximum values of tensile strength and elongation at break were observed, respectively, for 10% and 25% of polymer impregnation. As observed by SEM, the BC composites with lower amounts of polymer absorbed formed thicker fibers. Additionally, the high interfacial interaction between the added polymers and the cellulose nanofibers through hydrogen bonding allows an efficient distribution of the stress, resulting in an improvement of the mechanical properties. However, as the concentration of the added products increase, the tensile strength and Young modulus start to decrease. This observation can be explained by the complete coating of surface hydroxyl groups of the cellulose nanofibers, preventing their contribution to the mechanical strength and elasticity through H-bonding. As previously reported (Soykeabkaew *et al.*, 2009; Gea *et al.*, 2010; Asgher, Ahmad and Iqbal, 2017), the strong attractive hydrogen bonding between cellulose nanofibers tends to weaken owing to extensive surface coating, affecting negatively the mechanical properties. In our composites, the quantity of BC (reinforcement) is constant. As more polymers (matrix) are incorporated, the relative

percentage of the reinforcement decreases, the behavior of the composite becoming increasingly governed by the matrix. Therefore, the mechanical strength and elasticity of the composite becomes gradually dependent on the intermolecular bonding of the matrix polymers. In the case of the softener polydimethylsiloxane, the weak intermolecular forces between the methyl groups yield very low tensile strength (Paquien *et al.*, 2005; Jin *et al.*, 2018). Also, fluorine atoms have low polarizability that results in low surface energies and thus weak cohesive forces between fluorocarbon molecules (Lemal, 2004).

It is also observed that samples with higher amounts of incorporated polymers have higher elongation, due to the greater mobility allowed between the different layers of the BC membrane. Finally, no significant differences were achieved by sequentially incorporating **H** in samples pretreated with **S**. Overall, taking as reference the technical report ISO/TR20879 (ISO, 2007), that establishes the performance requirements for uppers components for footwear, the composites present suitable mechanical properties [casual footwear – Breaking strength $\geq 10 \text{ N}\cdot\text{mm}^{-1}$, elongation $\geq 7\%$ (along)]. Regarding tensile strength, all samples are above or near the reference value, although regarding the elongation at break only 50S, 25H and 25S + H samples match the requirements.

Table 16. Thickness, Young's modulus, tensile strength, and elongation at break.

Sample	Thickness (mm)	Young's modulus (MPa)	Tensile strength (MPa) ^a	Elongation at break (%)
BC	0.30 ± 0.01	9.19 ± 0.30	35.60 ± 3.10	3.44 ± 0.08
BC-1S	0.34 ± 0.01	18.38 ± 6.15	42.64 ± 7.26	3.45 ± 0.82
BC-10S	0.48 ± 0.03	6.14 ± 0.78	35.61 ± 2.59	5.10 ± 0.17
BC-25S	0.63 ± 0.04	1.57 ± 0.28	27.18 ± 1.40	6.90 ± 1.55
BC-50S	0.73 ± 0.02	1.35 ± 0.50	16.31 ± 0.26	7.67 ± 0.27
BC-1H	0.30 ± 0.01	23.10 ± 2.37	40.04 ± 10.36	2.82 ± 0.73
BC-10H	0.34 ± 0.02	11.72 ± 1.56	48.35 ± 8.80	5.92 ± 0.83
BC-25H	0.50 ± 0.02	3.90 ± 0.21	27.78 ± 0.77	7.97 ± 0.65
BC-50H	0.61 ± 0.08	3.35 ± 0.85	25.46 ± 2.18	6.04 ± 0.39
BC-10S + H	0.37 ± 0.02	5.17 ± 0.38	37.25 ± 3.92	5.48 ± 0.29
BC-25S + H	0.53 ± 0.02	3.37 ± 0.90	31.78 ± 6.71	8.94 ± 0.95
BC-50S + H	0.77 ± 0.03	2.32 ± 0.62	17.29 ± 0.63	6.37 ± 0.72

First set: 1S/25S; BC/50S; 1S/50S; 10S/50S; 25S/50S; Second set: 10H/25H; 10H/50H; Third set: BC/50S + H; 10S + H/50S + H; 25S + H/50S + H.

^a Multiple comparison tests between BC and each set of composites, means difference is significant at the 0.05 level.

3.5. Conclusion

In this study, through an exhaustion process, BC fibers were surface modified with Persoftal MS Con.01 and Baygard EFN, resulting in malleable and mechanically resistant composites, with hydrophobic character and breathability. The new BC-based composites may offer a sustainable alternative to cotton, leather and man-made cellulosic fibers, thus exhibiting strong potential for further high value-added differentiation and sustainable consumer products such as textiles and leather. BC-based composites may be regarded as strategic materials with enormous potential, focusing on natural and organic products development and represent an alternative to materials used today in textile and shoe industries.

Chapter 4

Development of BC/PDMS/PEG/AESO composites²

4.1. Abstract

Bacterial cellulose (BC) obtained by static culture was used to produce bio-based composites. A mixture of an amino-polydimethylsiloxane-based (PDMS) softener, polyethyleneglycol (PEG) 400 and acrylated epoxidized soybean oil (AESO), was incorporated into the BC membranes through an exhaustion process. The results show that BC composites with distinct performances can be easily designed by simply varying the polymers percentage contents. This strategy represents a simple approach towards the production of BC-based composites.

² This chapter is based on the following publication:

Silva, F. A. G. S., Fernandes, M., Souto, A. P., Ferreira, C., Dourado, F. and Gama, M. (2019) "Optimization of bacterial nanocellulose fermentation using recycled paper sludge and development of novel composites," *Applied Microbiology and Biotechnology*, 103(22), pp. 9143–9154.

4.2. Introduction

Acrylated epoxidized soybean oil (AESO) is obtained from soybean oil, a renewable resource abundantly available, via epoxidation and acryloilation. It contains three highly reactive functionalities, double (C=C) bonds, –OH groups, and epoxy rings. The C=C bonds in AESO is capable of self-polymerizing and copolymerizing with other components via a free-radical initiation, forming a three-dimensional network (Liu *et al.*, 2018).

Bacterial cellulose (BC) membranes were used for the development of nanocomposites, using formulations that includes: (i) a commercial softener based on polydimethylsiloxane (PDMS) (conferring malleability, robustness and softness); (ii) polyethyleneglycol (PEG) 400 (as a plasticizer, allowing to obtain a product with greater elasticity as well as contributing to improve the interfacial adhesion between the BC and the other polymers) and (iii) acrylated epoxidized soybean oil (AESO) (yielding a high biobased content BC composite with hydrophobic character). A simple and effective approach was developed, based on the use of an exhaustion process, aiming to produce BC nanocomposites.

4.3. Materials and methods

4.3.1. Materials

BC membranes were offered by Satisfibre S.A. (Portugal). Soybean oil, epoxidized acrylate (Sigma-Aldrich, Steinheim, Germany), Lauryl methacrylate (97%) (Acros Organics, Geel, Belgium), 1,6-hexanodiol diacrylate (80%) (Sigma-Aldrich, Steinheim, Germany), Tri (propylene glycol) diacrylate (Sigma-Aldrich, Steinheim, Germany), tert-Butyl peroxybenzoate (98%) (Sigma-Aldrich, Steinheim, Germany), Polyethylene glycol 400, (Merck Millipore, Darmstadt, Germany), were used as received without further purification. The softener Persoftal MS Conc.01 (Tanatex Chemicals) consists of an non-ionic aqueous dispersion of Siloxanes and Silicones, 3-((2-aminoethyl)amino)propyl Me, diMe, hydroxy-terminated (10-20%), with density of 0.99 g·cm⁻³ (23 °C) and viscosity of 405 mPa·s (23 °C).

4.3.2. Composites production

BC membranes were used as a scaffold for the production of composites by the incorporation of a mixture of Persoftal MS Conc.01 (PDMS-based polymer), PEG 400 and the resin AESO. AESO has a low cross-linking density and thus inferior mechanical strength due to the existence of long aliphatic chains

and low degree of unsaturation in AESO molecules. Also, it has high viscosity at room temperature that restricts its processability (Liu *et al.*, 2018). To reduce these limitations, a mixture containing different reactive monomers added to AESO (coded “AESO mixture”, Table 17), was prepared as follows (in mass percentages): AESO (50%), lauryl methacrylate (38.5%), 1,6-hexanodiol diacrylate (5%), tri(propylene glycol) diacrylate (5%), and the initiator tert-Butyl peroxybenzoate (1.5%). This mixture was prepared 24 h prior to use where all products were mixed and then placed under magnetic stirring for 1 h at 500 rpm.

For the composites’ production, purified wet BC membranes with about 3.0 cm in thickness, with a size of 13.0 × 16.0 cm and weighting 700 g were used. The membranes were first mechanically pressed to remove the excess of adsorbed water to a final wet mass of 135 g, corresponding to 5.5% dry mass in BC and a thickness of around 0.5 cm. The compressed membranes were then treated with the different polymers at different combination, by an exhaustion process, as detailed in Table 17.

Table 17. Formulations used in the production of BC composites.

Sample	Persoftal MS (g)	PEG 400 (g)	AESO mixture (g)
BC	-	-	-
BC-S ¹	75	0	0
BC-S/PEG400	60	15	0
BC-S/PEG400/AESO	20	20	35

¹S: Softener

For this, the pressed BC membranes were placed inside the stainless-steel cups and the polymers’ mixture was added at a mass ratio of BC:polymer mixture of 1:10.

The exhaustion process was then carried out in an Ibelus machine equipped with an infrared heating system, using stainless-steel cups with a capacity of approximately 220 cm³, with a rotation of 50 rpm, for 40 cycles. The desired temperature (60 °C) was achieved using a gradient of 2 °C·min⁻¹. The treatment lasted for 2 days at 60 °C, after which the samples were oven dried (WTC binder oven) at 90 °C for 24 h (until constant mass), followed by a curing step for 3 h at 180 °C.

4.3.3. Physical-chemical properties evaluation

4.3.3.1. *Fourier transform infrared (FT-IR) spectroscopy*

FT-IR spectra of the BC and BC composites were collected in the attenuated total reflection mode (ATR) at a spectral resolution of 16 cm^{-1} , with 60 scans, over the range $650\text{--}4000\text{ cm}^{-1}$ at room temperature, using a Nicolet Avatar 360 FT-IR spectrophotometer (Madison, WI, USA).

4.3.3.2. *Scanning electron microscopy (SEM)*

The surface morphology and cross section of the BC and BC composites was examined using an ultra-high-resolution field emission gun scanning electron microscopy (SEM) instrument (NOVA 200 Nano SEM, FEI Co. Hillsboro, OR, USA). To analyze the cross section, the samples were fractured after immersion in liquid nitrogen. All samples were coated with a thin layer of Au/Pd.

4.3.3.3. *Wettability*

The wettability of the samples was characterized via static contact angle measurements, performed using a Dataphysics instrument (Filderstadt, Germany) using OCA20 software (version 1.5, Dataphysics instrument, Filderstadt, Germany) with a video system for the capture of images in static mode, using the sessile drop method. A drop of $5\text{ }\mu\text{L}$ of distilled water was positioned on the composite's surface with a microliter syringe and observed over time for 180 s. At least five measurements at different places were taken for each sample. To measure the angle formed at the liquid/solid interface, images were captured with a special charge-coupled device camera that takes an image every 0.04 s.

4.3.3.4. *Water vapor permeability (WVP)*

WVP was evaluated according to the Standard BS 7209:1990 (British Standards Institution, 1990). According to this method, the test specimen is sealed over the top of a test dish which contains 46 mL of distilled water and the assembly is placed on a rotating turntable and allowed to rotate, under isothermal conditions, for a period of one hour to establish the equilibrium of water vapor pressure gradient across the sample. After this period the assembly is weighted and allowed to rotate for 24 h, and is weighted again. The result is represented by the Equation (2) and expressed in $\text{g}\cdot\text{m}^{-2}\cdot 24\text{ h}^{-1}$ (section 3.3.3.5).

4.3.3.5. Mechanical properties

For the tensile strength measurements, the full width of the sample (25 mm) was fixed and a length that allows an initial distance between the clamps of the strength tester equipment (Hounsfield HSK100, Salfords, UK) of 100 mm was set out between grips; the samples were then submitted to tensile. Three samples of each material were tested at a constant speed of 100 mm·min⁻¹.

4.4. Results and discussion

As observed from the increase in the thickness, specific mass and polymer content of the BC composites (Table 18), the exhaustion process effectively allowed the impregnation of BC with different formulations of Persoftal (S), PEG and AESO. The obtained composites were characterized by ATR FT-IR, SEM, contact angle and mechanical properties.

Table 18. Thickness, mass per unit area and polymers content of BC composites.

Sample	Thickness (mm)	Mass per unit area (g·m ⁻²)	Polymers content (%)
BC	0.48	325.5	
BC-S	0.97	808.8	59.8
BC-S/PEG400	1.09	1012.4	67.9
BC-S/PEG400/AESO	0.96	763.6	57.4

4.4.1. ATR FT-IR analyses of BC and BC composites

ATR FT-IR spectroscopy was used to characterize BC and its composites. As seen in Figure 10, the BC spectrum shows characteristic peaks of cellulose, such as the –OH stretching peak around 3344 cm⁻¹, CH stretching of alkanes and asymmetrical stretching of CH₂ at 2919 cm⁻¹, –OH bending of adsorbed water at 1650 cm⁻¹, CH₂ bending deformation at 1426 cm⁻¹ and 1366 cm⁻¹, –OH deformation at 1334 cm⁻¹, C–O–C deformation modes and stretching vibrations at 1159–1107 cm⁻¹, C–O–C and C–OH stretching vibration of the sugar ring at 1054–1029 cm⁻¹, and C–OH out-of-plane bending mode at 665 cm⁻¹ (Araújo *et al.*, 2018; Kawee, Lam and Sukyai, 2018; Yu *et al.*, 2018; Wahid *et al.*, 2019).

In the BC-S/PEG400 composite, the increase of some absorption bands can be attributed to PEG400, although they overlap with signals from cellulose and modified amino-PDMS. These bands are located at 3392–3346 cm⁻¹ (–OH stretching), 2962–2873 cm⁻¹ (CH₂ stretching), 1409 cm⁻¹ (asymmetric CH₂

deformation), 1351 cm^{-1} (CH_2 wagging), 1258 cm^{-1} (CH_2 twisting), $1076\text{--}1006\text{ cm}^{-1}$ (CH_2 symmetric deformation, C–O–C and C–OH stretching), and 950 cm^{-1} and 864 cm^{-1} (CH_2 rocking). Another peak at 1721 cm^{-1} (C=O stretching) can be a result of ester linkages between PEG and the surface hydroxyl groups of BC (Finocchio *et al.*, 2014; Araki and Mishima, 2015). With the incorporation of AESO, the main differences are observed in the spectrum of the inner part of the composite, where the characteristic peaks of the modified amino-PDMS at 794 cm^{-1} (NH_2 wagging) and 1258 cm^{-1} (Si-CH_3) disappear. This may indicate that AESO is essentially concentrated inside the composite. As observed by SEM, the internal and surface layers of the composite display a different morphology.

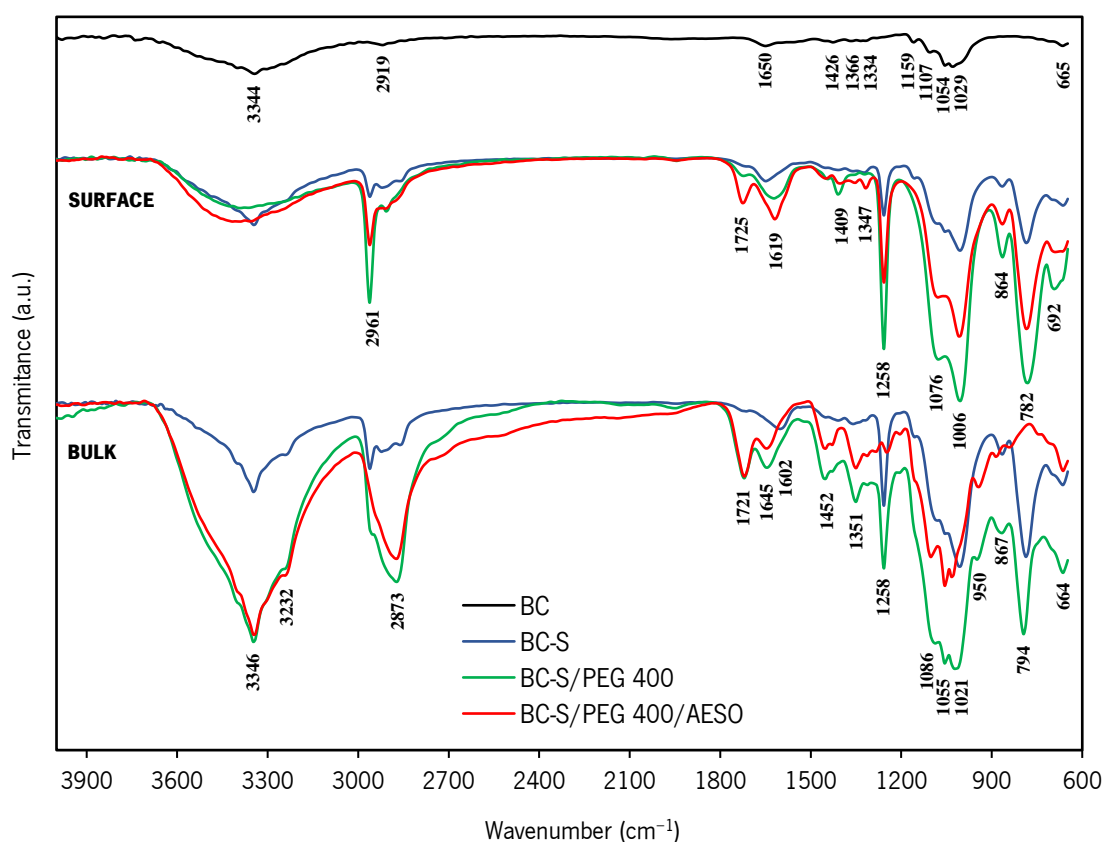


Figure 10. ATR-FT-IR spectra of BC and BC composites.

The spectra of both the surface and inner parts of the BC-S composite showed the emergence of high-intensity peaks located at 1258 cm^{-1} , corresponding to Si-CH_3 , and located at 798 cm^{-1} which is attributed to NH_2 wagging (Mohd *et al.*, 2016). The spectrum of the inner part of the composite also shows a new peak, located at 1602 cm^{-1} , assigned to NH_2 bending vibration. The vibration band attributed to Si–O–Si and Si–O–C bond ($1150\text{--}1135\text{ cm}^{-1}$), which corresponds to the condensation reaction between silanol

and hydroxyl group of cellulose and self-condensation reaction between silanol groups, is difficult to analyze as they overlap with the C–O–C skeletal vibration band. However, both spectra, surface and inner, show an increase in the intensity of these peaks, suggesting that the softener was grafted onto the –OH functional groups of BC (Mohd *et al.*, 2016; Saini *et al.*, 2016; Shao *et al.*, 2017). An increase of the band at 2862–2961 cm^{-1} , related to the CH_2 stretching vibrations of the propyl group was also observed (Saini *et al.*, 2016; Shao *et al.*, 2017).

4.4.2. Scanning electron microscopy (SEM)

To analyze the microstructure of the BC and its composites, SEM micrographs of the surface as well as of the cross sections were collected. As illustrated in Figure 11, the treatment of BC membranes with different polymers led to significant changes in their morphology. The characteristic three-dimensional nanofibrillar network was clearly observed on the surface of BC. In the composites, BC fibers are perfectly covered with the polymers and an increment of the fiber's diameter is observed, associated with a more compact and uniform surface.

The cross-section micrographs of all nanocomposites displayed the typical lamellar morphology of BC uniformly coated. Contrarily, for BC-S/PEG400/AESO, a distinct layer was detected, where nanofibers cannot be clearly distinguished. The impregnation process is performed under agitation; thus, it is likely that colloidal particles of the several polymers of the formulation will form, facilitating its penetration in the BC network.

We can speculate that the AESO mixture and modified amino-PDMS formed some agglomerates that remained mostly on the surface of the composite, whereas the AESO blend being in greater quantity penetrated to larger extent into the membrane. As shown by FT-IR (Figure 10), in the spectrum of the inner AESO composite, the presence of modified amino-PDMS was not detected. Upon drying the agglomerates filled almost all the pores provided a more compact surface where individual BC fibers are not visible. Images at higher magnifications also provided evidence of the strong interfacial adhesion between BC nanofibrils and the polymers, as shown by the cross-section images after fracturing and the homogeneous dispersion within the BC network, individual cellulose fibers being no longer visible.

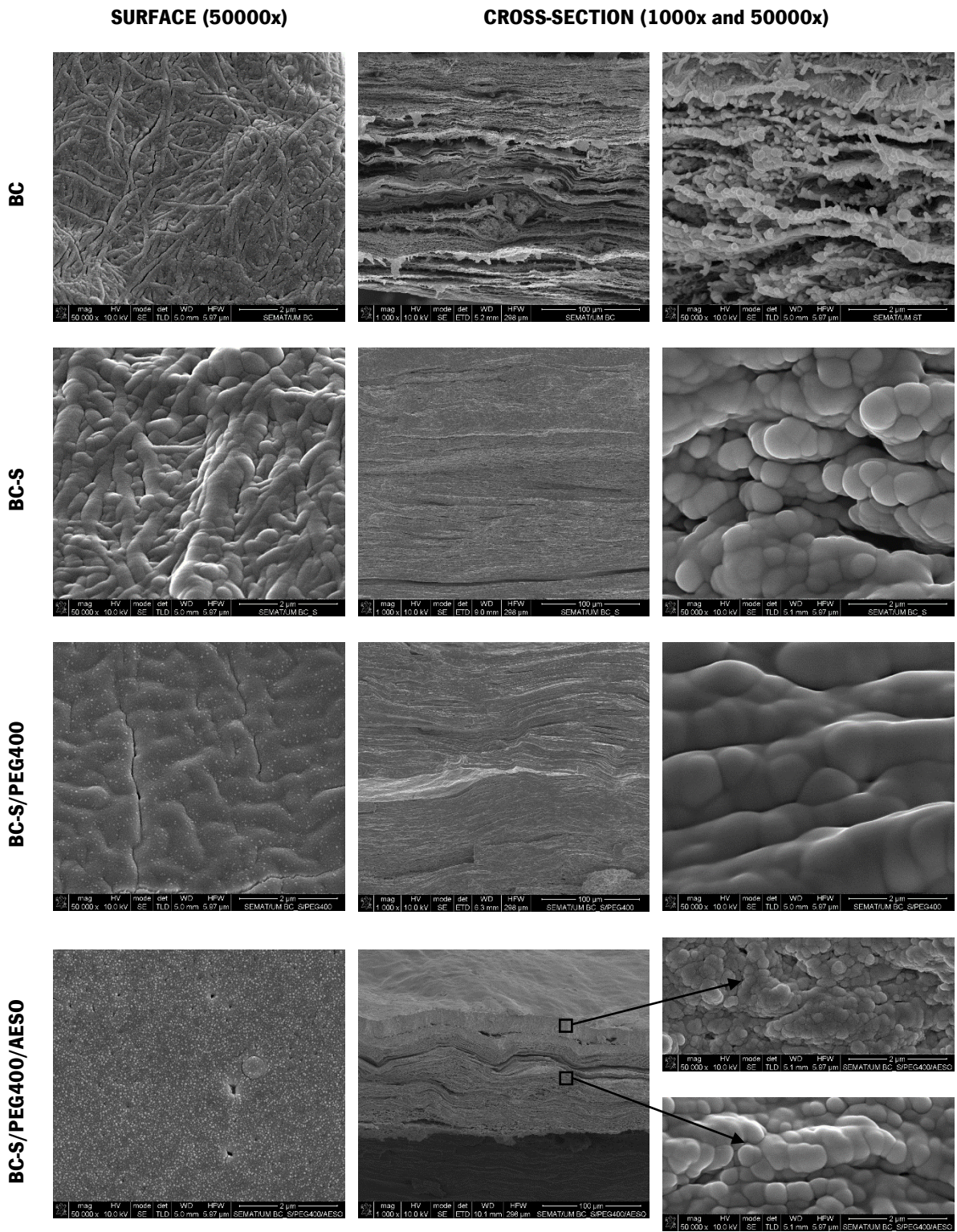


Figure 11. SEM images of BC and BC composites.

4.4.3. Wettability

The water contact angles analysis (Figure 12) further confirm the impregnation of the BC membranes, changing its surface wettability and offering better hydrophobicity compared with pure BC. The initial water contact angle increased in order BC < BC-S < BC-S/PEG400 < BC-S/PEG400/AESO. The surface flatness of the composites increases in the same order, as qualitatively assessed by SEM.

It is well accepted that the water–solid contact angle varies with a combined effect of both surface chemistry and roughness of the surface (Yousefi *et al.*, 2018). Thus, although topography may partially justify the increase in contact angle (the higher porosity of BC may contribute to a lower contact angle), this result is mainly related to the lower surface energy of the hydrophobic compounds impregnated with the composites. The more hydrophobic surface was obtained for BC-S/PEG400/AESO composite. The water contact angles for this surface was as high as 114.7° , indicating a low-energy surface with nonpolar functionalities from the incorporation of modified amino-PDMS and AESO resin. The water absorption/spreading profile over time can be a result from the surface pores that allows the access to polar groups or a capillary effect, but again the AESO containing composite is more resistant to the absorption/spreading processes (Li *et al.*, 2019).

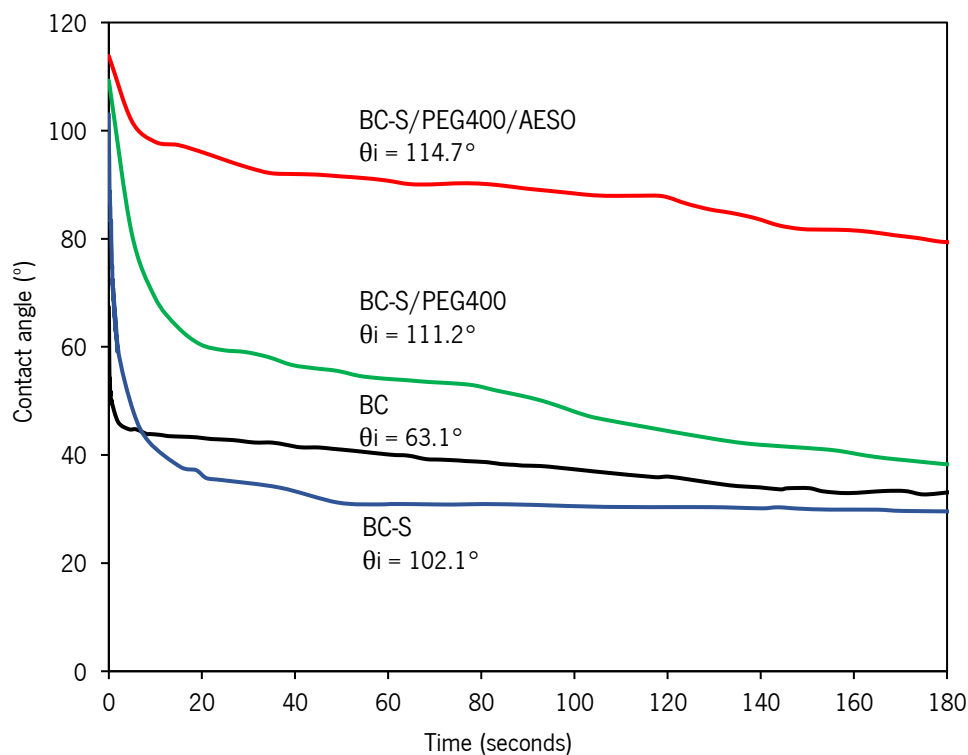


Figure 12. Contact angle of BC and BC composites.

4.4.4. Water vapor permeability (WVP)

The breathability, expressed in water vapor permeability (WVP), of textile and leather materials is an important property to assure body comfort. As observed in Figure 13, the WVP values of the BC composites decreased when compared to the original dry BC. However, all BC composites were still breathable. In solid polymers, the water vapor permeation mechanism is determined by a sequential process of adsorption/absorption, diffusion and desorption, first, water molecules adsorb onto the material's surface, until an equilibrium is established. Then the water molecules diffuse through the material driven by a concentration gradient and finally desorption occurs from the opposite surface (Lu, Tian *et al.* 2016). As shown by the results, water vapor could easily permeate through pure BC. Cellulose is strongly hydrophilic and although the molecular chains pack tight together after drying, water molecules can easily interact with the abundant hydroxyl groups on the cellulose molecules through hydrogen-bonds followed by diffusion (Li, Zhou *et al.* 2019). When modified amino-PDMS was incorporated into the BC matrix, the WVP values decreased noticeably. This composite presents better water resistance when compared with cellulose, affecting the adsorption process. In contrast, the addition of PEG400 to BC-S composite, increased WVP value due to its hydrophilic character. Although AESO has a hydrophobic character, there is an increase WVP. As observed from SEM, BC-S/PEG400/AESO composite possesses an irregular structure along its cross-section. We can speculate that some incompatibility between the polymers leads to the formation of agglomerates, creating more free volume and relative short pathway for water molecules to diffuse.

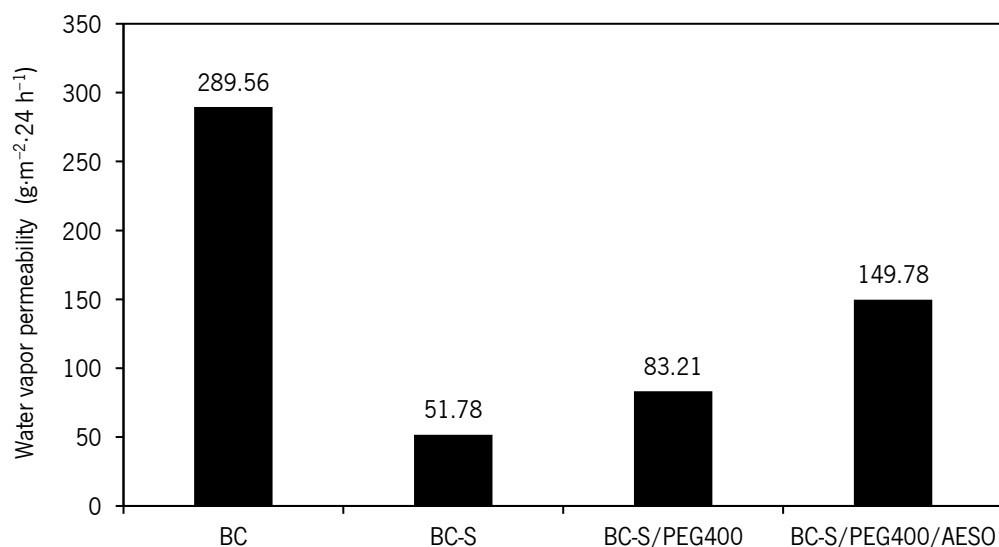


Figure 13. Water vapor permeability of BC and BC composites.

4.4.5. Mechanical properties

SEM and FT-IR analysis of the composites suggest that a good interfacial adhesion between the polymers mixture and BC was achieved. Despite the high amounts of the polymers impregnated (Table 18), the behavior of the composite is also governed by the BC matrix. Compared to BC, the mechanical properties of the composites were dramatically reduced, as shown in Figure 14. The biggest obstacle for the practical application of composites is the poor stress transfer between the reinforcement and polymer matrix. Generally, the stress transfer between the two phases is strongly dependent on the degree of interfacial bonding (Wei and McDonald, 2016). So, a lower tensile strength than that of neat BC was expected, as PDMS is an amorphous polymer and BC membrane is a highly crystalline material; also, the addition of other polymers to BC membrane detracts the inter-molecular hydrogen bonds between the BC fibers, decreasing the tensile strength of the composite.

The introduction of PEG did not significantly improve the tensile strength but the elongation at break increased noticeably. PEG can act as a plasticizer, providing more space between the BC fibers. On the other hand, when the AESO mixture was added, and since it was well dispersed in the matrix and, probably a better fiber-matrix interface bonding was formed, restricting the motion of PDMS molecule chains, which increased the stress transfer, resulting in a composite with higher tensile strength.

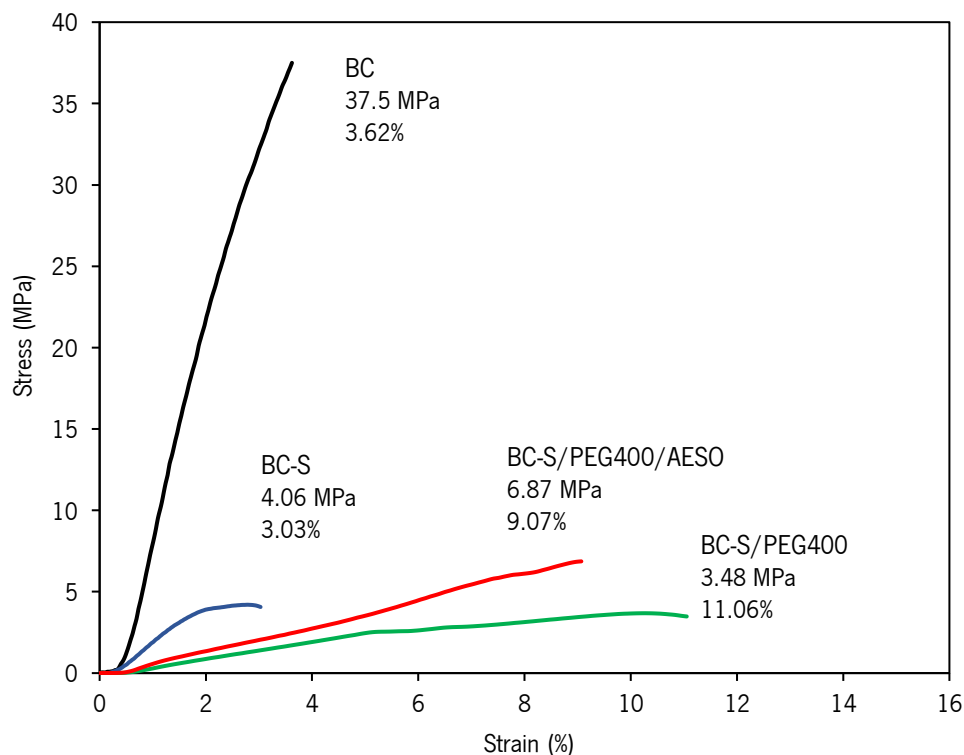


Figure 14. Stress-strain averaged curves of BC and BC composites obtained up to the rupture point

4.5. Conclusion

New BC-based composites with a high degree of sustainability were successfully produced through exhaustion with modified amino-PDMS, PEG 400 and AESO. FT-IR and SEM analyses provided evidence of the incorporation of these polymers into the BC membrane, resulting in its hydrophobic performance. Although BC has been used for the reinforcement of composites by several authors, there are very few studies using the intact BC membrane obtained by static fermentation, thus keeping intact the 3D BC network.

Chapter 5

Development of BC/emulsified AESO composites³

5.1. Abstract

This research investigated the development of bio-based composites comprising bacterial cellulose (BC), as obtained by static culture, and acrylated epoxidized soybean oil (AESO) as an alternative to leather. AESO was first emulsified; polyethylene glycol (PEG), polydimethylsiloxane (PDMS) and perfluorocarbon-based polymers were also added to the AESO emulsion, with the mixtures being diffused into the BC 3D nanofibrillar matrix by an exhaustion process. Scanning electron microscopy (SEM) and Fourier transform infrared (FT-IR) spectroscopy analysis demonstrated that the tested polymers penetrated well and uniformly into the bulk of the BC matrix. The obtained composites were hydrophobic and thermally stable up to 200 °C. Regarding their mechanical properties, the addition of different polymers lead to a decrease in the tensile strength and an increase in the elongation at break, overall presenting satisfactory performance as a potential alternative to leather.

³ This chapter is based on the following publication:

Fernandes, M., Souto, A. P., Gama, M. and Dourado, F. (2019) "Bacterial cellulose and emulsified AESO biocomposites as an ecological alternative to leather," *Nanomaterials*, 9(12), pp. 1710–1727.

5.2. Introduction

The tannery industry faces several challenges associated with high environmental impact, scarcity of raw materials and increasing consumer demand for environmentally friendly products. The worldwide production of leather is approximately 20 billion square feet per year (FAO, 2015). To produce 1 ton of leather, 6.7 tons of raw skin (Kanagaraj *et al.*, 2015), 57,000 liters of water (Wool, 2013), and 3.35 tons of chemicals are required (Black *et al.*, 2013). Worldwide, for bovine skin, 370 billion liters of water are consumed annually, generating 6.5 million tons of solid waste. This research intends to contribute to the reduction of the animal hide dependency by the development of composites from bacterial cellulose (BC) as structuring material and activated vegetable oils as a flexibilizing, mechanical reinforcing and hydrophobizing agent. BC is a biopolymer produced by bacterial fermentation that consists exclusively of a three-dimensional structure of pure cellulose nanofibers. Chemically, BC is identical to vegetable cellulose but the nano-scale of its fibers offers a significantly higher surface area (Wang, Tavakoli and Tang, 2019).

Vegetable oils (VOs) are abundant renewable resources with an increasing number of industrial applications. They offer the advantages of low cost, nontoxicity and biodegradability (Zhu *et al.*, 2004; Kim *et al.*, 2010; López and Santiago, 2013; Saithai *et al.*, 2013). Among the VOs, soybean oil is one of the most attractive due to its low price and abundant availability. To increase their reactivity, double bonds can be replaced by more reactive functional groups such as epoxide, acrylate, hydroxyl or maleate (Grishchuk and Karger-Kocsis, 2011; Saithai *et al.*, 2013; Senoz *et al.*, 2013; Gandini and Lacerda, 2015). Most commonly, double bonds are epoxidized and then acrylated, reacting with carboxyl groups of acrylic acids, allowing free radical polymerization (Gandini and Lacerda, 2015; Liu, Madbouly and Kessler, 2015).

Acrylated epoxidized soybean oil (AESO) has been studied extensively in the production of composites with high renewable content (Khot *et al.*, 2001; Akesson, Skrifvars and Walkenström, 2009; Lee *et al.*, 2013; Senoz *et al.*, 2013; Ramamoorthy *et al.*, 2014, 2018; Kocaman *et al.*, 2017; Liu *et al.*, 2018; Temmink, Baghaei and Skrifvars, 2018). Regarding leather and analogues, AESO was surface-grafted onto goat leather using UV-radiation (Nunez, Santiago and Lopez, 2008). A recent patent (Wool, 2013) demonstrated the possibility of manufacturing ecological leather analogues by mixing natural fibers with epoxidized and acrylated triglycerides and vinyl monomers, the mixture being chemically polymerized. The composite was then deposited in suitable molds and hot pressed. In another work (Cao *et al.*, 2013), an environmentally friendly leather substitute was developed by reinforcing a mixture of AESO resin with

cotton fabrics. Later, an ecological leather composed of organic cotton fabrics and AESO/MLAU (methacrylated lauric acid) (50/50) resin was tested in footwear (Cao *et al.*, 2014). Although the authors presented this product as water-resistant and breathable, no tests were performed to support these claims. Composites of BC with modified soybean oil have also been reported, namely in the development of composite foams (Blaker *et al.*, 2009; Koon-Yang Lee *et al.*, 2011; Sousa *et al.*, 2017) and optically transparent composites (Retegi *et al.*, 2012).

From the above, as is the purpose of this work, it is expected that by combining never dried BC membranes, as obtained by microbial fermentation, with a biodegradable polymer such as AESO, it may be possible to produce a truly green nanocomposite with potential applications in the leather industry. BC constitutes a three-dimensional polymeric structure with interconnected fibers, with macroporosity and therefore high aptitude to the anchorage of the AESO emulsified particles. Further, using emulsified VOs as low-cost natural substrates obviates the need to surface-modify BC, thus simplifying the preparation of BC-based composites while not affecting the BC's native properties. This strategy represents a novel and promising approach towards the development of an environmentally friendly product, exclusively from biological and recyclable materials, at low water and energy production costs.

5.3. Materials and methods

5.3.1. Materials

Bacterial cellulose membranes were offered by Satisfibre S.A. (Braga, Portugal). Soybean oil, epoxidized acrylate (Sigma-Aldrich, Steinheim, Germany), lauryl methacrylate (97%) (Acros Organics, Geel, Belgium), 1,6-hexanodiol diacrylate (80%) (Sigma-Aldrich, Steinheim, Germany), tri(propylene glycol) diacrylate (Sigma-Aldrich, Steinheim, Germany), Triton X-100 (Sigma-Aldrich, Steinheim, Germany), Span 80 (Sigma-Aldrich, Steinheim, Germany), isobutanol (Merck Millipore, Darmstadt, Germany), cumene hydroperoxide (80%) (Sigma-Aldrich, Steinheim, Germany), cobalt naphthenate (6%) (Sigma-Aldrich, Steinheim, Germany), and polyethylene glycol 400 (Merck Millipore, Darmstadt, Germany), were used as received. Persoftal MS Conc.01 and Baygard EFN (Tanatex Chemicals) were offered by ADI Center (Santo Tirso, Portugal).

5.3.2. Preparation of the acrylated epoxidized soybean oil (AESO) mixture

AESO was used in this work to produce a hydrophobic composite with high bio-based content. AESO is synthesized from soybean oil (renewable resource abundantly available) via epoxidation and acryloilation. It contains three highly reactive functionalities, double (C=C) bonds, –OH groups, and epoxy rings. The C=C bond in AESO is capable of self-polymerizing and copolymerizing with other components via a free-radical initiation, forming a three-dimensional network. However, it has a low crosslinking density and thus inferior mechanical strength due to the existence of long aliphatic chains and low degree of unsaturation in AESO molecules. Also, it has high viscosity at room temperature that restricts its processability (Liu *et al.*, 2018). To reduce these limitations, a mixture was prepared by adding different reactive monomers to AESO at room temperature. This mixture was composed of acrylated epoxidized soybean oil (50% m/m); lauryl methacrylate (40% m/m)-a fatty acid-based reactive diluent, potentially bio-based, which reduces the viscosity of the mixture (Cousinet *et al.*, 2015); 1,6-hexanodiol diacrylate (5% m/m); and tri(propylene glycol m/m) diacrylate (5% m/m)-bifunctional monomers which can enhance the crosslinking (Wei *et al.*, 2019).

5.3.3. Determination of the required hydrophilic–lipophilic balance (HLB) and AESO emulsion stability evaluation

The Hydrophilic–Lipophilic Balance (HLB) values are generally considered vital for the stabilization of surfactant-based emulsions. Tritons and Spans are a range of non-ionic surfactants stable in mild alkalis, acids and electrolytes and have no reaction with ionic ingredients or actives. To prepare stable AESO emulsions, the effect of HLB was first studied by preparing different combinations of two non-ionic surfactants (Triton X-100 and Span 80) and a co-surfactant (Butanol) in a ratio of 2:1, as presented in Table 19. The HLB values of the mixed surfactants were calculated by Equation (4) (ICI Americas Inc., 1980):

$$HLB_{mix} = (HLB_A X_A) + (HLB_B X_B) + (HLB_C X_C), \quad (4)$$

where HLB_{mix} , HLB_A , HLB_B , and HLB_C are the HLB values of the mixture, Triton X-100, Span 80, and Butanol, respectively, and X_A , X_B and X_C are the weight percentages of every surfactant in the mixture. HLB values from 5.20 (more lipophilic or oil soluble) up to 11.33 (more hydrophilic or water soluble) were obtained.

The oil-in-water (O/W) emulsions were prepared with a mass ratio of 20:2:78 (AESO mixture/surfactant combination/water), as follows: 2 g of the surfactant combination (Table 19) were added to 20 g of the AESO mixture, followed by the addition of 78 g of deionized water. The mixture was emulsified using a homogenizer (Unidrive X 1000 D, CAT, Staufen, Germany) at a speed of 30,000 rpm, for 1, 5 and 10 min. This process was carried out in an ice bath to avoid temperature rise during emulsification. After this, the emulsions were stored in test tubes at room temperature to investigate their stability over time (up to 10 days) under conditions of varied HLB and stirring time. The stability was evaluated by visually recording signs of phase separation and creaming; the droplet morphology of the emulsions was investigated by optical microscopy using a Leica DM750 M microscope (Leica Microsystems, Wetzlar, Germany) with a Leica MC 170HD camera, using a 10× eyepiece lens and 100× objective lens.

Table 19. Combinations of surfactants used to study the effect of HLB on the AESO emulsion stability.

Surfactant Combination	Triton X-100 (%) (HLB = 13.5) ¹	Span 80 (%) (HLB = 4.3) ¹	Butanol (%) (HLB = 7.0) (ICI Americas Inc., 1980)	HLB_{mix}
A	0.00	66.67	33.33	5.20
B	19.57	47.10	33.33	7.00
C	41.31	25.36	33.33	9.00
D	66.67	0.00	33.33	11.33

¹ Values taken from the technical specification sheets

5.3.4. Exhaustion of BC membranes with emulsified AESO

To test the incorporation of AESO in BC membranes, an emulsion was prepared by adding the initiator cumene hydroperoxide (CHP) (3% m/m) and the catalyst cobalt naphthenate (CONP) (0.8% m/m) to the AESO mixture. This initiator permits the polymerization of AESO at low temperatures (Dweib *et al.*, 2006), which prevents the aggregation or coalescence of the emulsified AESO particles. An emulsion with HLB of 11.3 (Table 19-D), which provided the best results obtained in the storage stability studies, was prepared using the same procedure described in section 5.3.3.

BC membranes (with about 3.0 cm in thickness, with a size of 12.0 × 2.5 cm and weighting 90 g) were each treated by exhaustion with 100 g of emulsified AESO mixture for 9 days at 40 °C (Sample 1) followed by a 3 h curing step at 90 °C (Sample 2), to accelerate the cross-link of the emulsified AESO mixture. The composites were then dried at 40 °C in an oven (WTC series, Binder GmbH, Tuttlingen, Germany) for 5 days. To avoid shrinkage of the samples during drying, the composites were attached to a zinc-plated wire support. Regarding the exhaustion process, it was carried out in an Ibelus machine (IL-720, Labelus, Braga, Portugal) equipped with an infrared heating system, using stainless-steel cups with a capacity of approximately 220 cm³, with a rotation of 50 rpm, 40 cycles, and a temperature gradient of 2 °C·min⁻¹. Samples were collected after the exhaustion process and before drying, for analysis by scanning electron cryomicroscopy (described below).

5.3.5. Production of composites with different polymers

Several composites were also produced by adding other polymers to the pre-emulsified AESO mixture. These were PEG 400, Persoftal MS Conc.01 (PDMS-based softener (S)) and Baygard EFN (perfluorocarbon-based hydrophobizer (H)). Softeners (Persoftal) and hydrophobizers (Baygard) used in the textile industry

are usually liquid dispersions or emulsions that, in addition to active agents (polysiloxanes or fluorocarbons), contain emulsifiers (e.g. ethoxylated fatty alcohols), dispersants, defoamers. Details on the characteristics of Persoftal and Baygard are presented in Table 13 (section 3.3.1). PEG is a polymer with functionalities such as steric stabilization, which can be used to prevent particle agglomeration (Lima, Souza and Rosa, 2018); it is a nonionic surfactant able to form long chain structures in aqueous solution; it is also a plasticizer agent with the ability to increase molecular spacing, thus offering flexibility (Khalaf *et al.*, 2019).

To produce the composites, BC membranes (with about 3.0 cm in thickness, with a size of 12.0 × 13.0 cm and weighting 450 g) were first squeezed to a final wet mass of 100 g. Then the compressed membranes were each treated by exhaustion with 100 g of an aqueous mixture as shown in Table 20, adding water to complete the 100 g.

Table 20. Proportions of the polymers in the aqueous mixture used in the production of BC composites.

Sample	AESO Emulsion (g)	PEG 400 (g)	Persoftal MS (g)	Baygard EFN (g)
BC/AESO	75	-	-	-
BC/AESO/PEG	75	4.5	-	-
BC/AESO/S	75	-	18	-
BC/AESO/PEG/S	75	4.5	18	-
BC/AESO/H	75	-	-	18
BC/AESO/PEG/H	75	4.5	-	18
BC/AESO/PEG/S/H	75	4.5	9	9

For the preparation of these mixtures, the AESO mixture emulsion was first prepared as described on sections 5.3.3 and 5.3.4. Then PEG, Persoftal or Baygard were added and the mixture was stirred at 500 rpm for 1 min.

The exhaustion treatment lasted for 5 days at 30 °C, in the same equipment above described, after which the samples were oven dried for 5 days at 40 °C, followed by a curing step for 3 h at 90 °C. As before, to avoid shrinkage of the samples during drying and curing, the composites were attached to a zinc-plated wire support.

The polymer content in the final composites was calculated through the Equation (5):

$$\text{Polymer Content} = \left(\frac{W_{\text{composite}} - W_{\text{BC}}}{W_{\text{composite}}} \right) \times 100, \quad (5)$$

where $W_{\text{composite}}$ corresponds to the dry mass of the composite, and W_{BC} corresponds to the dry mass of BC.

5.3.6. Characterization of the BC-based composites

5.3.6.1. Scanning electron cryomicroscopy (Cryo-SEM)

SEM analyses of the BC and BC composites were performed using a high-resolution Scanning Electron Microscope (JEOL JSM 6301F, JEOL, Tokyo, Japan) with X-Ray Microanalysis (Oxford INCA Energy 350, Oxford Instruments, Abingdon, England) and a CryoSEM (Gatan Alto 2500, Gatan, Pleasanton, CA, USA). The non-dried specimens were rapidly cooled (plunging it into sub-cooled nitrogen-slush nitrogen) and transferred under a vacuum to the cold stage of the preparation chamber. Then the samples were fractured, sublimated ('etched') for 120 s at -90 °C, and coated with Au/Pd by sputtering for 45 seconds with a 12 mA current. Afterward, the samples were transferred into the SEM chamber and analyzed at a temperature of -150 °C.

5.3.6.2. Scanning electron microscopy (SEM)

Analyses of the surface and cross-section morphology of the dried BC and BC composites were done using an ultra-high-resolution field emission gun SEM instrument (NOVA 200 Nano SEM, FEI Co. Hillsboro, OR, USA). To analyze the cross-section, the samples were first freeze-fractured with liquid nitrogen and coated with a thin layer of Au/Pd.

5.3.6.3. Fourier transform infrared (FT-IR) spectroscopy

A Nicolet Avatar 360 FT-IR spectrophotometer (Madison, WI, USA) was used to record the FT-IR spectra of the dried BC sheet and BC composites. The spectra were collected in the attenuated total reflection mode (ATR) at a spectral resolution of 16 cm^{-1} , with 60 scans, over the range 650 – 4000 cm^{-1} at room temperature. A background scan with no sample and no pressure was acquired before the spectra of the samples were collected.

5.3.6.4. Contact angle (CA) and surface free energy (SFE)

The surface wettability was accessed by contact angle measurements carried out in a DataPhysics instrument (Filderstadt, Germany) with a video system for the capture of images every 0.04 s in static mode using the sessile drop method, using OCA20 software (version 1.5, Dataphysics instrument, Filderstadt, Germany). A drop of 5 μL of distilled water was placed on the dried composite's surface with a microliter syringe and observed with a special charge-coupled device camera. Afterward, the water contact angle was observed over time for 180 s. At least five measurements at different places were taken for each sample. To calculate the surface energy (γ_s) of the BC composites and their polar (γ_s^p) and dispersive (γ_s^d) components, the Wu method (harmonic-mean) was used, Equation (1) (section 3.3.3.4) (Wu, 1971).

The following liquids with known surface energy and surface energy components were used: distilled water (γ : 72.8; γ^d : 29.1; γ^p : 43.7); polyethylene glycol 200 (γ : 43.5; γ^d : 29.9; γ^p : 13.6); and glycerol (γ : 63.4; γ^d : 37.4; γ^p : 26.0), units in $\text{mJ}\cdot\text{m}^{-2}$ (Oliveira *et al.*, 2013).

5.3.6.5. Differential scanning calorimetry (DSC)

DSC curves were obtained on a Mettler-Toledo DSC822 instrument (Giessen, Germany). Samples weighing about 5–7 mg (the exact mass was recorded before each assay) were heated in hermetically-sealed aluminum pans and tested in the temperature range of 25 to 450 $^{\circ}\text{C}$ at a heating rate of 10 $^{\circ}\text{C}\cdot\text{min}^{-1}$, under inert nitrogen atmosphere at 80 $\text{mL}\cdot\text{min}^{-1}$ flow rate.

5.3.6.6. Thermogravimetric analysis (TGA)

Thermogravimetric analysis was carried out in a Hitachi STA7200 (Tokyo, Japan). Samples weighing 5–7 mg (the exact mass was recorded before each assay) were placed in platinum pans and tested from 25 to 600 $^{\circ}\text{C}$ at a heating rate of 10 $^{\circ}\text{C}\cdot\text{min}^{-1}$ under a nitrogen flow rate of 200 $\text{mL}\cdot\text{min}^{-1}$.

5.3.6.7. Mechanical properties

Tensile strength and elongation at break measurements were evaluated according to the standard ISO 17706:2003 (ISO, 2003). The overall width of the sample (25 mm) was fixed and a length that allows an initial distance between the clamps of the tester equipment (Hounsfield HSK100, Salfords, UK) of 75 mm

was set out in grips and subjected to tensile and tear. Three samples of each dried material were tested at a constant speed of $100 \text{ mm}\cdot\text{min}^{-1}$.

5.4. Results and discussion

5.4.1. Emulsions stability and diffusion into BC

Both the HLB value of the surfactant mixture (Triton-X100/Span 80/Butanol) and emulsification time had a significant effect on the stability of the O/W emulsions, as evaluated by visual observation over 10 days. As shown in Figure 15b, at HLB of 5.20, the lowest creaming formation was observed in emulsions prepared with longer mixing times. Increasing the HLB value to 11.33, hence increasing the hydrophilic ratio of the surfactant's mixture, allowed for the stabilization of the emulsion for up to 10 days (Figure 15f), regardless of the emulsification time, as no creaming was observed after 10 days of storage.

The optical microscopy images of the emulsions prepared with different HLB values were taken immediately following preparation. At lower HLB (Figure 15a,c), emulsions exhibit larger droplet size (possibly containing also some multivesicular droplets, Figure 15a) and size variability, as opposed to those with higher HLB. Thus, a surfactants mixture with HLB 11.33 and 10 min of emulsification was selected for further work.

After determining the best HLB value for the preparation of the AESO emulsions, impregnation of BC was done through the exhaustion process. This process commonly used in textile technology involves placing the fabric or yarn in a chamber containing water and treatment products. The chamber is then sealed and the treatment solution heated and submitted to heavy stirring, which results in the products transitioning from the water to the fabric or yarn. This procedure was adopted in this work to process the BC membranes, incorporating the AESO emulsion into the cellulosic porous network. Although several authors addressed the development of composites using BC fibers, very few papers use the intact membranes obtained by static fermentation, as it is demonstrated in this work.

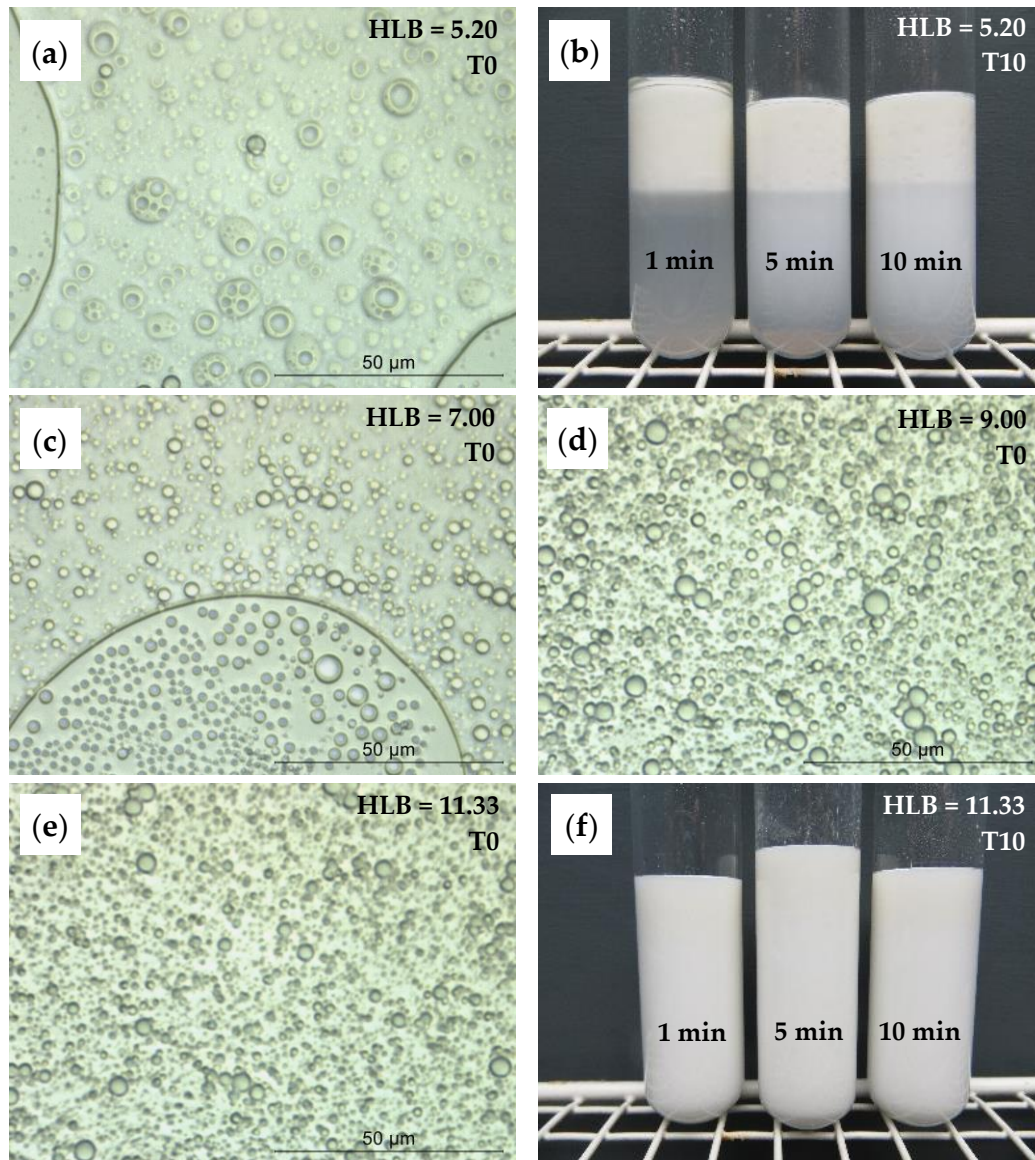


Figure 15. Optical micrographs (100 \times magnification) of freshly prepared AESO emulsions with different HLB and after 10 min of emulsification: **(a)** HLB 5.20, **(c)** HLB 7.00, **(d)** HLB 9.00, and **(e)** HLB 11.33; and visual appearance of AESO emulsions at different times of emulsification after 10 days storage: **(b)** HLB 5.20 and **(f)** HLB 11.33.

To confirm the presence of AESO particles inside the BC 3D nanofibrillar matrix, the composite samples were examined by Cryo-SEM. Figure 16 shows the 3D porous fiber network structure of BC (Figure 16a) and of the AESO particles adsorbed onto the surface of the nanofibers (Figure 16b), after 9 days at 40 $^{\circ}$ C, showing no signs of particle aggregation or coalescence. However, by increasing the temperature to 90 $^{\circ}$ C for 3 h, during the exhaustion process (Figure 16c), the coalescence of the AESO particles was observed, possibly due to the emulsion breakdown at a higher temperature and to lower viscosity, associated with an incomplete polymerization. Figure 16d shows a SEM micrograph of the dried BC/AESO

composite at a higher magnification. The collapse of the BC porous structure is observed upon drying, producing a structure with packed AESO particles. Further work was performed by drying the material at 40 °C before post curing at 90 °C, attempting to control the coalescence to some extent.

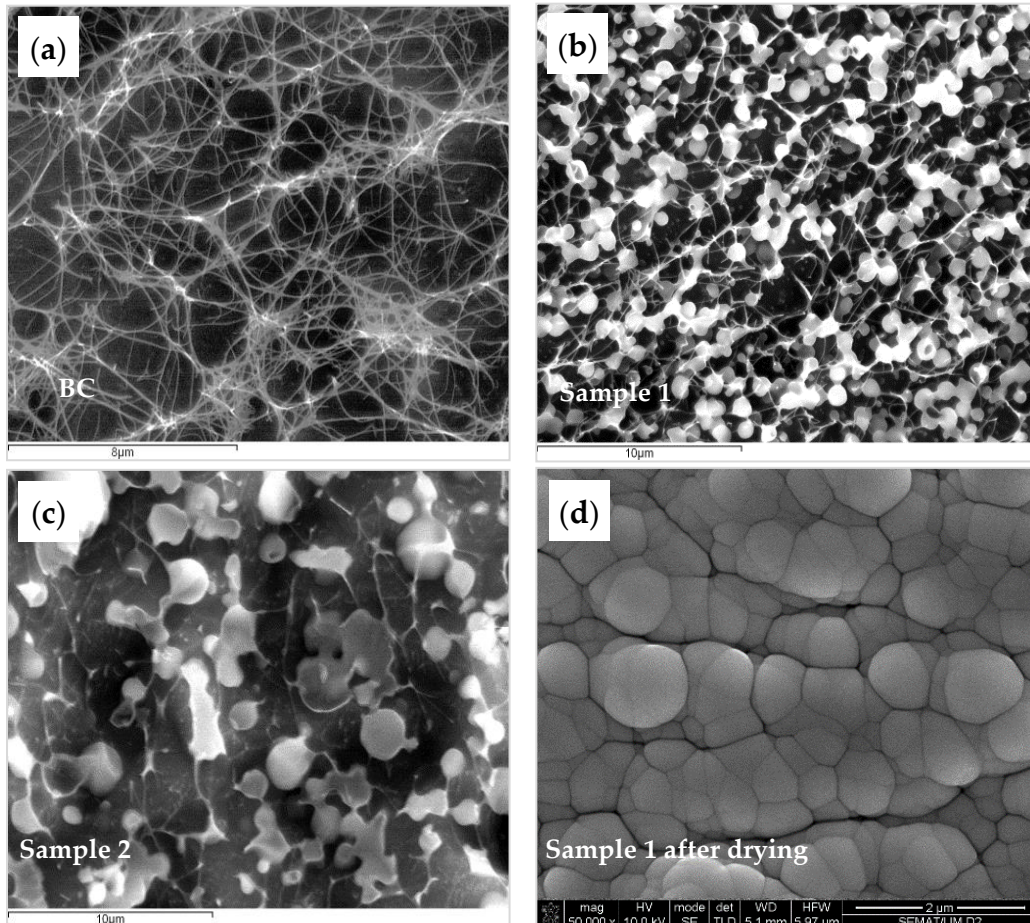


Figure 16. CryoSEM images: (a) BC membrane, (b) after exhaustion with AESO emulsion for 9 days at 40 °C (Sample 1), (c) after exhaustion with AESO emulsion for 9 days at 40 °C + 3 h at 90 °C (Sample 2); and (d) SEM image of the Sample 1 after drying at 40 °C.

5.4.2. Morphological Analysis

BC-based composites were also obtained through exhaustion with AESO emulsion combined with other polymers. The morphological properties of the dried BC and BC-based composites were evaluated by SEM (Figure 17). As expected, the surface and cross-section of dried BC (Figure 17a,e) presented a compacted structure of nanofibers, due to the replacement of cellulose–water–cellulose by cellulose–cellulose hydrogen bonding, the nanofibers being randomly arranged in layers with pores on the surface

and throughout the BC matrix (Khan *et al.*, 2018). The cross-section SEM analysis of the dried BC composites (Figure 17f–l) confirmed a good bulk penetration of the emulsified polymers during the exhaustion process, coating the BC nanofibers and promoting a more compact and bulky structure, as compared to native BC. SEM images of the surface of the BC composites (Figure 17b–d) show that the polymers also covered the membrane's surface, resulting in a rougher structure where the nanofibers are not distinguished. While sphere-like particles can be observed in cross-section images, the possibility of particle coalescence during drying cannot be excluded. Despite the complete coverage of the fibers by the polymers, the characteristic stratified BC structure is still observed in some cases (ex. BC/AESO: Figure 17f, and BC/AESO/PEG/H: Figure 17h).

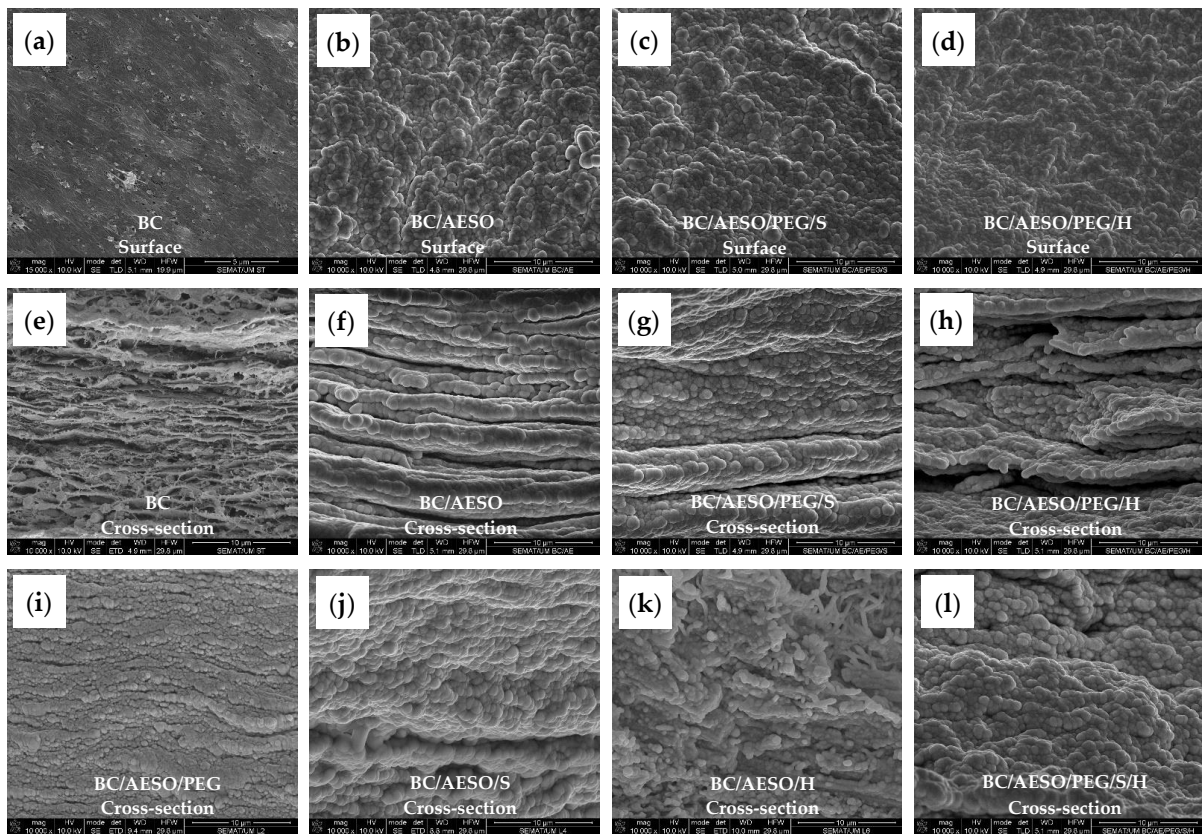


Figure 17. SEM images of BC and BC composites: surface and cross-section images, **(a,e)** BC; **(b,f)** BC/AESO; **(c,g)** BC/AESO/PEG/S; **(d,h)** BC/AESO/PEG/H; and cross-section images **(i)** BC/AESO/PEG, **(j)** BC/AESO/S, **(k)** BC/AESO/H, and **(l)** BC/AESO/PEG/S/H. Magnification: 15,000 \times (scale: 5 μ m) (a) and 10,000 \times (scale: 10 μ m) (b–l).

As compared to BC, the composites presented an increase in thickness and in the mass per unit area, due to the incorporation of the polymers (Table 21), which varied with the formulation. As compared to

BC impregnated with AESO mixture, both the added softener (S, Persofter) and hydrophobizer (H, Baygard) presented lower impregnation. However, the opposite effect is observed adding PEG to either S, H or both mixtures, suggesting that PEG promoted a higher BC impregnation content. In the case of the mixtures of AESO, S and/or H, it is not possible to determine whether these were incorporated into BC in the same proportions as that of the emulsified AESO.

Table 21. Thickness, mass per unit area and polymer content of the composites.

Sample	Thickness (mm)	Mass Per Unit Area ($\text{g}\cdot\text{m}^{-2}$)	Polymers content (%)
BC	0.48	238.0	-
BC/AESO	0.78	686.4	65.3
BC/AESO/PEG	0.55	576.0	58.7
BC/AESO/S	0.51	552.0	56.9
BC/AESO/PEG/S	0.79	921.6	74.2
BC/AESO/H	0.48	478.4	50.3
BC/AESO/PEG/H	0.72	886.4	73.1
BC/AESO/PEG/S/H	0.95	1032.5	76.9

5.4.3. Fourier transform infrared (FT-IR)

Fourier transform infrared (FT-IR) spectroscopy was used to characterize the functional groups on the dried BC and BC composites' surfaces (Figure 18). BC spectrum exhibited the characteristic cellulose vibration peaks, namely, -OH stretching peak at 3344 cm^{-1} , C-H stretching at 2919 cm^{-1} , -OH bending at 1650 cm^{-1} , $\text{-CH}_2\text{-}$ bending at 1426 cm^{-1} , C-O-C deformation modes and stretching vibrations at $1159\text{--}1107\text{ cm}^{-1}$, C-O-C and C-OH stretching vibration of the sugar ring at $1054\text{--}1029\text{ cm}^{-1}$, and C-OH out-of-plane bending mode at 665 cm^{-1} (Alonso *et al.*, 2018; He *et al.*, 2018; Sun *et al.*, 2018).

The spectrum of the BC/AESO composite showed a peak at 3343 cm^{-1} corresponding to the stretching vibrations of -OH groups. The peaks at $2922\text{--}2855\text{ cm}^{-1}$ and at $1457\text{--}1406\text{ cm}^{-1}$ are attributed to the asymmetric stretching vibrations and deformation of C-H in the $\text{-CH}_2\text{-}$ and -CH_3 bonds, respectively, assigned to the inherent aliphatic sequences of AESO. Another significant peak at 1721 cm^{-1} is attributed to the stretching vibration of C=O in esters and the one at 1637 cm^{-1} is ascribed to the double-bond signals of acrylate functionalities (-CH=CH_2). The peaks at 1295 cm^{-1} and $1163\text{--}1053\text{ cm}^{-1}$ correspond to C-O groups and C-O-C stretching vibration of ester, respectively. Finally, the peak at 811 cm^{-1}

corresponds to the bending vibration of =C–H, the double bonds on AESO characteristic of the epoxide group (Lu *et al.*, 2014; W. Liu *et al.*, 2017; Mandal and Maji, 2017).

In the BC/AESO/PEG composite, the increase of some absorption bands can be attributed to PEG400, although they overlap with signals from cellulose and AESO mixture. These bands are located at 3345 cm^{-1} (–OH stretching), 2918–2854 cm^{-1} (CH_2 stretching), 1644 cm^{-1} (–OH bending), 1456 cm^{-1} (asymmetric CH_2 deformation), 1351 cm^{-1} (CH_2 wagging), 1095–1029 cm^{-1} (CH_2 symmetric deformation, C–O–C and C–OH stretching), 950 cm^{-1} (CH_2 rocking), and 664 cm^{-1} (C–OH out-of-plane bending) (Araki and Mishima, 2015; Lima, Souza and Rosa, 2018).

In the composite BC/AESO/S, the appearance of new peaks was observed, namely, at 1258 cm^{-1} (CH vibration in Si– CH_3) and at 791 cm^{-1} (NH_2 and Si– CH_3), confirming the incorporation of modified amino-PDMS into the BC composite (Mohd *et al.*, 2016; Wu *et al.*, 2018; Zhang *et al.*, 2018). When PEG 400 was used in the polymer mixture, it was also observed at the peak at 1575 cm^{-1} that is attributed to the vibration modes of NH_2 groups (Zargar, Nourmohammadi and Amosbediny, 2015). The vibration bands of Si–O–C and Si–O–Si bridges at around 1165–1011 cm^{-1} are difficult to analyze as they overlap with the C–O–C vibrations from BC and PEG (Saini *et al.*, 2016; Shao *et al.*, 2017).

In the composites with perfluorocarbon (for BC/AESO/PEG/H), it was possible to identify the bands associated with CF_2 groups (asymmetric and symmetric CF_2 stretching at 1234 and 1141 cm^{-1} respectively and ‘amorphous’ CF_2 deformations at 702 cm^{-1}) (Mukherjee *et al.*, 2013). While in the composite BC/AESO/PEG/S/H, perfluorocarbon peaks are difficult to identify as they overlap with the characteristic peaks of the PDMS-based polymer.

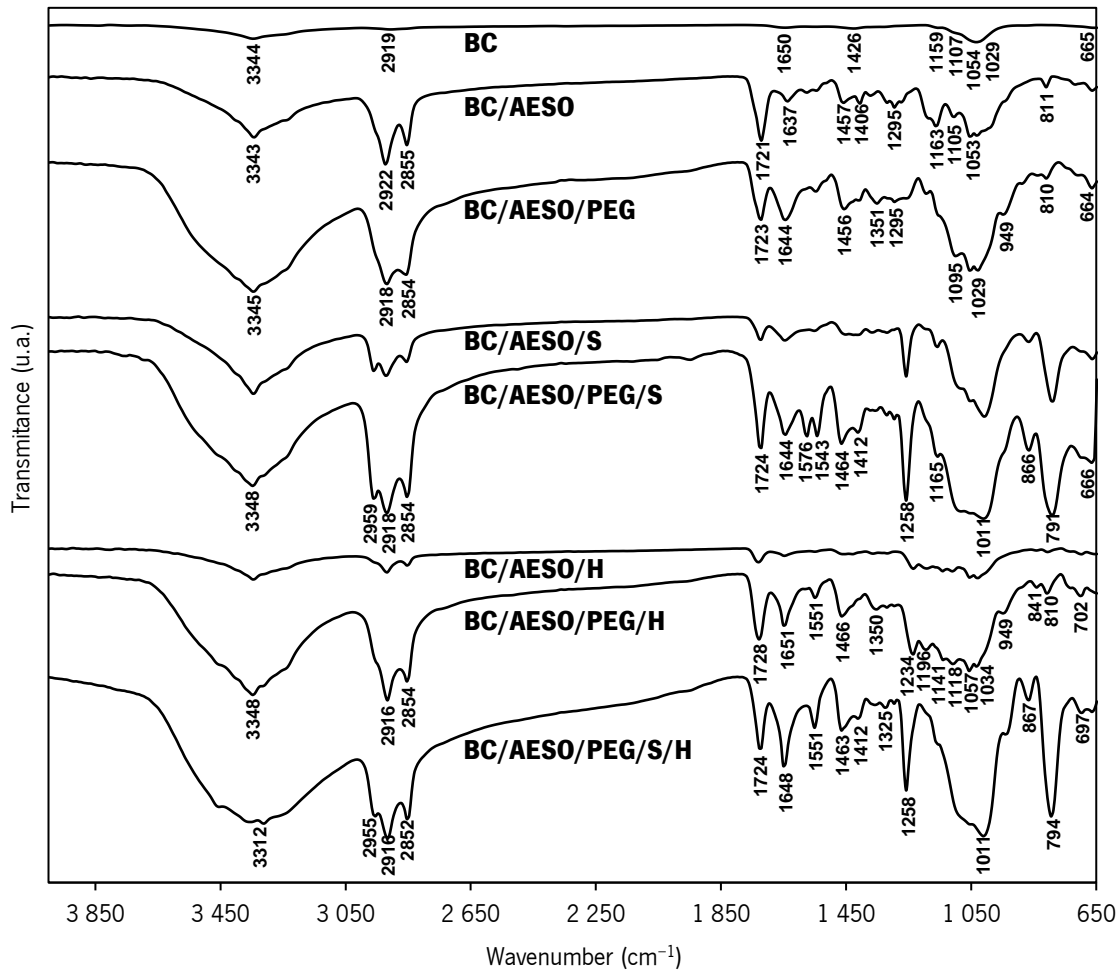


Figure 18. FT-IR spectra of BC and the composites.

5.4.4. Surface wettability and surface free energy

The BC composites are designed for leather (textile and footwear) applications; therefore, it is important to determine their surface hydrophobicity. The wetting properties of the BC and BC-based composites were investigated by measuring the water contact angles (WCAs). The obtained values are shown in Figure 19 and Figure 20. BC has a highly hydrophilic surface, bearing the lowest water droplet angle (63.1°), which increased for the BC composites to values between 79.0° and 138.0° , indicating a significant increase in hydrophobicity. Values of 95.8° and 79.0° were observed for BC/AESO and BC/AESO/PEG, respectively. AESO contains hydrophobic long-chain non-polar fatty acid chains (Li *et al.*, 2018) and consequently improves the water resistance of the composite. Despite being more hydrophobic, the WCAs over time decreased quickly in these composites, as compared to BC. This can be explained by the closed packed structure of the dried BC that limits the water diffusion through the tight space between the nanofibers, due to the strong and high number of cellulose–cellulose hydrogen bonds (Sun *et al.*, 2018).

As expected, the incorporation of PDMS (S) and perfluorocarbon-based (H) polymers into BC also significantly increased the WCAs. Both polymers have very low surface tension, $19.5\text{--}23.6\text{ mN}\cdot\text{m}^{-1}$ (X. Xu *et al.*, 2016; Tian *et al.*, 2018) and $6\text{--}18\text{ mN}\cdot\text{m}^{-1}$ (Milionis, Bayer and Loth, 2016), respectively, thus decreasing the free energy of the system and reducing the surface wettability. However, in the samples with PEG, this increase was not as substantial, since PEG can interact with the BC membrane by hydrogen bonds. As stated by Kondo *et al.* (Kondo and Sawatari, 1994), the ether oxygen in the poly(ethylene oxide) skeleton forms hydrogen bonds with the primary OH group at the C6 position of the anhydroglucose unit. Promising results were observed with all H-composites: higher contact angles (Figure 20) and very low absorption rate over time (Figure 19). The increase in hydrophobicity resulted from a decrease in the polar component of the surface tension and consequently in the total surface free energy of the composite, as shown in Figure 20. An exception to this trend was observed for BC/AESO/PEG, where an increase in the surface free energy was recorded. Among the different polymers tested, AESO was the one that offered less hydrophobicity, and the incorporation of the PEG, being hydrophilic as observed above, increased the value of the polar component.

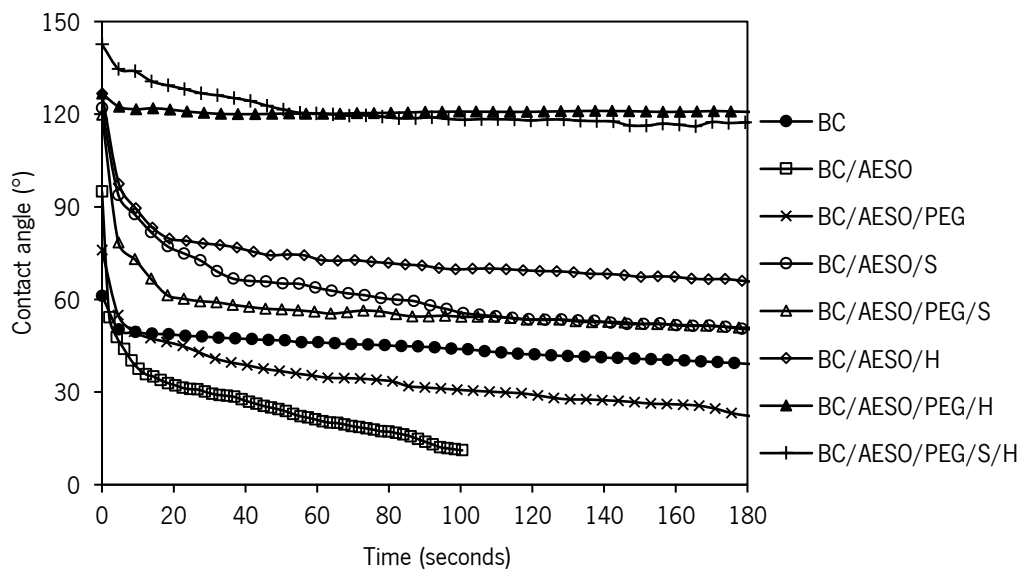


Figure 19. Water contact angle over time.

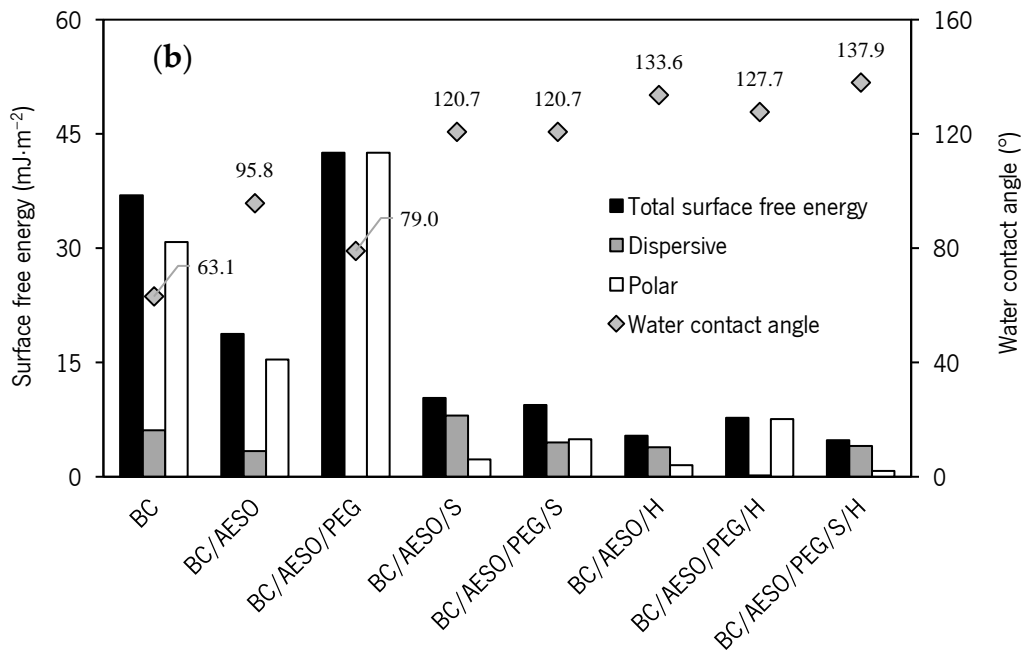


Figure 20. Static water contact angle and surface free energy.

5.4.5. Thermal properties

The thermal properties were evaluated by differential scanning calorimetry (DSC) and thermogravimetric analysis (TGA). DSC and TGA curves of BC and its composites obtained under nitrogen atmosphere are depicted in Figure 21a,b, respectively, and the corresponding relevant data are summarized in Table 22.

The DSC curve of BC reveals an endothermic degradation peak (T_m) at 362.2 °C, which is attributed to partial pyrolysis with the fragmentation of carbonyl and carboxylic bonds from anhydrous glucose units (Barud *et al.*, 2011). BC also shows a narrow weight loss at 351.0 °C (T_{dmax}), indicating fast degradation, involving dehydration, depolymerization of the main polymer network and the decomposition of glucosyl units followed by the formation of a charred residue (Frone *et al.*, 2018; Hu *et al.*, 2018).

In the case of the composites, an additional endothermic transition below 100 °C is observed in the DSC curves, it corresponds to the first step of weight loss in the temperature range of 30–150 °C observed in Figure 21b, which is ascribed to the loss of absorbed water. From Table 22, it is possible to observe that the composites with PEG 400 lost 5% of their mass at lower temperatures; this occurs because low-molecular polyethylene glycol contributes to higher hygroscopicity, the water being released by evaporation. These samples also present less charred residue, when compared with the composites without PEG. For most of the composites, a second event, in the range of 100–250 °C, is observed before the main degradation. This degradation stage can be considered the evaporation and

decomposition of unreacted monomers, catalysts, or other low molecular weight components in the composites (Liu *et al.*, 2015; Liu, Madbouly and Kessler, 2015; Zhang *et al.*, 2015; F. Liu *et al.*, 2017).

All DSC curves of the composites display exothermic transitions up to 200 °C, which we hypothesize to correspond to the polymerization of unreacted AESO (Liu, Xie and Qiu, 2017). A redox initiator system (the initiator cumene hydroperoxide (CHP) and the promoter cobalt naphthenate (CONP)) was used to polymerize AESO during the exhaustion process. This was performed at a relatively low temperature (30 °C), as described by other authors (Dweib *et al.*, 2006), attempting to avoid coalescence of the emulsified AESO (which is favored at a higher temperature due to the reduction of viscosity). However, as stated by Dweib *et al.* (2006), oxygen and water inhibit the free-radical polymerization reaction and the complete curing of the resins. In this work, emulsified AESO was cured, probably not completely, in aqueous media. Thus, the exothermic peak in DSC curves may be associated with the free-radical polymerization. Indeed, this peak does not appear in the AESO mixture curve tested without the addition of a catalyst on Figure 21a. The increase in temperature promoted the decomposition of the initiator CHP, generating more free radicals to complete the polymerization.

Further, the degradation of the composite network structure constitutes the second endothermic transition at higher temperatures. The beginning of the structural disruption is defined as the temperature where 10 wt% of the mass is lost. It was observed that $T_{10wt\%}$ for BC (326.4 °C) was higher than $T_{10wt\%}$ for all composites. Therefore, it can be inferred that native BC is more thermally stable than the polymeric composites.

The composites show less pronounced peaks with the main mass loss step, corresponding to the higher percentage of mass loss, observed in a broader temperature range. The T_{dmax} decreases in the order BC > BC/AESO > BC/AESO/PEG > BC/AESO/S > BC/AESO/PEG/S > BC/AESO/PEG/S/H > BC/AESO/H > BC/AESO/PEG/H and these results are in accordance with the DSC data. Although the composites are less stable thermally, they are stable up to 200 °C, so they can be applied in common leather applications.

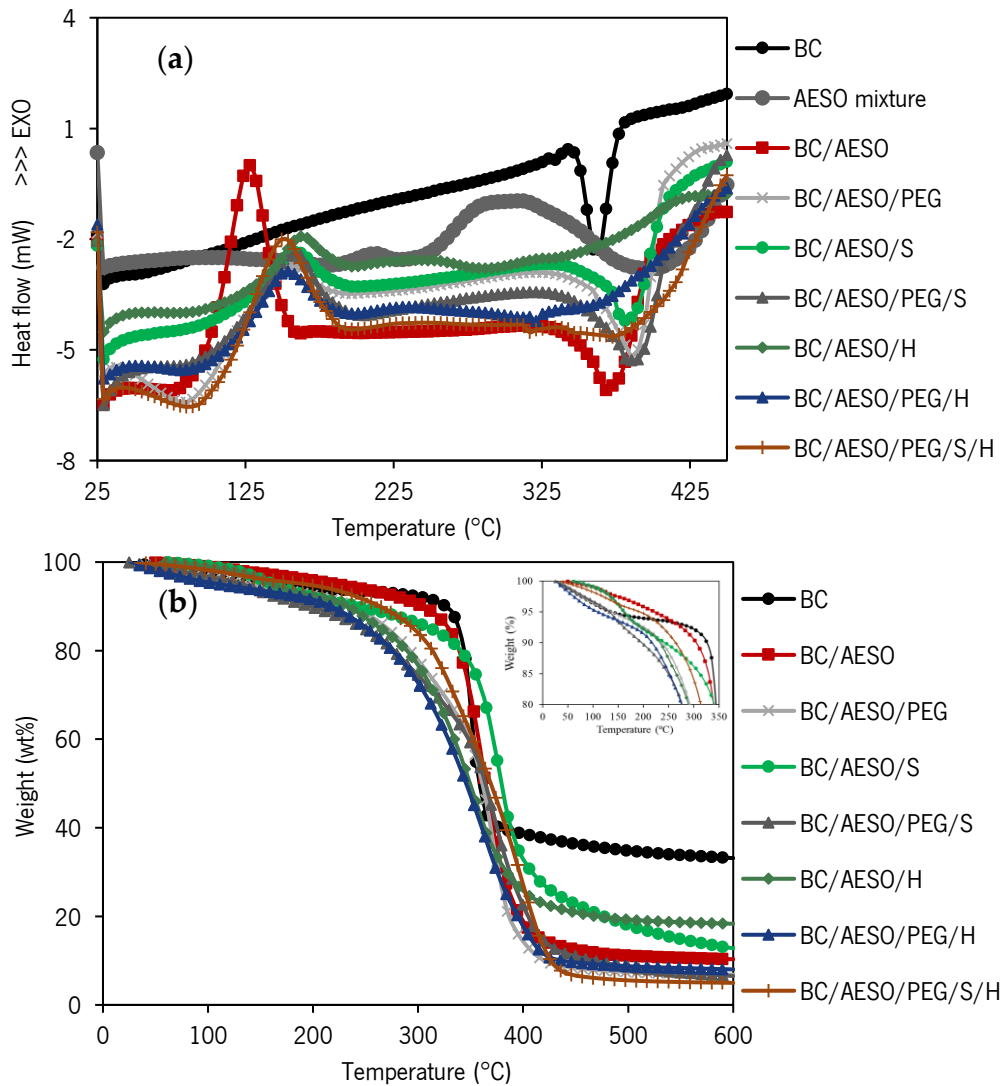


Figure 21. (a) DSC thermograms and (b) TGA curves of weight percentage of dried BC and BC composites.

Table 22. Thermal degradation data obtained from DSC, TGA and DTG curves of dried BC and BC composites.

Sample	T_c (°C) ^a	T_m (°C) ^b	$T_{5\text{ wt}\%}$ (°C) ^c	$T_{10\text{ wt}\%}$ (°C) ^d	T_{dmax} (°C) ^e
BC	-	362.2	136.1	326.4	351.0
BC/AESO	127.3	365.0	221.9	305.0	364.4
BC/AESO/PEG	153.2	387.2	136.8	236.8	372.7
BC/AESO/S	158.1	387.6	161.9	242.9	375.9
BC/AESO/PEG/S	157.3	389.9	132.5	196.9	374.3
BC/AESO/H	161.8	350.2	161.4	232.9	353.1
BC/AESO/PEG/H	151.9	365.5	109.5	217.4	361.9
BC/AESO/PEG/S/H	150.1	388.4	192.4	263.8	333.8/400.8

^a Temperature of the curing exotherm maximum; ^b Temperature of the degradation endothermal maximum; ^c Temperature at 5% mass loss; ^d Temperature at 10% mass loss; and, ^e Temperature(s) at the maximum mass loss rate.

5.4.6. Mechanical properties

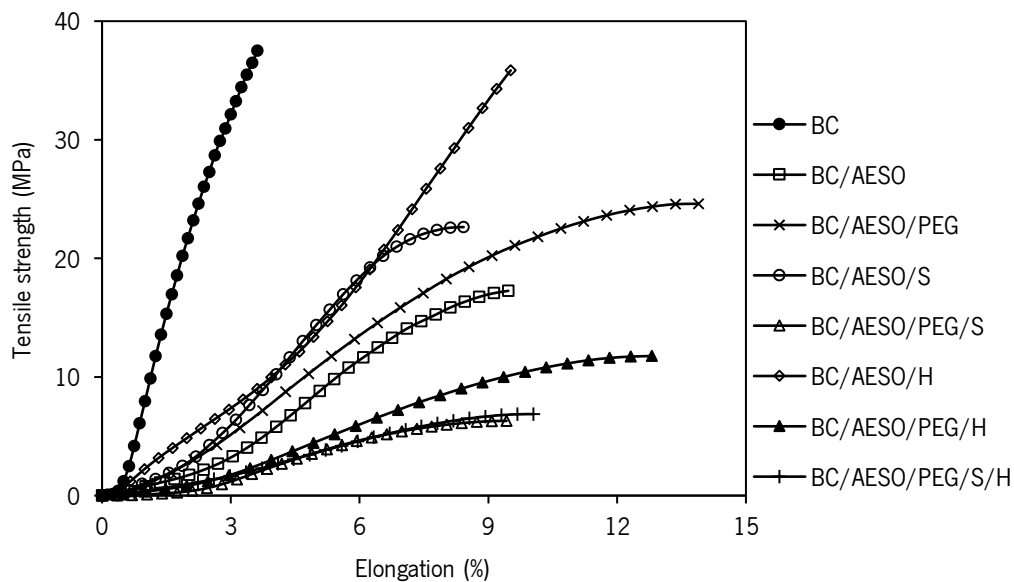
The average values and standard deviation of the tensile strength and elongation at break of the BC and BC-based composites are reported in Table 23, and the stress–strain curves are given in Figure 22. As deduced from Figure 22, neat BC displayed a rigid and brittle behavior, because of the extensive interactions between the polymer molecules that result in high tensile strength but low elongation at break. The incorporation of the plasticizers into polymers disrupts the intermolecular attractive forces between the main polymer chains and consequently increases the free volume and chain mobility, leading to an increase in extensibility (Boon, Lim and Gong, 2018; Sun *et al.*, 2018; Salarbashi, Bazeli and Tafaghodi, 2019). Thus, when compared to the neat BC membrane, the incorporation of emulsified polymer mixtures leads to a reduction in the values of the tensile strength and an increase in the elongation at break. As observed by SEM (Figure 17), the polymers appeared to have completely covered the surface of the BC nanofibers, resulting in an increase in the composites' thickness (Table 21). As observed by DSC, AESO was not completely polymerized, thus it may have not fully acted as a reinforcing agent but also as a plasticizer, allowing higher mobility between the different layers of the BC membrane.

The addition of either S or H, to BC/AESO, improved the mechanical and elongation properties of the composites, as compared to BC/AESO. However, only for this composite (BC/AESO) the addition of PEG allowed increasing the mechanical properties. In general, it was observed that the addition of different polymers leads to a decrease in tensile strength and an increase in elongation at break. The incorporation of PEG resulted in a consistent and significant increase in the elongation at break values due to its plasticizing effect.

Overall, taking as reference the technical report ISO/TR20879 (ISO, 2007), with respect to the mechanical properties, most of the composites are suitable to be used in footwear. Regarding tensile strength values, BC/AESO/PEG/S, BC/AESO/PEG/H, and BC/AESO/PEG/S/H samples (more polymer content as shown in Table 21) were below the reference value (casual footwear: $>10 \text{ N}\cdot\text{mm}^{-1}$) ($\text{MPa} \times \text{Thickness}$), but in the case of the elongation at break, all samples presented values within the required reference values.

Table 23. Tensile strength and elongation at break of dried BC and BC composites.

Sample	Tensile strength (MPa)	Elongation at break (%)
BC	37.5 ± 0.8	3.6 ± 0.6
BC/AESO	17.3 ± 0.7	9.5 ± 1.0
BC/AESO/PEG	24.6 ± 1.7	13.9 ± 0.8
BC/AESO/S	22.6 ± 3.3	8.4 ± 0.1
BC/AESO/PEG/S	6.3 ± 1.0	9.4 ± 2.3
BC/AESO/H	35.9 ± 3.0	9.5 ± 0.2
BC/AESO/PEG/H	11.8 ± 1.0	12.9 ± 2.0
BC/AESO/PEG/S/H	6.9 ± 0.2	10.0 ± 0.5

**Figure 22.** Stress strain curves of dried BC and BC composites.

5.5. Conclusion

This work provided a straightforward method to prepare BC composites with high potential for applications as a replacement for leather. We have successfully prepared composites based on BC, emulsified AESO resin, PEG, and PDMS- and perfluorocarbon-based polymers through a simple strategy to enhance the flexibility and hydrophobicity of the BC.

Based on SEM observations and FT-IR analysis, all the tested polymers penetrated well and uniformly into the BC matrix. The obtained composites showed hydrophobicity with the highest values of WCAs obtained for the composites with the perfluorocarbon-based product. Regarding the thermal and mechanical

properties, it was found that the composites presented lower thermal stability and tensile strength, although they are stable up to 200 °C and most of the composites can be applied in uppers for shoes.

Further optimization of the process may improve its performance through improved control of the polymerization reaction. Hence, this work opens new perspectives for potential applications of BC in the footwear industry.

Chapter 6

Development of BC-based composites polymerized with H₂O₂/AA, finishing and dyeing⁴

6.1. Abstract

This work aimed at the development of bacterial cellulose (BC)-based composites containing emulsified acrylated epoxidized soybean oil (AESO), polymerized with the redox initiator system hydrogen peroxide (H₂O₂) and L-ascorbic acid, and ferrous sulfate as catalyst. For this, the polymerization of the emulsified organic droplet was tested before and afterwards its incorporation into BC (by exhaustion). The composites were then finished with an antimicrobial agent (benzalkonium chloride) and dyed.

The obtained composites were characterized in terms of wettability, water vapor permeability (WVP), mechanical, thermal properties and antimicrobial properties. When AESO emulsion was polymerized prior to the exhaustion process, the obtained composites showed higher water WVP, tensile strength and thermal stability. Meanwhile, post-exhaustion polymerized AESO conferred the composite higher hydrophobicity and elongation. The composites finished with the antimicrobial agent showed activity against the *S. aureus*. Finally, intense colors were obtained more uniformly when they were incorporated simultaneously with the emulsified AESO with all the dyes tested.

⁴ This chapter is based on the following publication:

Fernandes, M., Souto, A. P., Dourado, F. and Gama, M. (2021) "Application of bacterial cellulose in the textile and shoe industry: Development of biocomposites," *Polysaccharides*, 2(3), pp. 566–581.

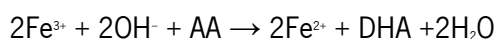
6.2. Introduction

The main objective of this research work is to create an alternative to leather by developing eco-friendly polymer composite materials based on biodegradable polymers, bacterial cellulose (BC) and modified vegetable oils (VOs).

In the previous chapter, composites based on BC and emulsified epoxidized soybean oil (AESO) were successfully prepared. However, the catalysts used were highly toxic to the environment. In the present chapter, AESO polymerization is carried out using a redox initiator system less aggressive to the environment, hydrogen peroxide (H₂O₂) (oxidant) and L-ascorbic acid (AA) (reductant) and ferrous sulfate (FeSO₄) as the catalyst: and under lower temperature (30 °C). The mechanism of redox reaction involves the transfer of a one-electron from the ferrous ion (Fe²⁺) to hydrogen peroxide, dissociating peroxide's oxygen–oxygen bond and generating one hydroxyl radical and one hydroxyl ion described as follows.



The reducing agent (AA) is transformed into dehydroascorbic acid (DHA) during the regeneration of Fe²⁺ to Fe³⁺, allowing the generation of new radicals, which is described as follows (Wang, 2013).



The biodegradability associated to VOs, although advantageous from an ecological and environmental point of view, implies their susceptibility to an enzymatic attack by microbial lipases. The scientific literature describes the enzymatic degradation of epoxidized, acryloylated and cross-linked VOs (Kiatsimkul, Sutterlin and Suppes, 2006). Using biocides could be a simple strategy to delay this biodegradability during the useful life cycle of the materials. In order to minimize the chances of a rapid degradability of the composites, the surface functionalization of the BC composites with antimicrobial properties was studied.

The dyeing of cellulosic fibers is commonly achieved using reactive, direct or vat dyes. They are applied by different processes, according to the conditions required to achieve a good diffusion and fixation rate, uniformity and adequate fastness. Exhaustion processes are carried out in aqueous solutions of dyes in the presence of suitable auxiliaries capable of promoting affinity between the dye and the fiber at the appropriate temperature and time to complete the diffusion of the dye, its adsorption and fixation onto the surface of the fiber (Burkinshaw, 2016). Although the general mechanisms involved in the BC-based composites dyeing can be generally drawn from the dyeing process of textile cellulosic fibers, adding polymeric mixtures in the production of the composites may change the dyeing process. Thus, in this

work, the dyeing of composites with different dyes was tested, by applying the dye i) simultaneously with the production of the composites and ii) in the obtained composites, as further described below.

6.3. Materials and methods

6.3.1. Materials

Bacterial cellulose membranes were offered by Satisfibre S.A. (Braga, Portugal). Soybean oil, epoxidized acrylate (Sigma-Aldrich, Steinheim, Germany), lauryl methacrylate (97%) (Acros Organics, Geel, Belgium), 1,6-hexanodiol diacrylate (80%) (Sigma-Aldrich, Steinheim, Germany), tri(propylene glycol) diacrylate (Sigma-Aldrich, Steinheim, Germany), Triton X-100 (Sigma-Aldrich, Steinheim, Germany), isobutanol (Merck Millipore, Darmstadt, Germany), hydrogen peroxide (30%) (Sigma-Aldrich, Steinheim, Germany), L-ascorbic acid (Sigma-Aldrich, Steinheim, Germany), ferrous sulfate (Merck Millipore, Darmstadt, Germany), and polyethylene glycol 400 (Merck Millipore, Darmstadt, Germany), were used as received. Persoftal MS Conc.01 and Baygard EFN (Tanatex Chemicals) were offered by ADI Center (Santo Tirso, Portugal). Antimicrobial finishing Si BAC (Smart Inovation, Barcelos, Portugal) and the dyes (DyStar, Porto, Portugal) were offered.

6.3.2. Development of composites with AESO emulsion polymerized before and after the exhaustion process

6.3.2.1. Emulsion polymerization and development of the composites

For the production of BC-based composites by the incorporation of a mixture of Persoftal MS Conc.01 (polydimethylsiloxane (PDMS)), polyethyleneglycol (PEG) 400 and acrylated epoxidized soybean oil (AESO), different mixtures were prepared as presented in Table 24.

First, a mixture was prepared by adding different reactive monomers to AESO to improve its processability and enhance the crosslinking. This mixture was composed of AESO (50% m/m); lauryl methacrylate (40% m/m)-a fatty acid-based reactive diluent, to reduce the viscosity of the mixture (Cousinet *et al.*, 2015); 1,6-hexanodiol diacrylate (5% m/m) and tri(propylene glycol) diacrylate (5% m/m)-bifunctional. The diacrylate monomers were used as crosslinking enhancers (Wei *et al.*, 2019). Then, a mixture with a mass ratio of 20:2:78 (AESO mixture/surfactant (Triton-X-100/Butanol 2/1)/water) was emulsified using a homogenizer (Unidrive X 1000 D, CAT, Staufen, Germany) at a speed of 25,000 rpm, for 12 min.

Table 24. Proportions of each component in the mixtures used in the production of BC composites.

AESO mixture (%)		AESO emulsion (%)		Polymers mixture (exhaustion) (%)	
AESO	50	AESO mixture	20	AESO emulsion	75
Lauryl methacrylate	40	Triton-X-100/Butanol (2/1)	2	Persoftal MS Con.01	20
1,6-hexanodiol diacrylate	5	Water	78	PEG 400	5
Tri(propylene glycol diacrylate	5				

The polymerization of the AESO emulsion was first tested using a redox initiator system, hydrogen peroxide (H₂O₂) (oxidant) and L-ascorbic acid (AA) (reductant), with ferrous sulfate (FeSO₄) as the catalyst. A flask containing the AESO mixture emulsion was placed in an ultrasound bath to avoid agglomeration and, per 100 g of the emulsion, 0.003 g of FeSO₄ were added followed by 1.5 g of H₂O₂ (30%) (previously dissolved in water); after 20 min, 0.9 g of AA (previously dissolved in water) were added to the mixture, in five portions, in intervals of 20 min each. The polymerization was carried out for 3 h more, at 25 °C.

For the production of the composites, 8 BC membranes with about 3.5 cm in thickness, a size of 13.0 × 24.0 cm and weighting 900 g (wet mass) were first mechanically pressed to remove the excess of water to a final wet mass of 200 g, corresponding to 5.5% dry mass in BC and a thickness of around 0.5 cm. The compressed membranes were then treated by exhaustion in 1200 mL of a mixture containing 75% of the emulsified AESO mixture, 20% Persoftal MS Con.01 and 5% PEG 400 (Table 24): four of which with the emulsified AESO mixture previously polymerized as described above (Composite A), and another four with the non- polymerized emulsified AESO mixture (Composites B).

The exhaustion process was carried out in an Ibelus machine equipped with an infrared heating system using a container with a capacity of approximately 2200 cm³, with a rotation of 50 rpm for 40 cycles. Starting from room temperature, the desired temperature (30 °C) was achieved using a gradient of 2 °C·min⁻¹. The treatment lasted for 7 days at 30 °C, after which the samples were oven dried (WTC binder oven) at 40 °C until constant mass. For the Composite B (samples produced with the non-polymerized AESO emulsion), after exhaustion and before drying, the membranes were treated again by exhaustion with a new solution containing the redox initiators and the catalyst for 3 days at 30 °C to polymerize the impregnated emulsion.

6.3.2.2. Characterization of the composites

The obtained composites were evaluated according to their wettability, water vapor permeability, mechanical properties, and thermal properties, as described in sections, 4.3.3.3., 4.3.3.4., 4.3.3.5., and 5.3.6.6., respectively.

The dynamic mechanical properties were measured on a Hitachi DMA7100 (Tokyo, Japan) equipment in tension mode. The storage modulus (E') was recorded from 25 to 250 °C, at a frequency of 1 Hz and heating rate of 2 °C·min⁻¹. The dimensions of the samples were 10 mm × 10 mm (tested area).

6.3.3. Finishing and dyeing

6.3.3.1. Antimicrobial finishing

The humidity and warm temperatures developed in footwear are favorable to the growth of bacteria, fungi, and molds, some of which contain lipases that may accelerate the biodegradation of the materials and release undesirable malodors. In order to evaluate the antimicrobial action of finishing treatments of BC composites with commercially available biocides, the Si BAC (Smart Inovation, Barcelos, Portugal) product was selected for which the active ingredient is benzalkonium chloride. Solutions containing the biocide, with different concentrations and the fixative (Smart Fix, Smart Inovation, Barcelos, Portugal), were prepared and applied to dried BC composites by exhausting at 40 °C in a bath ratio of 1:20 (m/v) (Table 25).

Table 25. Conditions used in the antimicrobial finishing of BC composites.

Sample	Si BAC (%) (w/w)	Smart Fix (%) (w/w)	Time (min)
Control	-	-	30
1 BAC	2	0.4	30
2 BAC	2	0.4	60
3 BAC	4	0.4	60

After drying until constant mass, the antimicrobial activity of the composites was evaluated using the agar diffusion plate test, ISO 20645:2006 (ISO, 2006). This method allows the qualitative determination of a surface antibacterial activity by detecting the presence of a halo around the edges of the sample (zone of inhibition) and the bacterial growth underneath. Suspensions of Gram positive *Staphylococcus aureus* (*S. aureus*) and Gram negative *Escherichia coli* (*E. coli*) were prepared in trypticase soy broth and left to grow overnight at 37 °C and 120 rpm. Then, their concentration was adjusted to 1×10⁷ CFUs/mL and added to tryptic soy agar. The agar was then poured into 55 mm diameter sterilized Petri dishes and, after

solidification, squared-sized BC composites of 1 × 1 cm were placed above them, guarantying maximum contact and incubated for 24 h at 37 °C.

6.3.3.2. *Dyeing of the composites*

Dyeing is an essential process in the development of textile and footwear products. In order to ascertain the dyeability of BC-based composites, different classes of dyes (direct, reactive, dispersed, and acid) were used. Their application was tested at the beginning of the exhaustion process during the production of the composites and in the dried composites.

Simultaneous dyeing and production of the BC-based composites were carried out as follows:

- a) Sirius Scarlet K-CF direct dye (0.1 g/100 g) was added to the mixture containing the AESO emulsion, PDMS and PEG 400 polymers, followed by the polymerization of the emulsion. The BC composites were then produced by the exhaustion process;
- b) Same process used in a) but with Procion Red H-E3N reactive dye;
- c) Same process used in a) but with Dianix Scarlet CC disperse dye;
- d) Procion Red H-E3N reactive dye (0.1 g/100 g) was added to the mixture containing the AESO emulsion previously polymerized and the other polymers. The BC composites were then produced by the exhaustion process;
- e) Procion Red H-E3N reactive dye (0.1 g/100 g) was added to the mixture containing the AESO emulsion and the other polymers. Then, the membranes were exhausted and finally polymerized;
- f) Same process used in e) but with Dianix Scarlet CC disperse dye.

For the dyeing of dry composites, the following tests were performed:

- g) Dyeing with the reactive dye Procion Red H-E3N (0.1 g/100 g) aqueous solution for 1.5 hours at 30 °C;
- h) Dyeing with the acid dye Solvaderm Black (0.1 g/100 g) aqueous solution for 1.5 hours at 30 °C; and
- i) Dyeing with the disperse dye Dianix Blue S-BG, (0.1 g/100 g) aqueous dispersion for 1.5 hours at different temperatures: 60, 80, 100, and 120 °C.

6.4. Results and discussion

6.4.1. Properties of the composites

The obtained composites were characterized regarding their wettability, water vapor permeability (WVP), mechanical and thermal properties, Table 26, Figure 23 and Figure 24.

As observed by the considerable increase in thickness (Table 26), the AESO emulsion mixture (Table 24) penetrated well into the BC membranes. The water contact angles values further confirmed the impregnation of the BC by changing its surface wettability ($WCA > 90^\circ$), which is slightly higher in the sample with the AESO polymerized after the exhaustion process (Composite B). As observed in Chapter 5, the incorporation of PDMS-based polymer into BC significantly increased the WCA of the composites. The low surface tension of PDMS, which is $19.5\text{--}23.6\text{ mN}\cdot\text{m}^{-1}$ (X. Xu *et al.*, 2016; Tian *et al.*, 2018), contributes to the decrease in the free energy and the surface wettability of the composite. Furthermore, AESO resin contains hydrophobic long-chain non-polar fatty acid chains (Li *et al.*, 2018), which improve the hydrophobicity of the composites.

Regarding the water vapor permeability, although the BC porosity was not completely obstructed by the incorporation of the polymer's mixture, the WVP values were much lower than those of pristine BC, which can be also explained by the higher thickness of the composites and their hydrophobic character. As shown in the previous chapters, the increased thickness and water resistance of the composites affected the adsorption process of the water vapor permeation mechanism.

Concerning the mechanical properties, as compared to BC, the tensile strength of the composites was lower but the elongation was much higher. These results can be explained by the extensive surface coating of the surface hydroxyl groups of the cellulose nanofibers which prevents their contribution to the mechanical strength through hydrogen bonding (Soykeabkaew *et al.*, 2009; Gea *et al.*, 2010; Asgher, Ahmad and Iqbal, 2017). Hence, the mechanical strength and elongation of the composites become dependent on the intermolecular bonding of the matrix polymers. The added polymers also had a plasticizing effect, which increased the free volume and allowed greater mobility between the different layers of the BC membrane (Boon, Lim and Gong, 2018; Sun *et al.*, 2018; Salarbashi, Bazeli and Tafaghodi, 2019). Composite B showed lower tensile strength value owing to the lower degree of polymerization of the crosslinked AESO, as will be discussed below.

Table 26. Properties of the BC and BC composites.

Sample	Thickness (mm)	WCA (°)	WVP (g·m⁻²·24 h⁻¹)	Tensile strength (MPa)	Elongation (%)
BC	0.48 ± 0.01	63.1 ± 4.7	289.6	37.5 ± 0.8	3.6 ± 0.6
Composite A (pre-polymerization)	1.27 ± 0.01	93.1 ± 5.7	65.1 ± 1.3	12.1 ± 1.8	15.5 ± 0.9
Composite B (post-polymerization)	1.22 ± 0.01	103.6 ± 3.2	28.8 ± 2.7	8.3 ± 0.4	19.1 ± 4.5

Thermogravimetric analysis (TGA) was used to evaluate the thermal properties and kinetics of degradation of the composites. The TGA and the derivative thermograms (DTG) are shown in Figure 23.

DTG curve of BC shows a single and narrow weight loss at 351.0 °C, indicating a fast degradation, involving dehydration, depolymerization of the main polymer network and the decomposition of glucosyl units followed by the formation of a charred residue (Frone *et al.*, 2018; Hu *et al.*, 2018). In the case of the composites, each of the samples presented two distinct peaks. Composite B (post-polymerization) shows one first event at 182.4 °C before the main degradation. This degradation stage can be considered the evaporation and decomposition of unreacted monomers, catalysts, or other low molecular weight components in the composites (Liu *et al.*, 2015; Liu, Madbouly and Kessler, 2015; Zhang *et al.*, 2015; F. Liu *et al.*, 2017). On the other hand, Composite A (pre-polymerization) had the first degradation peak at 328.3 °C and, hence, it can be inferred that the pre-polymerization using the redox initiator system hydrogen peroxide/L-ascorbic acid was more effective when compared to the post-polymerization. This can explain the lower WVP and tensile strength, higher contact angle and the higher elongation values of Composite B. The main mass loss step of both composites corresponding to the highest percentage of mass loss occurred at higher temperatures for the composites as compared to BC, respectively, at 392.6 °C and 373.1 °C for Composites A and B. This can be attributed to the decomposition of PDMS-based polymer and crosslinked AESO. The temperature corresponding to the maximum rate of weight-loss of the polymers was around 420 °C (Radhakrishnan, 2005; Sousa *et al.*, 2017).

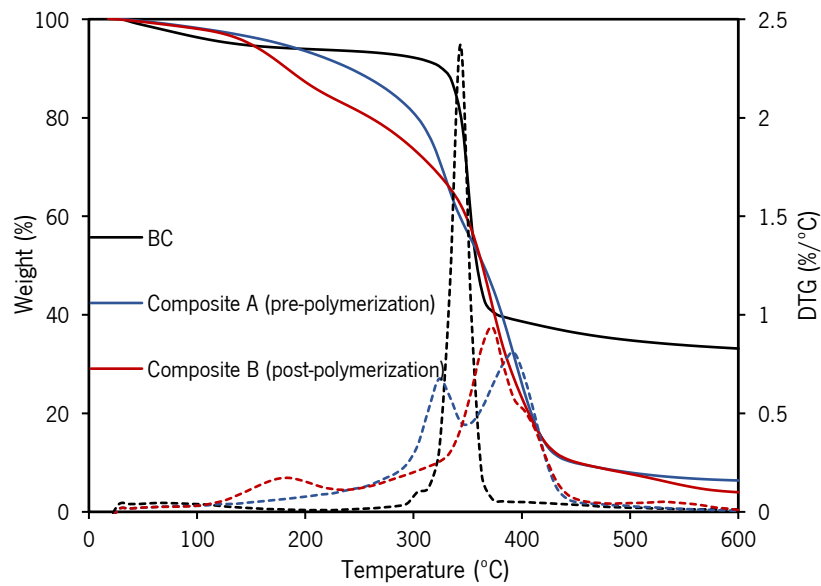


Figure 23. TGA curves (solid lines) and respective derivative (dashed lines) of BC and BC composites.

The storage modulus (E') obtained by dynamic mechanical analysis (DMA) of pure BC and the composites over a temperature range of 25 °C to 250 °C at a frequency of 1 Hz is presented in Figure 24.

The obtained data show that BC has high stiffness with a storage modulus at room temperature of 6.5 GPa due to the strong hydrogen bonds between the nanofibers. However, a considerably lower storage modulus was observed for the BC composites, which can be ascribed to the plasticizing effect of the impregnated polymers resulting in the segmental mobilization of the nanocellulose chains. Among the composites, Composite A showed a higher storage modulus for temperatures up to approximately 100 °C. These results are in good agreement with the tensile strength measurements, which were plausibly associated with a higher crosslinking density. In addition, it was also possible to observe that the storage modulus of Composite B decreased when the temperature rose to 55 °C and then increased when it rose to 130 °C. This could be due to the loss of unreacted material, as was observed in the TGA results, which consequently gave rise to densification of the composite structure during heating, allowing an improved stress transfer behavior at higher temperatures.

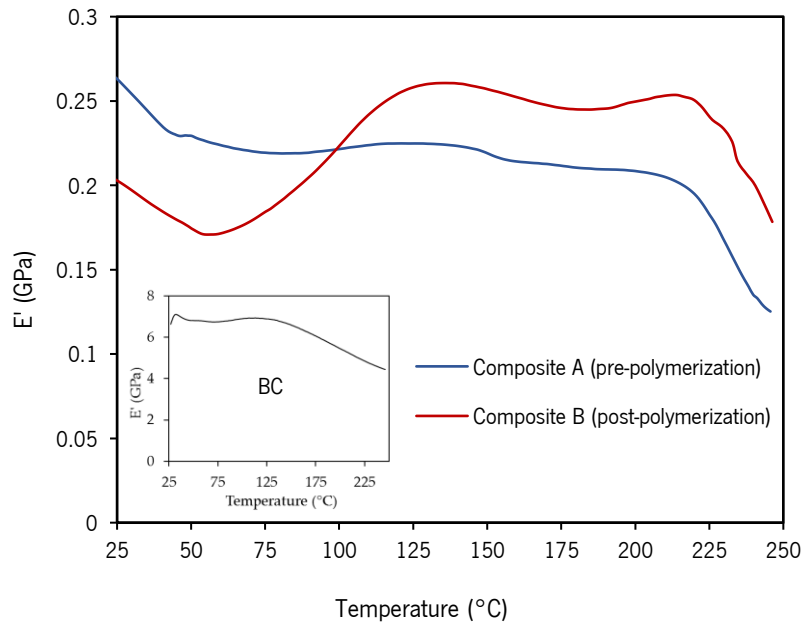


Figure 24. Evolution of the storage modulus (E') versus temperature at 1 Hz for BC (inserted graph) and BC composites as obtained by dynamic mechanical analysis

Comparing the results of these composites, by using the redox initiator system hydrogen peroxide and L-ascorbic acid with the ones from Chapter 5 a substantial improvement in the elongation at break (pre-polymerization and post-polymerization) and in the tensile strength (pre-polymerization) was achieved. Overall, the polymerization of the AESO emulsion using biodegradable catalysts was validated and since the polymerization occurred before the exhaustion process, this method was more effective in the preparation of the composites.

6.4.2. Antimicrobial activity

The antibacterial activity of the BC composites finished (surface-functionalized) with different concentrations and time of exhaustion of the biocide benzalkonium chloride (BAC), against *S. aureus* and *E. coli*, was determined using the zone of inhibition method. *S. aureus* and *E. coli* are among the most prevalent species of gram-positive and gram-negative bacteria, respectively. As shown in Figure 25, all samples with the biocide compound produced a zone of inhibition (halo) against the *S. aureus* (Gram-positive), and this area increased with concentration and with the time of treatment.

No inhibition was observed against the *E. coli*, possibly due to the poor antimicrobial capacity of the benzalkonium chloride (cationic) against gram-negative bacteria (Wei, Yang and Hong, 2011).

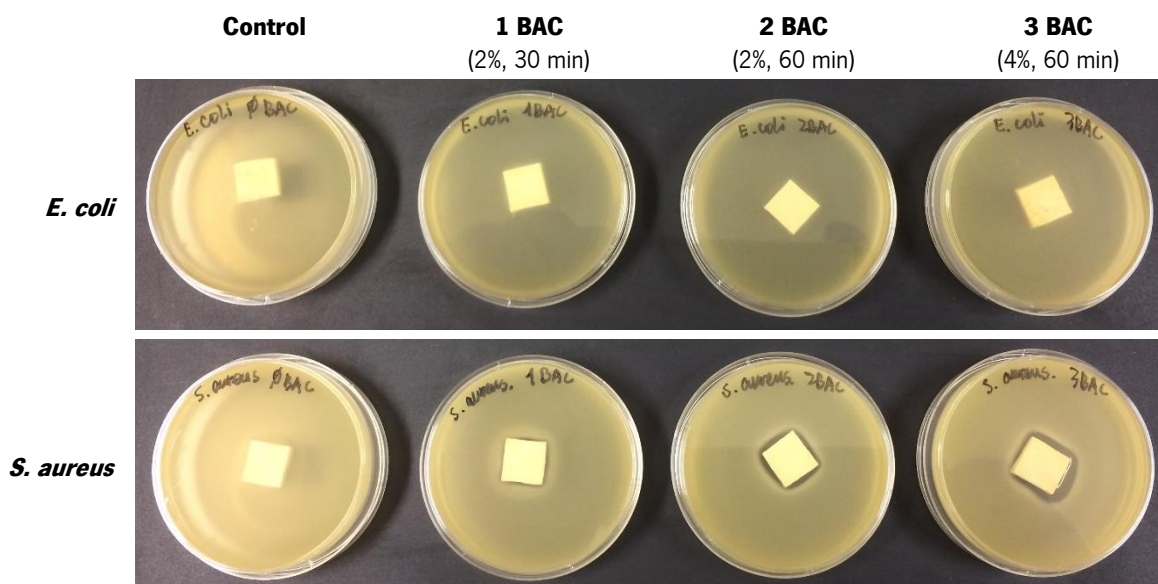


Figure 25. Antibacterial activity of the BC composites surface-functionalized with benzalkonium chloride-based product against *Escherichia coli* and *Staphylococcus aureus*.

6.4.3. Dyeing

Figure 26 shows some photos of the dyed composites. All samples showed intense colors, were very flexible and hydrophobic (inserted photo in Figure 26e as an example). For samples dyed during the exhaustion with the AESO mixture, Figure 26a-f, the dye diffused well into the membranes, resulting in more uniform colors. However, in samples dyed after the production of the composites, Figure 26g-h, the dye remained only at the outer layers (inserted photo in Figure 26g) and the color was less uniform. It was also possible to observe that by increasing the temperature during dyeing with the dispersed dye, Figure 26i, more intense colors were obtained and despite the greater shrinkage of the sample, this change contributed to obtaining a material with a texture more similar to that of leather.

From the above, incorporating the dye simultaneously with the AESO mixture is a more efficient approach towards dyeing BC composites. These results also allowed to present a simple and potentially low-cost strategy for this process, albeit it will be necessary to carry out color washing and rubbing fastness tests, as well as to optimize the process conditions, taking into account the variables of pH, bath ratio, temperature, dye concentration, auxiliary products and the duration of the process.

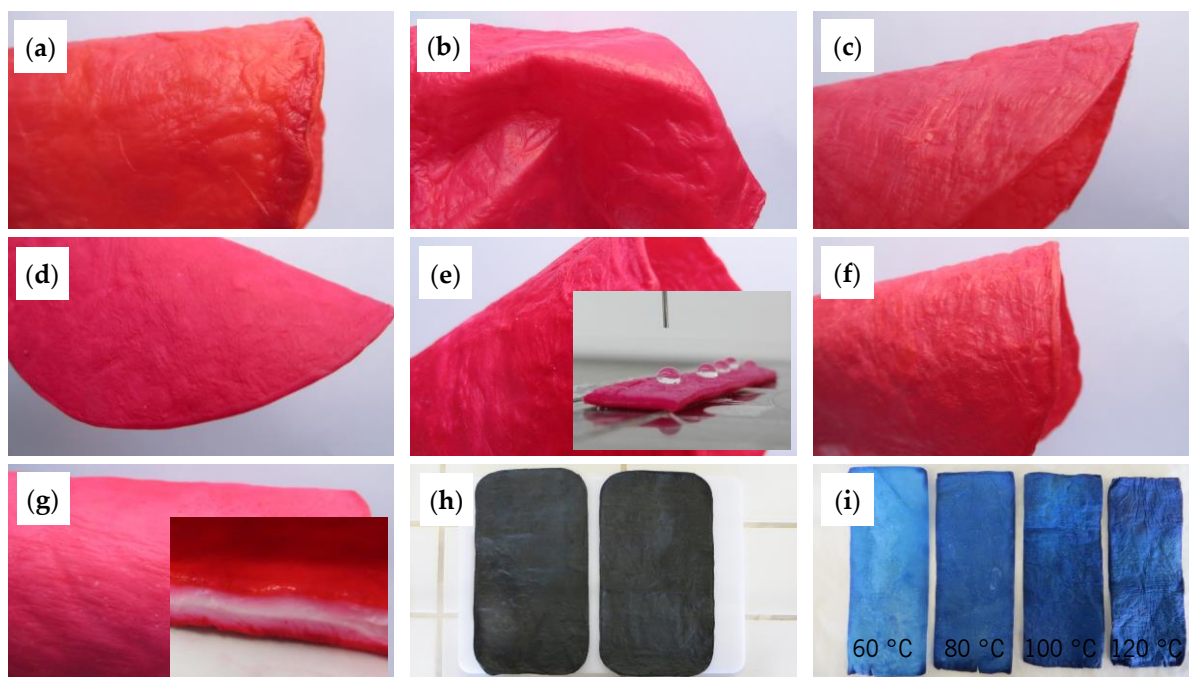


Figure 26. Photos of the dyed BC composites. Letters (a–i) correspond to the experimental conditions described in Section 6.3.3.2. Simultaneous dyeing and production of the BC-based composites (a–f) and dyeing of dry composites (g–i).

6.5. Conclusion

After carrying out this work, the possibility of producing BC composites by incorporating, through the exhaustion process, products based on AESO, PDMS, and PEG 400, using biodegradable catalysts was validated. The polymerization of the AESO emulsion before the exhaustion process proved to be more effective in terms of WVP, tensile strength and thermal stability. However more work is needed to optimize the process. Composites finished with biocides showed antimicrobial activity against *S. aureus* and incorporating the dye simultaneously with the AESO mixture was the most efficient approach towards composites with intense colors.

Chapter 7

Conclusions and suggestions for future work

7.1. Main conclusion

This project aimed at using bacterial cellulose (BC) as a structuring material, for the development of a new leather analogue from alternative biological products, specifically with modified vegetable oils and other hydrophobic polymers. In this concept, BC, a highly porous nanofibrillar natural material, was submitted to an exhaustion process, allowing the bulk impregnation of hydrophobic polymers, namely commercial nano/microparticles, Persoftal MS Con.01 (polydimethylsiloxane (PDMS)-based) and Baygard EFN (perfluorocarbon (PFC)-based), and acrylated epoxidized soybean oil (AESO).

In a first approach, BC-based nanocomposites were developed by impregnating BC membranes with PDMS- or PFC-based products, each, at different concentrations, and with both polymers in a sequential process. Both hydrophobic products penetrated well in the BC membranes, adsorbing tightly onto the surface of the nanofibers, across the entire depth of the material, as observed by scanning electron microscopy (SEM) and Fourier transform infrared (FT-IR). The incorporation of increasing amounts of PDMS- or PFC-based products increased the thickness and the mass per unit area of the composites, while decreasing the water vapor permeability (WVP). After incorporation of the polymers, higher contact angles (CAs) were obtained, indicative of more hydrophobic surfaces, and the use of PFC-based product seems to provide more hydrophobicity. The mechanical properties of the composites improved with the incorporation of the polymers, although, as the concentration of the added products increased, the tensile strength and Young's modulus decreased. It was also observed that samples with higher amounts of incorporated polymers, had higher elongation. Overall, the resulting composites were malleable, mechanically resistant, hydrophobic, and breathable.

Then, aiming at increasing the bio-based content of the composite, BC membranes were impregnated with activated vegetable oils, AESO, in a mixture containing also the PDMS-based polymer and

polyethylene glycol (PEG) 400. FT-IR and SEM analyses provided evidence of the incorporation of these polymers into the BC membrane, resulting in its hydrophobic performance. The incorporation of the AESO resin in the PDMS/PEG mixture contributed to an increase in the values of tensile strength and a decrease in the elongation, while the addition of the plasticizer PEG 400 increased the elongation and decreased the tensile strength.

Using a new approach, AESO resin was previously emulsified to allow better diffusion into the BC membranes and applied in mixtures containing also PEG 400, and PDMS- and PFC-based products. All the tested polymer mixtures penetrated well and uniformly into the BC matrix, as shown on SEM observations and FT-IR analysis. The obtained composites were hydrophobic and the highest values of CAs were obtained for the composites with the PFC-based product (CAs of 128-138°). Regarding the thermal properties, it was found that the composites presented lower thermal stability than the BC, although they were stable up to 200 °C. From differential scanning calorimetry (DSC) analysis, it was observed that AESO resin was not fully cured. Further optimization of the polymerization may improve its performance. When compared to BC/AESO composite, the addition of either PDMS- or PFC-based product, improved the mechanical and elongation properties of the composites and, in general, the incorporation of PEG resulted in a consistent and significant increase in the elongation at break values due to its plasticizing effect.

Finally, it was demonstrated that AESO emulsion can be polymerized using the redox initiator system H₂O₂/AA. When the composites were developed with the mixture containing the previously polymerized AESO emulsion, greater WVP, tensile strength and thermal stability were obtained, while the composites polymerized after the exhaustion presented higher hydrophobicity and elongation. It was also shown that the composites finished with an antimicrobial agent, had antimicrobial action against *S. aureus* bacterium. Also, composites with intense colors were obtained by incorporating the dye simultaneously with the polymer's mixture, resulting in a more uniform distribution of the color, as compared to post-dyed composites.

Summing up, this work demonstrated new approaches to develop composites based on bacterial cellulose and hydrophobic polymers, including modified soybean oil, opening new perspectives for the potential applications of BC and thus offer a high value-added differentiation and sustainable consumer products, such as textiles and leather. The exhaustion process here used, is already available at large scale and represents a simple and cost-effective approach towards the production of these composites.

7.2. Suggestions for future work

Based on the results obtained in this work, the following suggestions can be made for future work:

- The results showed that BC composites with distinct performances can be designed by simply varying the polymers percentage contents. Optimization of the polymer's mixture regarding the percentage of each component, may allow to improve the final properties of the composites, considering their applications in leather products.
- There were technical difficulties in the polymerization process, which should have been done under controlled temperature and inert atmosphere conditions. Full optimization of the AESO polymerization may allow better results in terms of the composite's final properties.
- Test the composites freeze-drying. Although it is an expensive process, it may be possible to increase the water vapor permeability.
- Optimization of the dyeing process, considering the variables of pH, bath ratio, temperature, dye concentration, auxiliary products, and the duration of the process.
- Finishing of the composites by spray-coating and/or by imprint a pattern to make its appearance more appealing.
- Evaluation of the properties of the composites considering the requirements for its application as an alternative to leather.
- Determination of the biodegradability of the composites.
- Study of the environmental impact (life cycle).

Chapter 8

References

- Abeer, M. M., Mohd, M. C. I. and Martin, C. (2014) "A review of bacterial cellulose-based drug delivery systems: their biochemistry, current approaches and future prospects," *Journal of Pharmacy and Pharmacology*, 66, pp. 1047–1061. doi: 10.1111/jphp.12234.
- Akesson, D., Skrifvars, M. and Walkenström, P. (2009) "Preparation of thermoset composites from natural fibres and acrylate modified soybean oil resins," *Journal of Applied Polymer Science*, 114, pp. 2502–2508. doi: 10.1002/app.
- Alonso, E., Faria, M., Faranak, M., Resnik, M., Ferreira, A. and Cordeiro, N. (2018) "Conductive bacterial cellulose-polyaniline blends: influence of the matrix and synthesis conditions," *Carbohydrate Polymers*, 183, pp. 254–262. doi: 10.1016/j.carbpol.2017.12.025.
- Ananas-anam (2017) *Introducing piñatex™ - ananas anam, Ananas-anam*. Available at: <http://www.ananas-anam.com/pinatex/> (Accessed: November 10, 2017).
- Andrade, F. K., Pertile, R. A. N., Dourado, F. and Gama, F. M. (2010) "Bacterial cellulose: properties, production and applications," in Lejeune, A. and Deprez, T. (eds.) *Cellulose: Structure and Properties, Derivatives and Industrial Uses*. New York: Nova Science Publishers, Inc, pp. 427–458.
- Araki, J. and Mishima, S. (2015) "Steric stabilization of 'charge-free' cellulose nanowhiskers by grafting of poly(ethylene glycol)," *Molecules*, 20, pp. 169–184. doi: 10.3390/molecules20010169.
- Araújo, I. M. S., Silva, R. R., Pacheco, G., Lustrì, W. R., Tercjak, A., Gutierrez, J., Júnior, J. R. S., Azevedo, F. H. C., Figuêredo, G. S., Vega, M. L., Ribeiro, S. J. L. and Barud, H. S. (2018) "Hydrothermal synthesis of bacterial cellulose – copper oxide nanocomposites and evaluation of their antimicrobial activity," *Carbohydrate Polymers*, 179, pp. 341–349. doi: 10.1016/j.carbpol.2017.09.081.
- Araújo, S., Silva, F. M. da and Gouveia, I. C. (2015) "The role of technology towards a new bacterial-cellulose-based material for fashion design," *Journal of Industrial and Intelligent Information*, 3(2), pp. 168–172. doi: 10.12720/jiii.3.2.168-172.
- Asgher, M., Ahmad, Z. and Iqbal, H. M. N. (2017) "Bacterial cellulose-assisted de-lignified wheat straw-PVA based bio-composites with novel characteristics," *Carbohydrate Polymers*, 161, pp. 244–252. doi: 10.1016/j.carbpol.2017.01.032.
- Barud, H. S., Souza, J. L., Santos, D. B., Crespi, M. S., Ribeiro, C. A., Messaddeq, Y. and Ribeiro, S. J. L. (2011) "Bacterial cellulose/poly (3-hydroxybutyrate) composite membranes," *Carbohydrate Polymers*, 83, pp. 1279–1284. doi: 10.1016/j.carbpol.2010.09.049.
- Basil-Jones, M. M., Edmonds, R. L., Allsop, T. F., Cooper, S. M., Holmes, G., Norris, G. E., Cookson, D. J., Kirby, N. and Haverkamp, R. G. (2010) "Leather structure determination by small-angle X-ray

- scattering (SAXS): Cross sections of ovine and bovine leather,” *Journal of Agricultural and Food Chemistry*, 58, pp. 5286–5291. doi: 10.1021/jf100436c.
- Bitlisli, B. O., Basaran, B., Karavana, H. A. and Aslan, A. (2005) “Importance of using genuine leather in shoe production in terms of foot comfort,” *Journal- Society of Leather Technologists and Chemists*, 89(3), pp. 107–110.
- Bizzi, C. A., Zanatta, R. C., Santos, D., Giacobe, K., Dallago, R. M., Mello, P. A. and Flores, E. M. M. (2020) “Ultrasound-assisted extraction of chromium from residual tanned leather: An innovative strategy for the reuse of waste in tanning industry,” *Ultrasonics Sonochemistry*, 64, p. 104682. doi: 10.1016/j.ultsonch.2019.104682.
- Black, M., Casanova, M., Rydin, S., Scalet, B. M., Roudier, S. and Sancho, L. D. (2013) *Best available techniques (BAT) - Reference document for the tanning of hides and skins*. Luxembourg: European Union. doi: 10.2788/13548.
- Blaker, J. J., Lee, K.-Y., Li, X., Menner, A. and Bismarck, A. (2009) “Renewable nanocomposite polymer foams synthesized from Pickering emulsion templates,” *Green Chemistry*, 11(9), pp. 1321–1326. doi: 10.1039/b913740h.
- Bodin, A., Concaro, S., Brittberg, M. and Gatenholm, P. (2007) “Bacterial cellulose as a potential meniscus implant,” *Journal of Tissue Engineering and Regenerative Medicine*, 1, pp. 406–408. doi: 10.1002/term.51.
- Bolt Threads (2020) *Bolt Technology – Meet Mylo™*, Bolt Threads. Available at: <https://boltthreads.com/technology/mylo/> (Accessed: August 25, 2020).
- Boon, D., Lim, K. and Gong, H. (2018) “Highly stretchable and transparent films based on cellulose,” *Carbohydrate Polymers*, 201, pp. 446–453. doi: 10.1016/j.carbpol.2018.08.080.
- BS 7209:1990. Specification for water vapour permeable apparel fabrics* (1990). London:BSI.
- Budhiono, A., Rosidi, B., Taher, H. and Iguchi, M. (1999) “Kinetic aspects of bacterial cellulose formation in nata-de-coco culture system,” *Carbohydrate Polymers*, 40(2), pp. 137–143. doi: 10.1016/S0144-8617(99)00050-8.
- Burkinshaw, S. M. (2016) *Physico-chemical aspects of textile coloration*. Edited by Society of Dyers and Colorists. West Sussex: John Wiley & Sons, Inc.
- Cai, D., Neyer, A., Kuckuk, R. and Heise, H. M. (2010) “Raman, mid-infrared, near-infrared and ultraviolet-visible spectroscopy of PDMS silicone rubber for characterization of polymer optical waveguide materials,” *Journal of Molecular Structure*, 976(1–3), pp. 274–281. doi: 10.1016/j.molstruc.2010.03.054.
- Cao, H., Wool, R. R. P., Bonanno, P., Dan, Q., Kramer, J. and Lipschitz, S. (2014) “Development and evaluation of apparel and footwear made from renewable bio-based materials,” *International Journal of Fashion Design, Technology and Education*, 7(1), pp. 21–30. doi: 10.1080/17543266.2013.859744.
- Cao, H., Wool, R., Sidoriak, E. and Dan, Q. (2013) “Evaluating mechanical properties of environmentally friendly leather substitute (eco-leather),” in *International Textile and Apparel Association (ITAA) Annual Conference Proceedings*. New Orleans.
- Castro, C., Zuluaga, R., Putaux, J. L., Caro, G., Mondragon, I. and Gañán, P. (2011) “Structural characterization of bacterial cellulose produced by *Gluconacetobacter swingsii* sp. from Colombian agroindustrial wastes,” *Carbohydrate Polymers*, 84(1), pp. 96–102. doi: 10.1016/j.carbpol.2010.10.072.
- Cazón, P., Velázquez, G. and Vázquez, M. (2019) “Characterization of bacterial cellulose films combined

- with chitosan and polyvinyl alcohol: Evaluation of mechanical and barrier properties," *Carbohydrate Polymers*, 216, pp. 72–85. doi: 10.1016/j.carbpol.2019.03.093.
- Chan, C. K., Shin, J. and Jiang, S. X. K. (2018) "Development of tailor-shaped bacterial cellulose textile cultivation techniques for zero-waste design," *Clothing and Textiles Research Journal*, 36(1), pp. 33–44. doi: 10.1177/0887302X17737177.
- Costa, A. F. de S., de Amorim, J. D. P., Almeida, F. C. G., de Lima, I. D., de Paiva, S. C., Rocha, M. A. V., Vinhas, G. M. and Sarubbo, L. A. (2019) "Dyeing of bacterial cellulose films using plant-based natural dyes," *International Journal of Biological Macromolecules*, 121, pp. 580–587. doi: 10.1016/j.ijbiomac.2018.10.066.
- Costa, A. F. de S., Rocha, M. A. V. and Sarubbo, L. A. (2017) "Review - Bacterial cellulose: an ecofriendly biotextile," *International Journal of Textile and Fashion Technology*, 7(1), pp. 11–26. Available at: <http://tjprc.org/view-archives.php>.
- Cousinet, S., Ghadban, A., Fleury, E., Lortie, F., Pascault, J. P. and Portinha, D. (2015) "Toward replacement of styrene by bio-based methacrylates in unsaturated polyester resins," *European Polymer Journal*, 67, pp. 539–550. doi: 10.1016/j.eurpolymj.2015.02.016.
- Czaja, W. K., Young, D. J., Kawecki, M. and Brown, R. M. (2007) "The future prospects of microbial cellulose in biomedical applications," *Biomacromolecules*, 8(1), pp. 1–12. doi: 10.1021/bm060620d.
- Dixit, S., Yadav, A., Dwivedi, P. D. and Das, M. (2015) "Toxic hazards of leather industry and technologies to combat threat: a review," *Journal of Cleaner Production*, 87, pp. 39–49. doi: 10.1016/j.jclepro.2014.10.017.
- Domskiene, J., Sederaviciute, F. and Simonaityte, J. (2019) "Kombucha bacterial cellulose for sustainable fashion," *International Journal of Clothing Science and Technology*, 31(5), pp. 644–652. doi: 10.1108/IJCST-02-2019-0010.
- Douglass, E. F., Avci, H., Boy, R., Rojas, O. J. and Kotek, R. (2018) "A review of cellulose and cellulose blends for preparation of bio-derived and conventional membranes, nanostructured thin films, and composites," *Polymer Reviews*, 58(1), pp. 102–163. doi: 10.1080/15583724.2016.1269124.
- Dourado, F., Leal, M., Martins, D., Fontão, A., Rodrigues, A. C. and Gama, M. (2016) "Celluloses as food ingredients/additives: Is there a room for BNC?," in Gama, M., Dourado, F., and Bielecki, S. (eds.) *Bacterial nanocellulose: From biotechnology to bio-economy*. Elsevier B.V, pp. 123–133. doi: 10.1017/CBO9781107415324.004.
- Duarte, A. P. and Bordado, J. C. (2015) "Cork - a renewable raw material: forecast of industrial potential and development priorities," *Frontiers in Materials*, 2, pp. 1–8. doi: 10.3389/fmats.2015.00002.
- Dweib, M. A., Hu, B., Shenton, H. W. and Wool, R. P. (2006) "Bio-based composite roof structure: Manufacturing and processing issues," *Composite Structures*, 74(4), pp. 379–388. doi: 10.1016/j.compstruct.2005.04.018.
- FAO (2015) *World statistical compendium for raw hides and skins, leather and leather footwear 1999-2015*. Rome: Food and Agriculture Organization of the United Nations (FAO). Available at: <http://www.fao.org/economic/est/est-commodities/hides-skins/en/>.
- Fibre2Fashion (2020) *Interview with Adrián López Velarde & Marte Cázares*, *Fibre2Fashion*. Available at: <https://www.fibre2fashion.com/interviews/face2face/desserto/adrián-lópez-velarde-marte-cázares/12568-1> (Accessed: August 25, 2020).
- Finocchio, E., Cristiani, C., Dotelli, G., Gallo, P. and Zampori, L. (2014) "Vibrational Spectroscopy Thermal

- evolution of PEG-based and BRIJ-based hybrid organo-inorganic materials. FT-IR studies,” *Vibrational Spectroscopy*, 71, pp. 47–56. doi: 10.1016/j.vibspec.2013.12.010.
- Fontaine, M., Clement, Y., Blanc, N. and Demesmay, C. (2019) “Hexavalent chromium release from leather over time natural ageing vs accelerated ageing according to a multivariate approach,” *Journal of Hazardous Materials*, 368, pp. 811–818. doi: 10.1016/j.jhazmat.2018.12.112.
- Foresti, M. L., Vázquez, A. and Boury, B. (2017) “Applications of bacterial cellulose as precursor of carbon and composites with metal oxide, metal sulfide and metal nanoparticles: A review of recent advances,” *Carbohydrate Polymers*, 157, pp. 447–467. doi: 10.1016/j.carbpol.2016.09.008.
- Fortunato, E., Gaspar, D., Duarte, P., Pereira, L., Águas, H., Vicente, A., Dourado, F., Gama, M. and Martins, R. (2016) “Optoelectronic devices from bacterial nanocellulose,” in Gama, M., Bielecky, S., and Dourado, F. (eds.) *Bacterial Nanocellulose: from biotechnology to bio-economy*. Amsterdam: Elsevier, pp. 179–197.
- Frone, A. N., Panaitescu, D. M., Chiulan, I., Nicolae, C. A., Casarica, A., Gabor, A. R., Trusca, R., Damian, C. M., Purcar, V., Alexandrescu, E. and Stanescu, P. O. (2018) “Surface treatment of bacterial cellulose in mild, eco-friendly conditions,” *Coatings*, 8(221), pp. 1–17. doi: 10.3390/coatings8060221.
- Fruitleather (2020) *Made from discarded fruit, Fruitleather Rotterdam*. Available at: <https://fruitleather.nl/introduction/> (Accessed: September 14, 2020).
- Gama, F. M. P. and Dourado, F. (2018) “Bacterial NanoCellulose: What future?,” *BiolImpacts*, 8(1), pp. 1–3. doi: 10.15171/bi.2018.01.
- Gandini, A. and Lacerda, T. M. (2015) “From monomers to polymers from renewable resources: Recent advances,” *Progress in Polymer Science*, 48, pp. 1–39. doi: 10.1016/j.progpolymsci.2014.11.002.
- Gao, H. L., Zhao, R., Cui, C., Zhu, Y. B., Chen, S. M., Pan, Z., Meng, Y. F., Wen, S. M., Liu, C., Wu, H. A. and Yu, S. H. (2020) “Bioinspired hierarchical helical nanocomposite macrofibers based on bacterial cellulose nanofibers,” *National Science Review*, 7(1), pp. 73–83. doi: 10.1093/nsr/nwz077.
- Garside, P. and Wyeth, P. (2003) “Identification of cellulosic fibres by FTIR spectroscopy - Thread and single fibre analysis by attenuated total reflectance,” *Studies in Conservation*, 48(4), pp. 269–275. doi: 10.1179/sic.2003.48.4.269.
- Gea, S., Bilotti, E., Reynolds, C. T., Soykeabkeaw, N. and Peijs, T. (2010) “Bacterial cellulose-poly(vinyl alcohol) nanocomposites prepared by an in-situ process,” *Materials Letters*, 64(8), pp. 901–904. doi: 10.1016/j.matlet.2010.01.042.
- Genberg, A. (2019) *Coffee Leather, Alice Genberg*. Available at: <https://www.alicegenberg.com/#/coffee-leather/%0ACoffee> (Accessed: September 1, 2020).
- Ghalachyan, A. (2018) *Evaluation of consumer perceptions and acceptance of sustainable fashion products made of bacterial cellulose*. Iowa State University. Available at: <https://lib.dr.iastate.edu/cgi/viewcontent.cgi?article=7590&context=etd>.
- Gil, L. (2015) “New cork-based materials and applications,” *Materials*, 8(2), pp. 625–637. doi: 10.3390/ma8020625.
- Gonçalves, F., Correia, P., Silva, S. P. and Almeida-Aguiar, C. (2015) “Evaluation of antimicrobial properties of cork,” *FEMS Microbiology Letters*, 363(3), pp. 1–6. doi: 10.1093/femsle/fnv231.
- Gonçalves, S., Rodrigues, I. P., Padrão, J., Silva, J. P., Sencadas, V., Lanceros-mendez, S., Girão, H., Gama, F. M., Dourado, F. and Rodrigues, L. R. (2016) “Acetylated bacterial cellulose coated with urinary bladder matrix as a substrate for retinal pigment epithelium,” *Colloids and Surfaces B: Biointerfaces*,

139, pp. 1–9. doi: 10.1016/j.colsurfb.2015.11.051.

Grishchuk, S. and Karger-Kocsis, J. (2011) “Hybrid thermosets from vinyl ester resin and acrylated epoxidized soybean oil (AESO),” *Express Polymer Letters*, 5(1), pp. 2–11. doi: 10.3144/expresspolymlett.2011.2.

Gulbinienė, A., Jankauskaitė, V. and Arcilauskaitė, R. (2003) “Effect of leather finishing on water vapour transmission. Part I. Water vapour transfer through pigment finished leather,” *Materials Science*, 9(3), pp. 275–280.

Hahn, J. (2020) *Tômtex is a leather alternative made from waste seafood shells and coffee*, Dezeen. Available at: <https://www.dezeen.com/2020/08/22/tomttx-leather-alternative-biomaterial-seafood-shells-coffee/> (Accessed: August 31, 2020).

Han, J., Shim, E. and Kim, H. R. (2019) “Effects of cultivation, washing, and bleaching conditions on bacterial cellulose fabric production,” *Textile Research Journal*, 89(6), pp. 1094–1104. doi: 10.1177/0040517518763989.

Hao, K. (2017) *Would you wear a leather jacket grown in a lab?*, Quartz. Available at: <https://qz.com/901643/would-you-wear-a-leather-jacket-grown-in-a-lab/> (Accessed: October 19, 2017).

Hashem, M., Ibrahim, N. A., El-shafei, A., Refaie, R. and Hauser, P. (2009) “An eco-friendly–novel approach for attaining wrinkle – free/soft-hand cotton fabric,” *Carbohydrate Polymers*, 78(4), pp. 690–703. doi: 10.1016/j.carbpol.2009.06.004.

He, J., Zhao, H., Li, X., Su, D., Zhang, F., Ji, H. and Liu, R. (2018) “Superelastic and superhydrophobic bacterial cellulose/silica aerogels with hierarchical cellular structure for oil absorption and recovery,” *Journal of Hazardous Materials*, 346, pp. 199–207. doi: 10.1016/j.jhazmat.2017.12.045.

Hemrich, J., Fikkert, J. and Berg, M. van den (1993) “Porous structural forms resulting from aggregate modification in polyurethane dispersions by means of isothermic foam coagulation,” *Journal of Coated Fabrics*, 22, pp. 268–278.

Hervy, M., Blaker, J. J., Braz, A. L. and Lee, K.-Y. (2018) “Mechanical response of multi-layer bacterial cellulose nanopaper reinforced polylactide laminated composites,” *Composites Part A: Applied Science and Manufacturing*, 107, pp. 155–163. doi: 10.1016/j.compositesa.2017.12.025.

Hijosa, C., Gallart, A. R., Romero, J. J., Paul, R. and Brouta-Agnésia, M. (2013) “US 2013/0149512 A1 - Natural Nonwoven Materials.”

Hiokki, K. (2014) “Leather-Like Materials,” in *Kirk-Othmer Encyclopedia of Chemical Technology*. John Wiley & Sons, Inc. doi: <https://doi.org/10.1002/0471238961.1205012008091511.a01.pub2>.

Hole, L. G. and Whittaker, R. E. (1971) “Structure and properties of natural and artificial leathers,” *Journal of Materials Science*, 6, pp. 1–15.

Hu, W., Chen, S., Xu, Q. and Wang, H. (2011) “Solvent-free acetylation of bacterial cellulose under moderate conditions,” *Carbohydrate Polymers*, 83(4), pp. 1575–1581. doi: 10.1016/j.carbpol.2010.10.016.

Hu, W., Chen, S., Yang, J., Li, Z. and Wang, H. (2014) “Functionalized bacterial cellulose derivatives and nanocomposites,” *Carbohydrate Polymers*, 101(1), pp. 1043–1060. doi: 10.1016/j.carbpol.2013.09.102.

Hu, Y., Sheng, J., Yan, Z. and Ke, Q. (2018) “Completely amorphous cellulose biosynthesized in agitated culture at low temperature,” *International Journal of Biological Macromolecules*, 117, pp. 967–973. doi: 10.1016/j.ijbiomac.2018.06.013.

- Huang, J. W., Lv, X. G., Li, Z., Song, L. J., Feng, C., Xie, M. K., Li, C., Li, H. Bin, Wang, J. H., Zhu, W. D., Chen, S. Y., Wang, H. P. and Xu, Y. M. (2015) “Urethral reconstruction with a 3D porous bacterial cellulose scaffold seeded with lingual keratinocytes in a rabbit model,” *Biomedical Materials*, 10(5), p. 055005. doi: 10.1088/1748-6041/10/5/055005.
- ICI Americas Inc. (1980) “Meaning of HLB: Advantages and limitations,” in *The HLB system: A time-saving guide to emulsifier selection*. Wilmington, Delaware, USA: ICI Americas Inc., pp. 1–4. doi: 10.1002/jsfa.6444.
- Iguchi, M., Yamanaka, S. and Budhiono, A. (2000) “Bacterial cellulose – a masterpiece of nature’s arts,” *Journal of Materials Science*, 35, pp. 261–270. doi: 10.1023/A:1004775229149.
- ISO (2003) “ISO 17706:2003 Footwear – Test methods for uppers – Tensile strength and elongation.”
- ISO (2006) “ISO 20645:2006 Textile fabrics – Determination of antibacterial activity – Agar diffusion plate test.”
- ISO (2007) “ISO/TR 20879:2007 Footwear – Performance requirements for components for footwear – Uppers.”
- Jang, W. D., Hwang, J. H., Kim, H. U., Ryu, J. Y. and Lee, S. Y. (2017) “Bacterial cellulose as an example product for sustainable production and consumption,” *Microbial Biotechnology*, 10(5), pp. 1181–1185. doi: 10.1111/1751-7915.12744.
- Jebel, F. S. and Almasi, H. (2016) “Morphological, physical, antimicrobial and release properties of ZnO nanoparticles-loaded bacterial cellulose films,” *Carbohydrate Polymers*, 149, pp. 8–19. doi: 10.1016/j.carbpol.2016.04.089.
- Jin, M. Y., Liao, Y., Tan, C. H. and Wang, R. (2018) “Development of high performance nanofibrous composite membranes by optimizing polydimethylsiloxane architectures for phenol transport,” *Journal of Membrane Science*, 549(August 2017), pp. 638–648. doi: 10.1016/j.memsci.2017.10.051.
- Johnson, L. M., Gao, L., Shields, C. W., Smith, M., Efimenko, K., Cushing, K., Genzer, J. and López, G. P. (2013) “Elastomeric microparticles for acoustic mediated bioseparations,” *Journal of Nanobiotechnology*, 11(1). doi: 10.1186/1477-3155-11-22.
- Joseph, A. and Joshi, G. M. (2018) “High performance of fluoro polymer modified by hexa-titanium boride nanocomposites,” *Journal of Materials Science: Materials in Electronics*, 29(6), pp. 4749–4769. doi: 10.1007/s10854-017-8431-z.
- Jozala, A. F., Lencastre-Novaes, L. C. de, Lopes, A. M., Santos-Ebinuma, V. de C., Mazzola, P. G., Pessoa-Jr, A., Grotto, D., Gerenutti, M. and Chaud, M. V. (2016) “Bacterial nanocellulose production and application: a 10-year overview,” *Applied Microbiology and Biotechnology*, 100(5), pp. 2063–2072. doi: 10.1007/s00253-015-7243-4.
- Kamal, A. S. M., Misnon, M. I. and Fadil, F. (2020) “The effect of sodium hydroxide concentration on yield and properties of bacterial cellulose membranes,” in *IOP Conference Series: Materials Science and Engineering*, pp. 0–7. doi: 10.1088/1757-899X/732/1/012064.
- Kamal, A. S. M., Misnon, M. I., Zakaria, M. N., Kadir, M. I. A. and Ahmad, M. R. (2018) “Characteristics of cotton, polyester and rayon fabrics coated with *Acetobacter xylinum*,” *International Journal of Engineering & Technology*, 7, pp. 181–184.
- Kamiński, K., Jarosz, M., Grudzień, J., Pawlik, J., Zastawnik, F., Pandyra, P. and Kołodziejczyk, A. M. (2020) “Hydrogel bacterial cellulose: a path to improved materials for new eco-friendly textiles,” *Cellulose*, 27(9), pp. 5353–5365. doi: 10.1007/s10570-020-03128-3.

- Kanagaraj, J., Senthilvelan, T., Panda, R. C. and Kavitha, S. (2015) “Eco-friendly waste management strategies for greener environment towards sustainable development in leather industry: a comprehensive review,” *Journal of Cleaner Production*, 89, pp. 1–17. doi: 10.1016/j.jclepro.2014.11.013.
- Kawee, N., Lam, N. T. and Sukyai, P. (2018) “Homogenous isolation of individualized bacterial nano fibrillated cellulose by high pressure homogenization,” *Carbohydrate Polymers*, 179(October 2017), pp. 394–401. doi: 10.1016/j.carbpol.2017.09.101.
- Khalaf, A. I., El Nashar, D. E., Helaly, F. M. and Soliman, A. (2019) “Evaluation of controlled release PVC/PEG polymeric films containing 5-fluorouracil for long-term antitumor,” *Polymer Bulletin*, 76, pp. 3555–3568. doi: 10.1007/s00289-018-2562-0.
- Khan, S., Ul-Islam, M., Ullah, M. W., Israr, M., Jang, J. H. and Park, J. K. (2018) “Nano-gold assisted highly conducting and biocompatible bacterial cellulose-PEDOT:PSS films for biology-device interface applications,” *International Journal of Biological Macromolecules*, 107, pp. 865–873. doi: 10.1016/j.ijbiomac.2017.09.064.
- Khot, S. N., Lascalea, J. J., Can, E., Morye, S. S., Williams, G. I., Palmese, G. R., Kusefoglu, S. H. and Wool, R. P. (2001) “Development and application of triglyceride-based polymers and composites,” *Journal of Applied Polymer Science*, 82, pp. 703–723. doi: 10.1002/app.1897.
- Kiatsimkul, P. pahn, Sutterlin, W. R. and Suppes, G. J. (2006) “Selective hydrolysis of epoxidized soybean oil by commercially available lipases: Effects of epoxy group on the enzymatic hydrolysis,” *Journal of Molecular Catalysis B: Enzymatic*, 41(1–2), pp. 55–60. doi: 10.1016/j.molcatb.2006.04.008.
- Kim, D. Y., Nishiyama, Y. and Kuga, S. (2002) “Surface acetylation of bacterial cellulose,” *Cellulose*, 9(3–4), pp. 361–367. doi: 10.1023/A:1021140726936.
- Kim, H. M., Kim, H. R., Hou, C. T. and Kim, B. S. (2010) “Biodegradable photo-crosslinked thin polymer networks based on vegetable oil hydroxy fatty acids,” *Journal of the American Oil Chemists’ Society*, 87(12), pp. 1451–1459. doi: 10.1007/s11746-010-1634-6.
- Kılıç, E., Zengin, A. C. A., Aydın, S., Ork, N. and Zengin, G. (2017) “The influence of fatliquoring process on protective characteristics of leather gloves,” in *International Scientific Conference “Innovative solutions for sustainable development of textiles and leather industry,”* pp. 167–172.
- Klemm, D., Heublein, B., Fink, H. P. and Bohn, A. (2005) “Cellulose: Fascinating biopolymer and sustainable raw material,” *Angewandte Chemie - International Edition*, 44(22), pp. 3358–3393. doi: 10.1002/anie.200460587.
- Klemm, D., Kramer, F., Moritz, S., Lindström, T., Ankerfors, M., Gray, D. and Dorris, A. (2011) “Nanocelluloses: A new family of nature-based materials,” *Angewandte Chemie - International Edition*, 50(24), pp. 5438–5466. doi: 10.1002/anie.201001273.
- Klerk, H. M. De, Kearns, M. and Redwood, M. (2019) “Controversial fashion, ethical concerns and environmentally significant behaviour - The case of the leather industry,” *International Journal of Retail & Distribution Management*, 47(1), pp. 19–38. doi: 10.1108/IJRDM-05-2017-0106.
- Kocaman, S., Karaman, M., Gursoy, M. and Ahmetli, G. (2017) “Chemical and plasma surface modification of lignocellulose coconut waste for the preparation of advanced biobased composite materials,” *Carbohydrate Polymers*, 159, pp. 48–57. doi: 10.1016/j.carbpol.2016.12.016.
- Kondo, T. and Sawatari, C. (1994) “Intermolecular hydrogen bonding in cellulose/poly(ethylene oxide) blends: thermodynamic examination using 2,3-di-O- and 6-O-methylcelluloses as cellulose model compounds,” *Polymer*, 35(20), pp. 4423–4428. doi: 10.1016/0032-3861(94)90102-3.

- Kuraray (2018) *Clarino™*, Kuraray America. Available at: <http://www.clarino-am.com/science.php> (Accessed: March 16, 2018).
- Laurenti, R., Redwood, M., Puig, R. and Frostell, B. (2016) “Measuring the environmental footprint of leather processing technologies,” *Journal of Industrial Ecology*, 21(5), pp. 1180–1187. doi: 10.1111/jiec.12504.
- Leber, J. (2016) *Real leather grown in a lab is moving closer to your closet*, *Fast Company*. Available at: <https://www.fastcompany.com/3061337/real-leather-grown-in-a-lab-is-moving-closer-to-you-closet> (Accessed: October 19, 2017).
- Lee, K.-Y., Blaker, J. J. and Bismarck, A. (2009) “Surface functionalisation of bacterial cellulose as the route to produce green polylactide nanocomposites with improved properties,” *Composites Science and Technology*, 69(15–16), pp. 2724–2733. doi: 10.1016/j.compscitech.2009.08.016.
- Lee, K.-Y., Buldum, G., Mantalaris, A. and Bismarck, A. (2014) “More than meets the eye in bacterial cellulose: Biosynthesis, bioprocessing, and applications in advanced fiber composites,” *Macromolecular Bioscience*, 14, pp. 10–32. doi: 10.1002/mabi.201300298.
- Lee, K.-Y., Quero, F., Blaker, J. J., Hill, C. A. S., Eichhorn, S. J. and Bismarck, A. (2011) “Surface only modification of bacterial cellulose nanofibres with organic acids,” *Cellulose*, 18(3), pp. 595–605. doi: 10.1007/s10570-011-9525-z.
- Lee, K.-Y., Wong, L. L. C., Blaker, J. J., Hodgkinson, J. M. and Bismarck, A. (2011) “Bio-based macroporous polymer nanocomposites made by mechanical frothing of acrylated epoxidised soybean oil,” *Green Chemistry*, 13(11), pp. 3117–3123. doi: 10.1039/c1gc15655a.
- Lee, S. (2011) *Grow your own clothes*, *TED Talk*. Available at: https://www.ted.com/talks/suzanne_lee_grow_your_own_clothes/transcript (Accessed: November 2, 2016).
- Lee, T. S., Choi, H. Y., Choi, H. N., Lee, K.-Y., Kim, S.-H., Lee, S. G. and Yong, D. K. (2013) “Effect of surface treatment of ramie fiber on the interfacial adhesion of ramie/acetylated epoxidized soybean oil (AESO) green composite,” *Journal of Adhesion Science and Technology*, 27(12), pp. 1335–1347. doi: 10.1080/01694243.2012.697326.
- Lee, Y.-A., Li, R. and Nam, C. (2016) “Consumers’ acceptance of sustainable apparel products made of bacterial cellulose materials,” in *International Textile and Apparel Association (ITAA) Annual Conference Proceedings*. Vancouver, pp. 1–3. Available at: https://lib.dr.iastate.edu/cgi/viewcontent.cgi?article=1488&context=itaa_proceedings.
- Lee, Y.-A., Xiang, C., Ghalachyan, A., Ramasubramanian, G., Li, R., Madbouly, S. and Farr, C. (2014) “Exploring optimal solutions for sustainable product development using renewable bacteria cellulose fiber and biopolymer composites,” in *2014 ITAA Proceedings #71*. Charlotte, pp. 8–9.
- Lee, Y. A. (2016) “Case study of renewable bacteria cellulose fiber and biopolymer composites in sustainable design practices,” in Muthu, S. S. and Gardetti, M. A. (eds.) *Sustainable Fibres for Fashion Industry*. Singapore: Springer. doi: 10.1007/978-981-10-0522-0.
- Lemal, D. M. (2004) “Perspective on Fluorocarbon Chemistry,” *Journal of Organic Chemistry*, 69(1), pp. 1–11. doi: 10.1021/jo0302556.
- Li, C., Xiao, H., Wang, X. and Zhao, T. (2018) “Development of green waterborne UV-curable vegetable oil-based urethane acrylate pigment prints adhesive: Preparation and application,” *Journal of Cleaner Production*, 180, pp. 272–279. doi: 10.1016/j.jclepro.2018.01.193.

- Li, L., Zhou, Z., Yang, B., Ji, X., Huang, H., Zhong, G. and Xu, L. (2019) “Robust cellulose nanocomposite films based on covalently cross-linked network with effective resistance to water permeability,” *Carbohydrate Polymers journal*, 211, pp. 237–248. doi: 10.1016/j.carbpol.2019.01.084.
- Life Materials (2017) *MuSkin – samples and small production amounts*. Available at: <https://lifematerials.eu/en/shop/muskin/> (Accessed: November 10, 2017).
- Lima, G. F. De, Souza, A. G. De and Rosa, D. S. (2018) “Effect of adsorption of polyethylene glycol (PEG), in aqueous media, to improve cellulose nanostructures stability,” *Journal of Molecular Liquids*, 268, pp. 415–424. doi: 10.1016/j.molliq.2018.07.080.
- Liu, C., Liu, Z., Tisserat, B. H., Wang, R., Schuman, T. P., Zhou, Y. and Hu, L. (2015) “Microwave-assisted maleation of tung oil for bio-based products with versatile applications,” *Industrial Crops & Products*, 71, pp. 185–196. doi: 10.1016/j.indcrop.2015.02.066.
- Liu, F., Miao, L., Wang, Y., Xue, X. and Yang, H. (2017) “Progress in organic coatings green fabrication of ultraviolet curable epoxy acrylate-silica hybrid coatings,” *Progress in Organic Coatings*, 109, pp. 38–44. doi: 10.1016/j.porgcoat.2017.04.015.
- Liu, K., Madbouly, S. A. and Kessler, M. R. (2015) “Biorenewable thermosetting copolymer based on soybean oil and eugenol,” *European Polymer Journal*, 69, pp. 16–28. doi: 10.1016/j.eurpolymj.2015.05.021.
- Liu, W., Fei, M., Ban, Y., Jia, A. and Qiu, R. (2017) “Preparation and evaluation of green composites from microcrystalline cellulose and a soybean-oil derivative,” *Polymers*, 9(10), p. 541. doi: 10.3390/polym9100541.
- Liu, W., Fei, M. en, Ban, Y., Jia, A., Qiu, R. and Qiu, J. (2018) “Concurrent improvements in crosslinking degree and interfacial adhesion of hemp fibers reinforced acrylated epoxidized soybean oil composites,” *Composites Science and Technology*, 160, pp. 60–68. doi: 10.1016/j.compscitech.2018.03.019.
- Liu, W., Xie, T. and Qiu, R. (2017) “Biobased thermosets prepared from rigid isosorbide and flexible soybean oil derivatives,” *ACS Sustainable Chemistry and Engineering*, 5(1), pp. 774–783. doi: 10.1021/acssuschemeng.6b02117.
- Live kindly (2018) *Fashion designer creates vegan leather softer than real cow hide, Live kindly*. Available at: <https://www.livekindly.co/vegan-lino-linoleum-leather-softer-than-cow-hide/> (Accessed: September 1, 2020).
- López, S. H. and Santiago, E. V. (2013) “Acrylated-epoxidized soybean oil-based polymers and their use in the generation of electrically conductive polymer composites,” in El-Shemy, H. A. (ed.) *Soybean - Bio-Active Compounds*. London: IntechOpen Limited, pp. 231–263. doi: 10.5772/52992.
- Lu, J. and Wool, R. P. (2004) “Development of new green SMC resins and nanocomposites from plant oils,” in *4th Annual SPE Automotive Composites Conference, Troy, MI, USA, 14-15 September 2004*.
- Lu, P., Xiao, H., Zhang, W. and Gong, G. (2014) “Reactive coating of soybean oil-based polymer on nanofibrillated cellulose film for water vapor barrier packaging,” *Carbohydrate Polymers*, 111, pp. 524–529. doi: 10.1016/j.carbpol.2014.04.071.
- Ludwicka, K., Jędrzejczak-Krzepkowska, M., Kubiak, K., Kolodziejczyk, M., Pankiewicz, T. and Bielecki, S. (2016) “Medical and cosmetic applications of bacterial nanocellulose,” in Gama, M., Dourado, F., and Bielecki, S. (eds.) *Bacterial Nanocellulose: From Biotechnology to Bio-Economy*. Amsterdam: Elsevier B.V, p. 262. doi: <http://dx.doi.org/10.1016/B978-0-444-63458-0.00007-X>.
- Mandal, M. and Maji, T. K. (2017) “Comparative study on the properties of wood polymer composites

based on different modified soybean oils,” *Journal of Wood Chemistry and Technology*, 37(2), pp. 124–135. doi: 10.1080/02773813.2016.1253099.

Material District (2019) *Leather-free handbag made of bacterial cellulose*, *Material District*. Available at: <https://materialdistrict.com/article/handbag-bacterial-cellulose/> (Accessed: August 25, 2020).

Materials District (2019) *Furniture made from apple leather*, *Materials District*. Available at: <https://materialdistrict.com/article/furniture-apple-leather/> (Accessed: August 28, 2020).

Mautner, A., Lee, K.-Y., Tammelin, T., Mathew, A. P., Nedoma, A. J., Li, K. and Bismarck, A. (2015) “Cellulose nanopapers as tight aqueous ultra-filtration membranes,” *Reactive and Functional Polymers*, 86, pp. 209–214. doi: 10.1016/j.reactfunctpolym.2014.09.014.

Milionis, A., Bayer, I. S. and Loth, E. (2016) “Recent advances in oil-repellent surfaces,” *International Materials Reviews*, 61(2), pp. 101–106. doi: 10.1080/09506608.2015.1116492.

Mishra, R. K., Sabu, A. and Tiwari, S. K. (2018) “Materials chemistry and the futurist eco-friendly applications of nanocellulose: Status and prospect,” *Journal of Saudi Chemical Society*. doi: 10.1016/j.jscs.2018.02.005.

Miyamoto, H., Tsuduki, M., Ago, M., Yamane, C., Ueda, M. and Okajima, K. (2014) “Influence of dyestuffs on the crystallinity of a bacterial cellulose and a regenerated cellulose,” *Textile Research Journal*, 84(11), pp. 1147–1158. doi: 10.1177/0040517513517960.

Mizuno, M., Kamiya, Y., Katsuta, T., Oshima, N., Nozaki, K. and Amano, Y. (2012) “Creation of bacterial cellulose-fabric complexed material,” *SEN'I GAKKAISHI*, 68(2), pp. 42–47.

Modern Meadow (2020) *Technology - Modern Meadow*, *Modern Meadow*. Available at: <https://www.modernmeadow.com/technology> (Accessed: September 2, 2020).

Mohd, N. H., Farahein, N., Ismail, H., Zahari, J. I., Farahhanim, W., Kargarzadeh, H., Ramli, S., Ahmad, I., Yarmo, M. A. and Othaman, R. (2016) “Effect of aminosilane modification on nanocrystalline cellulose properties,” *Journal of Nanomaterials*, 2016.

Mondal, S., Pal, S., Bal, R. and Maity, J. (2018) “Fabrication of two sites hydrophobicity on cotton surface – a fluoropolymerization approach,” *Journal of Adhesion Science and Technology*, 4243, pp. 1–10. doi: 10.1080/01694243.2018.1458407.

Mukherjee, T., Rimal, S., Koskey, S., Chyan, O., Singh, K. J. and Myers, A. M. (2013) “Bonding structure of model fluorocarbon polymer residue determined by functional group specific chemical derivatization,” *ECS Solid State Letters*, 2(3), pp. 11–14. doi: 10.1149/2.008303ssl.

Mukhopadhyay, A., Preet, A. and Midha, V. (2018) “Moisture transmission behaviour of individual component and multi-layered fabric with sweat and pure water,” *Journal of the Textile Institute*, 109(3), pp. 383–392. doi: 10.1080/00405000.2017.1348435.

Naeem, M. A., Alfred, M., Saba, H., Siddiqui, Q., Naveed, T. and Shahbaz, U. (2019) “A preliminary study on the preparation of seamless tubular bacterial nanocomposite fabrics,” *Journal of Composite Materials*, 53(26–27). doi: 10.1177/0021998319842295.

Nam, C. and Lee, Y.-A. (2016) “RETHINK II. Kombucha Shoes for Scarlett and Rhett,” in *International Textile and Apparel Association (ITAA) Annual Conference Proceedings*, pp. 1–2.

Nasr, A. I. (2017) “Influence of some mechanical finishing processes on manufactured leather properties,” *Majalah Kulit, Karet, dan Plastik*, 33(2), pp. 99–107. doi: 10.20543/mkcp.v33i2.3139.

Ng, A. (2017) “Grown microbial 3D fiber art, Ava: Fusion of traditional art with technology,” in

- International Symposium on Wearable Computers, ISWC*. Maui, pp. 209–214. doi: 10.1145/3123021.3123069.
- Ng, F. M. C. and Wang, P. W. (2016) “Natural self-grown fashion from bacterial cellulose: A paradigm shift design approach in fashion creation,” *The Design Journal*, 19(6), pp. 837–855. doi: 10.1080/14606925.2016.1208388.
- Ng, M. C. F. and Wang, W. (2015) “A study of the receptivity to bacterial cellulosic pellicle for fashion,” *Research Journal of Textile and Apparel*, 19(4), pp. 65–69. doi: 10.1108/RJTA-19-04-2015-B007.
- Nisoa, M. and Wanichapichart, P. (2010) “Surface hydrophobic modification of cellulose membranes by plasma-assisted deposition of hydrocarbon films,” *Songklanakarinn Journal of Science and Technology*, 32(1), pp. 97–101. doi: 10.1016/j.surfcoat.2004.10.013.
- Nogi, M. and Yano, H. (2008) “Transparent nanocomposites based on cellulose produced by bacteria offer potential innovation in the electronics device industry,” *Advanced Materials*, 20, pp. 1849–1852. doi: 10.1002/adma.200702559.
- Nunez, F. U., Santiago, E. V. and Lopez, S. H. (2008) “Structural, thermal and morphological characterization of UV-graft polymerization of acrylated-epoxidized soybean oil onto goat leather,” *Chemistry & Chemical Technology*, 2(3), pp. 191–197.
- Oliveira, F. R., Fernandes, M., Carneiro, N. and Pedro Souto, A. (2013) “Functionalization of wool fabric with phase-change materials microcapsules after plasma surface modification,” *Journal of Applied Polymer Science*, 128(5). doi: 10.1002/app.38325.
- Padrão, J., Gonçalves, S., Silva, J. P., Sencadas, V., Lanceros-Méndez, S., Pinheiro, A. C., Vicente, A. A., Rodrigues, L. R. and Dourado, F. (2016) “Bacterial cellulose-lactoferrin as an antimicrobial edible packaging,” *Food Hydrocolloids*, 58, pp. 126–140. doi: 10.1016/j.foodhyd.2016.02.019.
- Palmleather (2017) *Palmleather - Our story, Palmleather*. Available at: http://palmleather.nl/?page_id=1028 (Accessed: June 1, 2017).
- Paquien, J. N., Galy, J., Gérard, J. F. and Pouchelon, A. (2005) “Rheological studies of fumed silica-polydimethylsiloxane suspensions,” *Colloids and Surfaces A: Physicochemical and Engineering Aspects*, 260(1–3), pp. 165–172. doi: 10.1016/j.colsurfa.2005.03.003.
- Peters, A. (2016) *This beautiful carbon-neutral “Leather” is grown from mushrooms, Fast Company*. Available at: <https://www.fastcompany.com/3062236/this-beautiful-carbon-neutral-leather-is-grown-from-mushrooms> (Accessed: October 11, 2017).
- Pinto, E. R. P., Barud, H. S., Silva, R. R., Palmieri, M., Polito, W. L., Calil, V. L., Cremona, M., Ribeiro, S. J. L. and Messaddeq, Y. (2015) “Transparent composites prepared from bacterial cellulose and castor oil based polyurethane as substrates for flexible OLEDs,” *Journal of Materials Chemistry C*, 3(44), pp. 11581–11588. doi: 10.1039/c5tc02359a.
- Pleumphon, C., Thiangtham, S., Pechyen, C., Manuspiya, H. and Ummartyotin, S. (2017) “Development of conductive bacterial cellulose composites: An approach to bio-based substrates for solar cells,” *Journal of Biobased Materials and Bioenergy*, 11(4), pp. 321–329. doi: 10.1166/jbmb.2017.1686.
- Pommet, M., Juntaro, J., Heng, J. Y. Y., Mantalaris, A., Lee, A. F., Wilson, K., Kalinka, G., Shaffer, M. S. P. and Bismarck, A. (2008) “Surface modification of natural fibers using bacteria: Depositing bacterial cellulose onto natural fibers to create hierarchical fiber reinforced nanocomposites,” *Biomacromolecules*, 9(6), pp. 1643–1651. doi: 10.1021/bm800169g.
- Portela, R., Leal, C. R., Almeida, P. L. and Sobral, R. G. (2019) “Bacterial cellulose: a versatile biopolymer

- for wound dressing applications,” *Microbial Biotechnology*, 12(4), pp. 586–610. doi: 10.1111/1751-7915.13392.
- Potivara, K. and Phisalaphong, M. (2019) “Development and characterization of bacterial cellulose reinforced with natural rubber,” *Materials*, 12(14). doi: 10.3390/ma12142323.
- Pradipasena, P., Chollakup, R. and Tantratian, S. (2018) “Formation and characterization of BC and BC-paper pulp films for packaging application,” *Journal of Thermoplastic Composite Materials*, 31(4), pp. 500–513. doi: 10.1177/0892705717712633.
- Radhakrishnan, T. S. (2005) “Thermal degradation of poly(dimethylsilylene) and poly(tetramethyldisilylene-co-styrene),” *Journal of Applied Polymer Science*, 99, pp. 2679–2686. doi: 10.1002/app.22813.
- Rajwade, J. M., Paknikar, K. M. and Kumbhar, J. V. (2015) “Applications of bacterial cellulose and its composites in biomedicine,” *Applied Microbiology and Biotechnology*, 99(6), pp. 2491–2511. doi: 10.1007/s00253-015-6426-3.
- Ramamoorthy, S. K., Kundu, C. K., Adekunle, K., Bashir, T. and Skrifvars, M. (2014) “Properties of green composites with regenerated cellulose fiber and soybean-based thermoset for technical applications,” *Journal of Reinforced Plastics and Composites*, 33(2), pp. 193–201. doi: 10.1177/0731684413504325.
- Ramamoorthy, S. K., Skrifvars, M., Alagar, R. and Akhtar, N. (2018) “End-of-life textiles as reinforcements in biocomposites,” *Journal of Polymers and the Environment*, 26, pp. 487–498. doi: 10.1007/s10924-017-0965-x.
- Rathinamoorthy, R., Aarthi, T., Aksaya Shree, C. A., Haridharani, P., Shruthi, V. and Vaishnikka, R. L. (2019) “Development and characterization of self-assembled bacterial cellulose nonwoven film,” *Journal of Natural Fibers*. doi: 10.1080/15440478.2019.1701609.
- Raut, A. (2019) *Malai: A sustainable, vegan alternative to leather*, *Architectural Digest*. Available at: <https://www.architecturaldigest.in/content/malai-a-sustainable-vegan-alternative-to-leather/> (Accessed: September 2, 2020).
- Retegi, A., Algar, I., Martin, L., Altuna, F., Stefani, P., Zuluaga, R., Gañán, P. and Mondragon, I. (2012) “Sustainable optically transparent composites based on epoxidized soy-bean oil (ESO) matrix and high contents of bacterial cellulose (BC),” *Cellulose*, 19(1), pp. 103–109. doi: 10.1007/s10570-011-9598-8.
- Riccio, C. (2017) *Muskin, the vegetable leather made from mushrooms*, *LifeGate*. Available at: <http://www.lifegate.com/people/lifestyle/muskin-leather-mushrooms> (Accessed: November 10, 2017).
- Rixtel, R. van (2019) *Lino leather*, *Dutch Design Daily*. Available at: dutchdesigndaily.com/complete-overview/lino-leather/ (Accessed: September 1, 2020).
- Robinson, M. (2016) *Everything you own could one day be made from mushrooms*, *Business Insider*. Available at: <http://www.businessinsider.com/mycoworks-2016-7> (Accessed: November 10, 2017).
- Rojas-Downing, M. M., Nejadhashemi, A. P., Harrigan, T. and Woznicki, S. A. (2017) “Climate change and livestock: Impacts, adaptation, and mitigation,” *Climate Risk Management*, 16, pp. 145–163. doi: 10.1016/j.crm.2017.02.001.
- Rotor, A. V (2017) *The making of nata de coco shoes, avrotor*. Available at: <http://avrotor.blogspot.com/2017/12/the-making-of-nata-de-coco-shoes.html> (Accessed: November 6, 2017).
- Ruan, C., Zhu, Y., Zhou, X., Abidi, N., Hu, Y. and Catchmark, J. M. (2016) “Effect of cellulose crystallinity

- on bacterial cellulose assembly,” *Cellulose*, 23(6), pp. 3417–3427. doi: 10.1007/s10570-016-1065-0.
- Sá, C. A. M. P. de (2011) “WO 2011149370 A1 - Cork fabric and process for the production thereof.” Available at: <http://www.google.com/patents/WO2011149370A1?cl=en>.
- Sai, H., Fu, R., Xing, L., Xiang, J., Li, Z., Li, F. and Zhang, T. (2015) “Surface modification of bacterial cellulose aerogels’ web-like skeleton for oil/water separation,” *ACS Applied Materials and Interfaces*, 7(13), pp. 7373–7381. doi: 10.1021/acsami.5b00846.
- Sai, H., Xing, L., Xiang, J., Cui, L., Jiao, J., Zhao, C., Li, Z., Li, F. and Zhang, T. (2014) “Flexible aerogels with interpenetrating network structure of bacterial cellulose-silica composite from sodium silicate precursor via freeze drying process,” *RSC Advances*, 4(57), pp. 30453–30461. doi: 10.1039/C4RA02752C.
- Saini, S., Belgacem, M. N., Salon, M.-C. B. and Bras, J. (2016) “Non leaching biomimetic antimicrobial surfaces via surface functionalisation of cellulose nanofibers with aminosilane,” *Cellulose*, 23(1), pp. 795–810. doi: 10.1007/s10570-015-0854-1.
- Saithai, P., Lecomte, J., Dubreucq, E. and Tanrattanakul, V. (2013) “Effects of different epoxidation methods of soybean oil on the characteristics of acrylated epoxidized soybean oil-co-poly(methyl methacrylate) copolymer,” *Express Polymer Letters*, 7(11), pp. 910–924. doi: 10.3144/expresspolymlett.2013.89.
- Salarbashi, D., Bazeli, J. and Tafaghodi, M. (2019) “Environment-friendly green composites based on soluble soybean polysaccharide: A review,” *International Journal of Biological Macromolecules*, 122, pp. 216–223. doi: 10.1016/j.ijbiomac.2018.10.110.
- Santos, S. M., Carbajo, J. M., Gómez, N., Quintana, E., Ladero, M., Sanchez, A., Chinga-Carrasco, G. and Villar, J. C. (2016) “Use of bacterial cellulose in degraded paper restoration. Part II: application on real samples,” *Journal of Materials Chemistry*, 51, pp. 1553–1561. doi: 10.1007/s10853-015-9477-z.
- Sathish, M., Madhan, B., Sreeram, K. J., Rao, J. R. and Nair, B. U. (2016) “Alternative carrier medium for sustainable leather manufacturing - a review and perspective,” *Journal of Cleaner Production*, 112, pp. 49–58. doi: 10.1016/j.jclepro.2015.06.118.
- Schenk, A. K. (2014) *Study of the impact of the nonwoven substrate formation on artificial leather*. North Carolina State University.
- Scherner, M., Reutter, S., Klemm, D., Sterner-Kock, A., Guschlbauer, M., Richter, T., Langebartels, G., Madershahian, N., Wahlers, T. and Wippermann, J. (2014) “In vivo application of tissue-engineered blood vessels of bacterial cellulose as small arterial substitutes: Proof of concept?,” *Journal of Surgical Research*, 189(2), pp. 340–347. doi: 10.1016/j.jss.2014.02.011.
- Schorn & Groh (2020) *NUO. Real wood as soft as leather.*, Schorn & Groh GmbH. Available at: <https://en.sg-veneers.com/products/nuo-real-smooth-wood.html%0AThe> (Accessed: September 15, 2020).
- Senoz, E., Stanzione, J. F., Reno, K. H., Wool, R. P. and Miller, M. E. N. (2013) “Pyrolyzed chicken feather fibers for biobased composite reinforcement,” *Journal of Applied Polymer Science*, 128(2), pp. 983–989. doi: 10.1002/app.38163.
- Shah, N., Ul-Islam, M., Khattak, W. A. and Park, J. K. (2013) “Overview of bacterial cellulose composites: A multipurpose advanced material,” *Carbohydrate Polymers*, 98(2), pp. 1585–1598. doi: 10.1016/j.carbpol.2013.08.018.
- Shao, W., Wu, J., Liu, H., Ye, S., Jiang, L. and Liu, X. (2017) “Novel bioactive surface functionalization of

- bacterial cellulose membrane,” *Carbohydrate Polymers*, 178, pp. 270–276. doi: 10.1016/j.carbpol.2017.09.045.
- Shim, E. and Kim, H. R. (2019) “Coloration of bacterial cellulose using in situ and ex situ methods,” *Textile Research Journal*, 89(7), pp. 1297–1310. doi: 10.1177/0040517518770673.
- Sick-Leitner, M. (2015) *SOYA C(O)U(L)TURE – Useful Things arise out of Waste*, *Ars Electronica Blog*. Available at: <https://ars.electronica.art/aeblog/en/2015/09/30/soya-coulture/> (Accessed: September 14, 2020).
- Silva, S. P., Sabino, M. A., Fernandes, E. M., Correlo, V. M., Boesel, L. F. and Reis, R. L. (2005) “Cork: properties, capabilities and applications,” *International Materials Reviews*, 50(6), pp. 345–365. doi: 10.1179/174328005X41168.
- Song, J. E., Cavaco-Paulo, A., Silva, C. and Kim, H. R. (2020) “Improvement of bacterial cellulose nonwoven fabrics by physical entrapment of lauryl gallate oligomers,” *Textile Research Journal*, 90(2), pp. 166–178. doi: 10.1177/0040517519862886.
- Song, J. E., Silva, C., Cavaco-Paulo, A. M. and Kim, H. R. (2019) “Functionalization of bacterial cellulose nonwoven by poly(Fluorophenol) to improve its hydrophobicity and durability,” *Frontiers in Bioengineering and Biotechnology*, 7, pp. 1–10. doi: 10.3389/fbioe.2019.00332.
- Song, J. E., Su, J., Noro, J., Cavaco-Paulo, A., Silva, C. and Kim, H. R. (2018) “Bio-coloration of bacterial cellulose assisted by immobilized laccase,” *AMB Express*, 8(19). doi: 10.1186/s13568-018-0552-0.
- Sousa, A. F., Ferreira, S., Lopez, A., Borges, I., Pinto, R. J. B., Silvestre, A. J. D. and Freire, C. S. R. (2017) “Thermosetting AESO-bacterial cellulose nanocomposite foams with tailored mechanical properties obtained by Pickering emulsion templating,” *Polymer*, 118, pp. 127–134. doi: 10.1016/j.polymer.2017.04.073.
- Soykeabkaew, N., Sian, C., Gea, S., Nishino, T. and Peijs, T. (2009) “All-cellulose nanocomposites by surface selective dissolution of bacterial cellulose,” *Cellulose*, 16(3), pp. 435–444. doi: 10.1007/s10570-009-9285-1.
- Stewart, J. (2020) *Two men created “leather” from cactus to save animals and the environment*, *My Modern Met*. Available at: <https://mymodernmet.com/vegan-cactus-leather-desserto/> (Accessed: August 25, 2020).
- Sudha, T. B., Thanikaivelan, P., Aaron, K. P., Krishnaraj, K. and Chandrasekaran, B. (2009) “Comfort, chemical, mechanical, and structural properties of natural and synthetic leathers used for apparel,” *Journal of Applied Polymer Science*, 114, pp. 1761–1767. doi: 10.1002/app.
- Sun, Y., Meng, C., Zheng, Y., Wang, Y., Qiao, K., Yue, L., Xie, Y. and He, W. (2018) “The effects of two biocompatible plasticizers on the performance of dry bacterial cellulose membrane: a comparative study,” *Cellulose*, 25, pp. 5893–5908. doi: 10.1007/s10570-018-1968-z.
- Sureshkumar, P. S., Thanikaivelan, P., Phebe, K., Krishnaraj, K., Jagadeeswaran, R. and Chandrasekaran, B. (2012) “Investigations on structural, mechanical, and thermal properties of pineapple leaf fiber-based fabrics and cow softy leathers: An approach toward making amalgamated leather products,” *Journal of Natural Fibers*, 9(1), pp. 37–50. doi: 10.1080/15440478.2012.652834.
- Tamilselvi, A., Jayakumar, G. C., Sri Charan, K., Sahu, B., Deepa, P. R., Kanth, S. V. and Kanagaraj, J. (2019) “Extraction of cellulose from renewable resources and its application in leather finishing,” *Journal of Cleaner Production*, 230, pp. 694–699. doi: 10.1016/j.jclepro.2019.04.401.
- Tang, K. P. M., Kan, C. W. and Fan, J. T. (2014) “Evaluation of water absorption and transport property

- of fabrics,” *Textile Progress*, 46(1), pp. 1–132. doi: 10.1080/00405167.2014.942582.
- Tang, L., Han, J., Jiang, Z., Chen, S. and Wang, H. (2015) “Flexible conductive polypyrrole nanocomposite membranes based on bacterial cellulose with amphiphobicity,” *Carbohydrate Polymers*, 117, pp. 230–235. doi: 10.1016/j.carbpol.2014.09.049.
- Temmink, R., Baghaei, B. and Skrifvars, M. (2018) “Development of biocomposites from denim waste and thermoset bio-resins for structural applications,” *Composites Part A: Applied Science and Manufacturing*, 106, pp. 59–69. doi: 10.1016/j.compositesa.2017.12.011.
- Tian, Y., Ina, M., Cao, Z., Sheiko, S. S. and Dobrynin, A. V (2018) “How to measure work of adhesion and surface tension of soft polymeric materials,” *Macromolecules*, 51(11), pp. 4059–4067. doi: 10.1021/acs.macromol.8b00738.
- Tomé, L. C., Brandão, L., Mendes, A. M., Silvestre, A. J. D., Pascoal, C., Alessandro, N., Freire, C. S. R. and Marrucho, I. M. (2010) “Preparation and characterization of bacterial cellulose membranes with tailored surface and barrier properties,” *Cellulose*, 17(6), pp. 1203–1211. doi: 10.1007/s10570-010-9457-z.
- Tomita, Y., Tsuji, T. and Kondo, T. (2009) “Fabrication of microbial cellulose nanofiber network sheets hydrophobically enhanced by introduction of a heat-printed surface,” *Sen-I Gakkaishi*, 65(2), pp. 73–79.
- Tu, C. (2016) *The fungi in your future*, *Science Friday*. Available at: <https://www.sciencefriday.com/articles/the-fungi-in-your-future/> (Accessed: October 11, 2017).
- Tyurin, I., Getmantseva, V., Andreeva, E. and Kashcheev, O. (2019) “The study of the molding capabilities of bacterial cellulose,” in *AUTEX 2019 - 19th World Textile Conference on Textiles at the Crossroads*. Ghent. Available at: <https://ojs.ugent.be/autex/article/view/11745/11183>.
- Ugbaja, M. I., Ejila, A., Mamza, P. A. and Mbada, I. N. (2016) “Water vapour permeability and wet rub fastness of finished leathers - Effect of acrylic polymer dispersion formulations,” *Science Journal of Chemistry*, 4(2), pp. 14–18. doi: 10.11648/j.sjc.20160402.11.
- United Nations (2015) *Transforming our world: the 2030 Agenda for Sustainable Development*. New York. Available at: https://www.un.org/ga/search/view_doc.asp?symbol=A/RES/70/1&Lang=E.
- Vegea (2017) *VEGEA® - Innovative biomaterials created from wine*, *Vegea*. Available at: <http://www.vegeacompany.com/en/> (Accessed: November 10, 2017).
- Wahid, F., Hu, X., Chu, L., Jia, S., Xie, Y. and Zhong, C. (2019) “Development of bacterial cellulose/chitosan based semi-interpenetrating hydrogels with improved mechanical and antibacterial properties,” *International Journal of Biological Macromolecules*, 122, pp. 380–387. doi: 10.1016/j.ijbiomac.2018.10.105.
- Wan, Y. Z., Luo, H., He, F., Liang, H., Huang, Y. and Li, X. L. (2009) “Mechanical, moisture absorption, and biodegradation behaviours of bacterial cellulose fibre-reinforced starch biocomposites,” *Composites Science and Technology*, 69(7–8), pp. 1212–1217. doi: 10.1016/j.compscitech.2009.02.024.
- Wan, Z., Wang, L., Ma, L., Sun, Y. and Yang, X. (2017) “Controlled hydrophobic biosurface of bacterial cellulose nanofibers through self-assembly of natural zein protein,” *ACS Biomaterials Science & Engineering*, 3(8), pp. 1595–1694. doi: 10.1021/acsbomaterials.7b00116.
- Wang, J., Tavakoli, J. and Tang, Y. (2019) “Bacterial cellulose production, properties and applications with different culture methods – A review,” *Carbohydrate Polymers*, 219, pp. 63–76. doi: 10.1016/j.carbpol.2019.05.008.
- Wang, S. (2013) *Redox-initiated adiabatic emulsion polymerization*. Lehigh University.

- Wang, S., Jiang, F., Xu, X., Kuang, Y., Fu, K., Hitz, E. and Hu, L. (2017) "Super-strong, super-stiff macrofibers with aligned, long bacterial cellulose nanofibers," *Advanced Materials*, 29(35), pp. 1–8. doi: 10.1002/adma.201702498.
- Wei, B., Yang, G. and Hong, F. (2011) "Preparation and evaluation of a kind of bacterial cellulose dry films with antibacterial properties," *Carbohydrate Polymers*, 84, pp. 533–538. doi: 10.1016/j.carbpol.2010.12.017.
- Wei, G., Xu, H., Chen, L., Li, Z. and Liu, R. (2019) "Isosorbide-based high performance UV-curable reactive diluents," *Progress in Organic Coatings*, 126, pp. 162–167. doi: 10.1016/j.porgcoat.2018.10.028.
- Wei, L. and McDonald, A. G. (2016) "A review on grafting of biofibers for biocomposites," *Materials*, 9(303). doi: 10.3390/ma9040303.
- Wiśniewska, M., Chibowski, S., Urban, T. and Terpiłowski, K. (2019) "Investigations of chromium(III) oxide removal from the aqueous suspension using the mixed flocculant composed of anionic and cationic polyacrylamides," *Journal of Hazardous Materials*, 368, pp. 378–385. doi: 10.1016/j.jhazmat.2019.01.068.
- Wood, D., Hang, L. and Salusso, C. J. (2015) "Production and characterization of bacterial cellulose fabrics," in *International Textile and Apparel Association (ITAA) Annual Conference Proceedings*. Santa Fe, pp. 11–13.
- Wool, R. (2013) "US 2013/0337711 A1 - Composites having leather-like characteristics."
- Wu, S. (1971) "Calculation of interfacial tension in polymer systems," *Journal of Polymer Science Part C: Polymer Symposia*, 34(1), pp. 19–30. doi: 10.1002/polc.5070340105.
- Wu, X., Li, J., Li, G., Ling, L., Zhang, G., Sun, R. and Wong, C.-P. (2018) "Heat-triggered poly(siloxane-urethane)s based on disulfide bonds for self-healing application," *Journal of Applied Polymer Science*, 46532, pp. 1–9. doi: 10.1002/app.46532.
- Wu, Z., Chen, S., Wu, R., Sheng, N., Zhang, M., Ji, P. and Wang, H. (2020) "Top-down peeling bacterial cellulose to high strength ultrathin films and multifunctional fibers," *Chemical Engineering Journal*, 391, p. 123527. doi: 10.1016/j.cej.2019.123527.
- Wu, Z. Y., Liang, H. W., Chen, L. F., Hu, B. C. and Yu, S. H. (2016) "Bacterial cellulose: A robust platform for design of three dimensional carbon-based functional nanomaterials," *Accounts of Chemical Research*, 49(1), pp. 96–105. doi: 10.1021/acs.accounts.5b00380.
- Xu, Q., Fan, L., Yuan, Y., Wei, C., Bai, Z. and Xu, J. (2016) "All-solid-state yarn supercapacitors based on hierarchically structured bacterial cellulose nanofiber-coated cotton yarns," *Cellulose*, 23(6), pp. 3987–3997. doi: 10.1007/s10570-016-1086-8.
- Xu, X., Jagota, A., Paretkar, D. and Hui, C. (2016) "Surface tension measurement from the indentation of clamped thin films," *Soft Matter*, 12, pp. 5121–5126. doi: 10.1039/c6sm00584e.
- Yang, Q., Ma, H., Dai, Z., Wang, J., Dong, S., Shen, J. and Dong, J. (2017) "Improved thermal and mechanical properties of bacterial cellulose with the introduction of collagen," *Cellulose*, 24(9), pp. 3777–3787. doi: 10.1007/s10570-017-1366-y.
- Yao, J., Chen, S., Chen, Y., Wang, B., Pei, Q. and Wang, H. (2017) "Macrofibers with high mechanical performance based on aligned bacterial cellulose nanofibers," *ACS Applied Materials & Interfaces*, 9(24), pp. 20330–20339. doi: 10.1021/acsami.6b14650.
- Yim, S. M., Song, J. E. and Kim, H. R. (2017) "Production and characterization of bacterial cellulose

- fabrics by nitrogen sources of tea and carbon sources of sugar,” *Process Biochemistry*, 59, pp. 26–36. doi: 10.1016/j.procbio.2016.07.001.
- Yorgancioglu, A., Başaran, B. and Sancakli, A. (2020) *Value addition to leather industry wastes and by-products: Hydrolyzed collagen and collagen peptides*, *IntechOpen*. doi: 10.5772/intechopen.92699.
- Yousefi, B., Gharehaghaji, A. A., Asghar, A. and Jeddi, A. (2018) “The combined effect of wrinkles and noncircular shape of fibers on wetting behavior of electrospun cellulose acetate membranes,” *Journal of Polymer Science Part B: Polymer Physics*, 56, pp. 1012–1020. doi: 10.1002/polb.24617.
- Yu, B., Cheng, H., Zhuang, W., Zhu, C., Wu, J., Niu, H., Liu, D., Chen, Y. and Ying, H. (2018) “Stability and repeatability improvement of horseradish peroxidase by immobilization on amino-functionalized bacterial cellulose,” *Process Biochemistry*, 79, pp. 40–48. doi: 10.1016/j.procbio.2018.12.024.
- Zahid, M., Heredia-Guerrero, J. A., Athanassiou, A. and Bayer, I. S. (2017) “Robust water repellent treatment for woven cotton fabrics with eco-friendly polymers,” *Chemical Engineering Journal*, 319, pp. 321–332. doi: 10.1016/j.cej.2017.03.006.
- Zargar, R., Nourmohammadi, J. and Amosbediny, G. (2015) “Preparation, characterization, and silanization of 3D microporous PDMS structure with properly sized pores for endothelial cell culture,” *International Union of Biochemistry and Molecular Biology*, 63(2), pp. 190–199. doi: 10.1002/bab.1371.
- Zengin, G., Sardroudi, S. P., Bitlisli, B. O. and Zengin, A. C. A. (2016) “Effect of various tanning processes on characteristics of lining leathers,” in *ICAMS 2016 - Proceedings of the 6th International Conference on Advanced Materials and Systems*. doi: 10.24264/icams-2016.iii.21.
- Zhang, C., Yan, M., Cochran, E. W. and Kessler, M. R. (2015) “Biorenewable polymers based on acrylated epoxidized soybean oil and methacrylated vanillin,” *Materials Today Communications*, 5, pp. 18–22. doi: 10.1016/j.mtcomm.2015.09.003.
- Zhang, W., Kalulu, M., Wang, X.-H., Xia, X.-K., Han, X.-L. and Jiang, Y. (2018) “Reverse hydrophobic PDMS surface to hydrophilic by 1-step hydrolysis reaction,” *Polymers for Advanced Technologies*, 29(7), pp. 2103–2109. doi: 10.1002/pat.4319.
- Zhao, W., Zhang, X., Tian, C. and Gao, Z. (2015) “Analysis of wetting characteristics on microstructured hydrophobic surfaces for the passive containment cooling system,” *Science and Technology of Nuclear Installations*, 2015, p. 6. doi: 10.1155/2015/652731.
- Zhong, C. (2020) “Industrial-scale production and applications of bacterial cellulose,” *Frontiers in Bioengineering and Biotechnology*, 8, pp. 1–19. doi: 10.3389/fbioe.2020.605374.
- Zhu, J., Chandrashekhara, K., Flanigan, V. and Kapila, S. (2004) “Curing and mechanical characterization of a soy-based epoxy resin system,” *Journal of Applied Polymer Science*, 91, pp. 3513–3518. doi: 10.1002/app.13571.
- Zürbig, C., Kruse, H.-H. and Buchkremer, K. (2015) “Leather imitates,” *ULLMANN’S*, p. 13. doi: 10.1002/14356007.a15_283.pub2.